DEVELOPMENT OF ENHANCED FBMC AND DYNAMIC SPECTRUM ALLOCATION SCHEME FOR INTERFERENCE MITIGATION IN 5G HETEROGENEOUS NETWORK

BY

NURZATI IWANI BINTI OTHMAN

A thesis submitted in fulfilment of the requirement for the degree of Doctor of Philosophy (Engineering).

Kulliyyah of Engineering
International Islamic University Malaysia

JULY 2023

ABSTRACT

The 4G network implements Orthogonal Frequency Division Multiplexing (OFDM) as its multiplexing method. Using the said method, the network is expected to be able to cope with severe channel conditions without the use of complex equalization filters. However, very high Peak to Average Power Ratio (PAPR) and Out-of-Band (OOB) emissions are still being experienced where the system's throughput and spectrum efficiency are significantly reduced. Maxis, one of the major telco operators in Malaysia, reported that they experienced a 33% in speed reduction for its 4G network throughout the year 2019. The currently dedicated spectrum for 4G is reaching its limits and there is a large as well as growing demand for wireless access and applications. The strategies for more intelligent use of the spectrum are urgently required. Thus, in this research, the overall objective is to assemble a new augmented multiplexing method and an enhanced spectrum management technique. The newly proposed multiplexing method for the future 5G is called the Filter Bank Multicarrier (FBMC) with a Lowpass Windowed Finite Impulse Response (FIR) filter (LWF-FBMC). The improved interference management procedure is identified as enhanced dynamic spectrum allocation (E-DSA) that incorporates a cooperative type of Game Theory (GT) called the Nash bargaining solution. These two proposed solutions are very much hoped to be able to maximize the throughput requirements of 5G. In addition, it is expected to address the interference mitigation aspects. This study utilized three types of Software Defined Radios (SDRs) for designing and analyzing the configurations. The SDRs used were the LabVIEW Communications System Design Suite (LV Comm), GNU Radio, and MATLAB software. For hardware implementation, the National Instrument's Universal Software Radio Peripheral reconfigurable I/O (NI USRP RIO) was used. In the methodology, the construction of the newly proposed LWF-FBMC was done using the LV Comm. The power spectral density (PSD) analyses between OFDM and LWF-FBMC were carried out to compare their level of OOB emissions by analyzing their power spectral densities. In developing the E-DSA, the effectiveness of the DSA for 4G was first analyzed using GNU Radio. The algorithm was then enhanced to be E-DSA and tested in an urban 5G heterogeneous network scenario that involves both macrocell and microcell users. The simulated configurations were then integrated with the NI USRP RIO transceiver to compare their power spectral densities in real-time. For the results, it was shown that the LWF-FBMC can achieve higher spectral efficiency than the OFDM by 15.4%. The newly configured E-DSA scheme can improve the 5G network's throughput by 104% when compared with the DSA for 4G network. The NI USRP RIO's results also indicated that the spectral efficiency of LWF-FBMC is higher by 50% than that of OFDM. However, for the simulation-hardware integration part, only the multiplexing methods were compared without analyzing the effects of implementing E-DSA due to the limited time and resources. For future works, it is best to examine this as well. In conclusion, with these improvements, it can be said that both methods, the LWF-FBMC and the E-DSA can help in alleviating the interference for the up-and-coming 5G system.

ملخص البحث

تنفذ شبكة 4G تعدّد الإرسال لشعبة التّردّد المتعامد (OFDM) بوصفها طريقة تعدّد الإرسال. يجب أن يكون قادرًا على التّعامل مع ظروف القناة الشّديدة دون استخدام مرشّحات المعادلة المعقدة. ومع ذلك، فإنّ نسبة الذّروة إلى متوسّط الطّاقة (PAPR) وانبعاثات خارج النّطاق (OOB) التي يعاني منها OFDM تقلّل بشكل كبير من إنتاجية النّظام وكفاءة طيفه. فعلى سبيل المثال، أبلغت إحدى شركات ذات مشغلي الاتصالات الرّئيسيّة في ماليزيا، معروف باسم ماكسيس (Maxis) عن حدوث انخفاض بنسبة 33٪ في السّرعة لشبكة 4G على مدار عام 2019م. يصل الطّيف المخصّص حاليًا لـ 4G إلى حدوده وهناك طلب كبير ومتزايد على الوصول اللّاسلكي والتّطبيقات. وافتقرت حاجة ماسّة إلى استراتيجيات للاستخدام الأكثر ذكاءً للطيف. ومن ثمَّ في هذا البحث، فيركز الهدف العام إلى تجميع طريقة تعدّد الإرسال المعزّزة الجديدة وتقنية إدارة الطّيف المعزّز. تسمّى طريقة الإرسال المتعدد المقترحة حديثًا لشبكة الجيل الخامس المستقبلية Filter Bank Multicarrier (FBMC) مع مرشّح -LWF) Lowpass Windowed Finite Impulse Response (FIR) FBMC. تم تحديد إجراء الإدارة المحسن على أنه تمّ توزيع الطّيف الدّيناميكي المحسن (E-DSA) الذي يتضمّن نوعًا تعاونيًا من نظرية اللّعبة (GT) يسمّى حلّ مساومة ناش. ومن المتوقع على أن يكون هذان الحلّان الجديدان المقترحان قادرين على استيعاب الكفاءة الطّيفية العالية وتعظيم متطلّبات إنتاجية 5G. وحملاً على ما مرّ، فإنّ من المتوقع أن يعالج جوانب التّخفيف من التّداخل. اعتمدت هذه الدّراسة على ثلاثة أنواع من أجهزة الرّاديو المحدّدة للبرامج (SDRs) لتصميم وتحليل التّكوينات. كانت SDRs المستخدمة هي (LV) LabVIEW Communications Design Suite Comm وGNU Radio وMATLAB. للتّحقّق من صحّة تصاميم المحاكاة، تمّ استخدام I/O الطّرفي للرّاديو العالمي التّابع للأداة الوطنيّة (NI USRP RIO). وتقوم هذه الدّراسة على المنهج أي تم تحديد أداء الكفاءات الطّيفيّة بين OFDM النّموذجيّ وFBMC باستخدام برنامج MATLAB. ومن ثمّ، تمّ بناء LWF-FBMC المقترح حديثًا باستخدام LV Common. وتمّ إجراء تحليلات كثافة طيف

الطّاقة (PSD) بين OFDM و LWF-FBMC لمقارنة كفاءاتهم الطّيفية. عند تطوير E-DSA، تمّ تحليل فعاليّة DSA لـ 4G أولاً باستخدام راديو GNU. بعد ذلك تحسين الخوارزمية لتكون E-DSA واختبارها في سيناريو شبكة 5G غير متجانس حضري يتضمّن مستخدمي macrocell و microcell. تمّ التّحقّق من صحّة التّكوينات المحاكاة باستخدام جهاز الإرسال والاستقبال RIO NI USRP لمقارنة كفاءاتها الطّيفية في الوقت الفعلي. بالنّسبة للنّتائج، تمّ توضيح أن LWF-FBMC يمكن أن تحقّق كفاءة طيفيّة أعلى من OFDM بنسبة 15.4٪. يمكن لمخطط E-DSA المعد حديثًا تحسين إنتاجيّة شبكة 5G بنسبة 144٪، ممّا يشير إلى أنه يمكن تخفيف التّداخل. وأشارت نتائج NI USRP RIO أيضًا إلى أن الكفاءة الطّيفية لـ LWF-FBMC أعلى بنسبة 50٪ من OFDM. مع هذه التّحسينات، يمكن القول إن كلتا الطّريقتين، LWF-FBMC و E-DSA يمكن أن تساعد في تخفيف التّداخل لنظام 5G الصاعد.
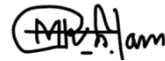
APPROVAL PAGE

The thesis of Nurzati Iwani Binti Othman has been approved by the following:

_____
Ahmad Fadzil Ismail
Supervisor

_____
Khairayu Badron
Co-supervisor

_____
Md Rafiqul Islam
Co-supervisor

_____
Aisha Hassan Abdalla Hashim
Internal Examiner

_____
Aduwati Sali
External Examiner

_____
Adamu Abubakar Ibrahim
Chairman

DECLARATION

I hereby declare that this thesis is the result of my own investigations, except where otherwise stated. I also declare that it has not been previously or concurrently submitted as a whole for any other degrees at IIUM or other institutions.

Nurzati Iwani Binti Othman

Signature……………………………   Date……20th July 2023……

INTERNATIONAL ISLAMIC UNIVERSITY MALAYSIA

DECLARATION OF COPYRIGHT AND AFFIRMATION OF FAIR USE OF UNPUBLISHED RESEARCH

DEVELOPMENT OF ENHANCED FBMC AND DYNAMIC SPECTRUM ALLOCATION SCHEME FOR INTERFERENCE MITIGATION IN 5G HETEROGENEOUS NETWORK

I declare that the copyright holder of this thesis are jointly owned by the student and IIUM.

Affirmed by Nurzati Iwani Binti Othman

………………………………   20th July 2023
                                        …………………..
Signature   Date

ACKNOWLEDGEMENTS

All glory is due to Allah, the Almighty, whose Grace and Mercies have been with me throughout the duration of my programme. Although, it has been tasking, His Mercies and Blessings on me ease the herculean task of completing this thesis.

I am most indebted to by supervisor, Prof. Dr. Ir. Ahmad Fadzil bin Ismail, whose enduring disposition, kindness, promptitude, thoroughness and friendship have facilitated the successful completion of my work. I put on record and appreciate his detailed comments, useful suggestions and inspiring queries which have considerably improvedthis thesis. His brilliant grasp of the aim and content of this work led to his insightful comments, suggestions and queries which helped me a great deal. Despite his commitments, he took time to listen and attend to me whenever requested. The moral support he extended to me is in no doubt a boost that helped in building and writing thedraft of this research work. I am also grateful to my co-supervisors, Asst. Prof. Dr. Ir. Khairayu Badron and Prof. Dr. Md Rafiqul Islam, whose support and cooperation contributed to the outcome of this work.

Lastly, my gratitude goes to my beloved husband and lovely children; for their prayers, understanding and endurance while away.

Once again, we glorify Allah for His endless mercy on us one of which is enabling us to successfully round off the efforts of writing this thesis. Alhamdulillah.

TABLE OF CONTENTS

LIST OF TABLES

LIST OF FIGURES

CHAPTER ONE

INTRODUCTION

1.1 BACKGROUND OF THE STUDY

1.1.1 5G Heterogeneous Network

5G technology aims to enhance the energy and spectral efficiency of a network consisting of various types of devices by implementing a combination of newly designed system concepts suitable for a multi-tier heterogeneous network. Figure 1.1 shows the 5G requirements that are expected to be met.
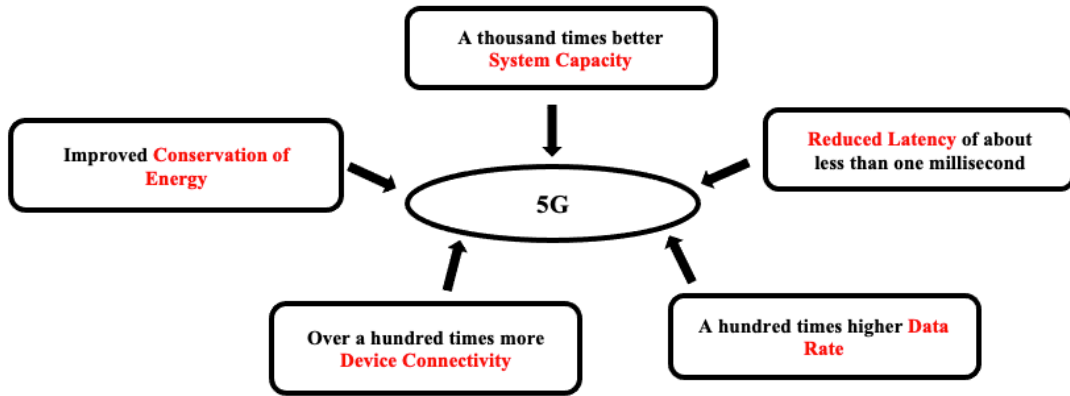
Figure 1.1 5G Requirements

A detailed explanation of the requirements for 5G wireless systems is outlined in Table 1.1 below:

Table 1.1 Detailed 5G requirements

5G Requirements	Description
Energy harvesting for energy-efficient communication	Energy can be harvested from: Environmental energy sources such as wind and solar energy. Radio signals such as radio frequency (RF) energy with coherent efficiency.

	This can extend the battery's lifetime and enhance energy efficiency (Han, 2017).
Multiple Random Access Technologies (RATs)	Combination of current RATs such as Global System for Mobile Communications (GSM), Evolved High-Speed Packet Access (HSPA+), and Long-Term Evolution (LTE) and 5G in the same network for improved system performance (Ericsson, 2013).
Densification of the base station (BS)	A more compact deployment of device-to-device (D2D) communication links, relays, and low-power nodes than today's macrocell networks (Fooladivanda and Rosenberg, 2013).
Prioritized spectrum access	Two types of priorities for spectrum access will be developed: Traffic-based: Users with different requirements, such as latency and reliability. Tier-based: Users with different tiers. This shall guarantee the protection of the macro users. On the other hand, traffic-based priority exists because of the various needs of the users, such as the reliability and latency requirements as well as their energy constraints.
Machine-type Communication (MTC) devices	MTC devices: Vehicles, home appliances, sensors, and many more. Will outnumber conventional communication devices such as tablets and smartphones (De Andrade, Astudillo and Da Fonseca, 2014)
Millimetre-wave communication	Millimetre-wave frequency bands: 28 GHz and 38 GHz bands. Can overcome the issue of under-utilized spectrum resources (Singh and Chawla, 2017).

Network-assisted device-to-device (D2D) communication	More concentration on D2D communications where the control signalling will be performed by the BS (Nakamura et al., 2013).
Latency and Data Rate	Targeted experienced data rates: 300 Mbps (downlink) and 60 Mbps (uplink) for dense urban locations. Targeted end-to-end latencies: 2 to 5 milliseconds. (Metis, 2013)

The transformation of the fourth generation (4G) communication network to the fifth generation (5G) is motivated by a substantial increase in the demand for continuous connectivity and improved quality of service (QoS). The idea of 5G is to substantially improve users' quality of experience (QoE) by integrating several diversified devices and machines under the same network. The network configuration is an incorporation of diverse systems such as Heterogeneous Network (H-Net), internet of things, beamforming, relay node, millimetre-wave communication, and device-to-device (D2D) communication (Siddiqui et al., 2021).
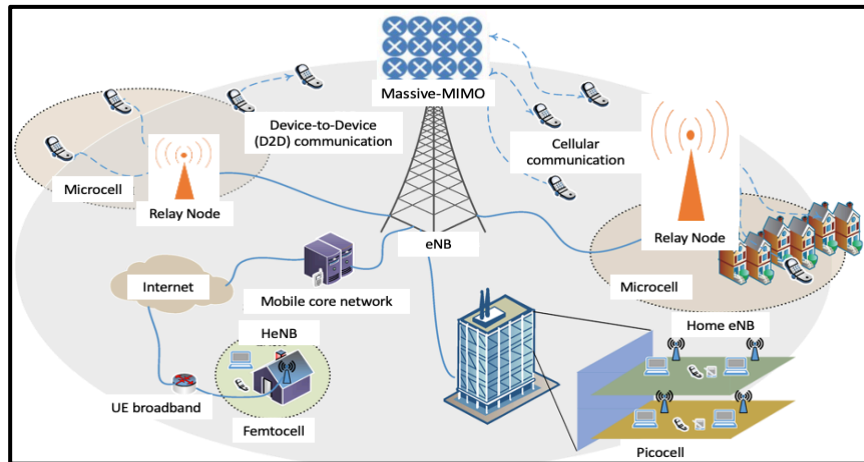
Figure 1.2 A Multi-tier Network Composed of Macrocells, Picocells, Femtocells, Relays, and D2D links

Figure 1.2 shows such a multi-tier network. This highly dense configuration will cause interference from both the downlink and uplink transmissions of the devices and base stations. With proper interference management within the network, resources such as

transmission power, spectrum availability, and transmission time can be allocated to all users to obtain maximized throughput.

For the existing 5G network, which is affected by numerous kinds of interferences, H-Net is a potential solution to mitigate it (Qasim et al., 2020). Due to the chaotic and disorganised network design, the inter-cell, intra-cell, adjacent-channel, self-, and inter-channel interferences severely degrade this extremely dense small-cell system. Inter-channel interference (ICI) in the present 5G H-Net can grow twofold compared to the conventional cellular network design, as seen by the development of ultra-dense tiny cell networks (Bhushan et al., 2014). As a result, ICI is heavily involved in the current 5G multi-cell low-power base station, and the characteristics it offered in its predecessor's mobile technologies are somewhat different from the new radio 5G network. Hence, an enhanced ICI management and mitigation technique should be created for future cellular technology. Furthermore, all other vulnerable interferences must be cancelled to ensure excellent QoS and equity among the users in a cellular network.

1.1.2 Spectrum Allocation for 5G

Since the development of 5G mobile communications technology, there have been numerous heated disputes on how to give the right amount of spectrum to different uses. According to Beltrán and Massaro (2018), in particular, spectrum scarcity and drawn-out procedures to eliminate and relocate low-intensity users have rekindled interest in spectrum sharing. While abiding by the incumbents' interference restrictions, dynamic spectrum-sharing technologies allow third-party users to share licenced spectrum bands with them. The massive underutilization of spectrum by all licenced network services across all interest bands serves as the driving force for research and development in spectrum-sharing schemes, both in the time and space domains. (Mekuria and Dludla, 2018).

Spectrum allocation for 5G is divided into three main bands, namely low, high, and extremely high, according to Ahmad et al. (2016). The band at lower frequencies, especially at 700 MHz, allows both deep indoor coverage and wide-area 5G coverage. The required capacity to support many connected devices and guarantee fast speed for simultaneously connected devices is provided by the spectrum at high frequencies with reasonably large bandwidths below 6 GHz (around 3.4 GHz to 3.8 GHz). The most optimal balance between

capacity and coverage is provided by this spectrum. The spectrum offers ultra-high capacity and very low latency at very high frequencies above 24 GHz (for example, 24.25 GHz to 27.5 GHz) with very big bandwidths. The coverage of the cells at these frequencies is minimal (from 50 m to 200 m).
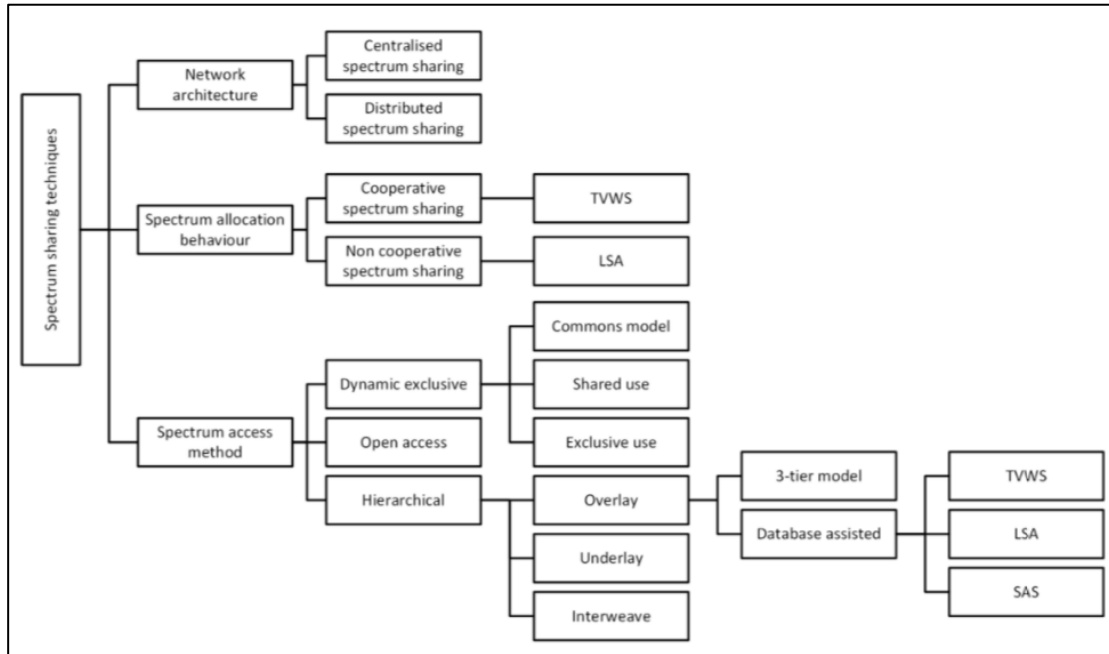
Figure 1.3 Spectrum Sharing Techniques (Abdulhakeem, et al., 2022)

Network design, spectrum allocation behaviour, and spectrum access method are the three primary spectrum-sharing approaches toward the construction of 5G that are detailed in Figure 1.3. Network architecture can be distributed or centralized (infrastructure-oriented) (infrastructure-less). There are two types of spectrum allocation behaviour: cooperative and non-cooperative. Either dynamic exclusive, open access or hierarchical model are available as spectrum access methods.

The majority of research on game theory's spectrum allocation is currently based on non-cooperative game models, where secondary users' (SUs') objectives are to maximise their game gains regardless of how their strategies affect other SUs. In this paper, a more effective dynamic spectrum allocation model is presented with the aim of optimizing the aggregate income of all SUs in the network. This model is based on Nash bargaining in a cooperative game.

1.2 STATEMENT OF THE PROBLEM

During the Covid-19 pandemic that started in 2020, most employees in Malaysia were instructed to work from their homes instead of their offices to prevent the spread of the virus. These activities led to an increase in internet traffic demand in residential areas between 50% and 70% causing network congestions that resulted in a 40% reduction in Internet speed, as reported by the Malaysian Communications and Multimedia Commission (MCMC) (2020).

According to the Department of statistics Malaysia, the percentage of individuals using Information and communication technology (ICT) services and equipment in Malaysia, such as computers, internet and mobile phone, has increased from the year 2020 until 2021 due to the pandemic. In this regard, the ICT sector is not the only sector affected by this scenario. Figure 1.4 shows the potential roles of 5G technology for sectors such as healthcare, education and retail.
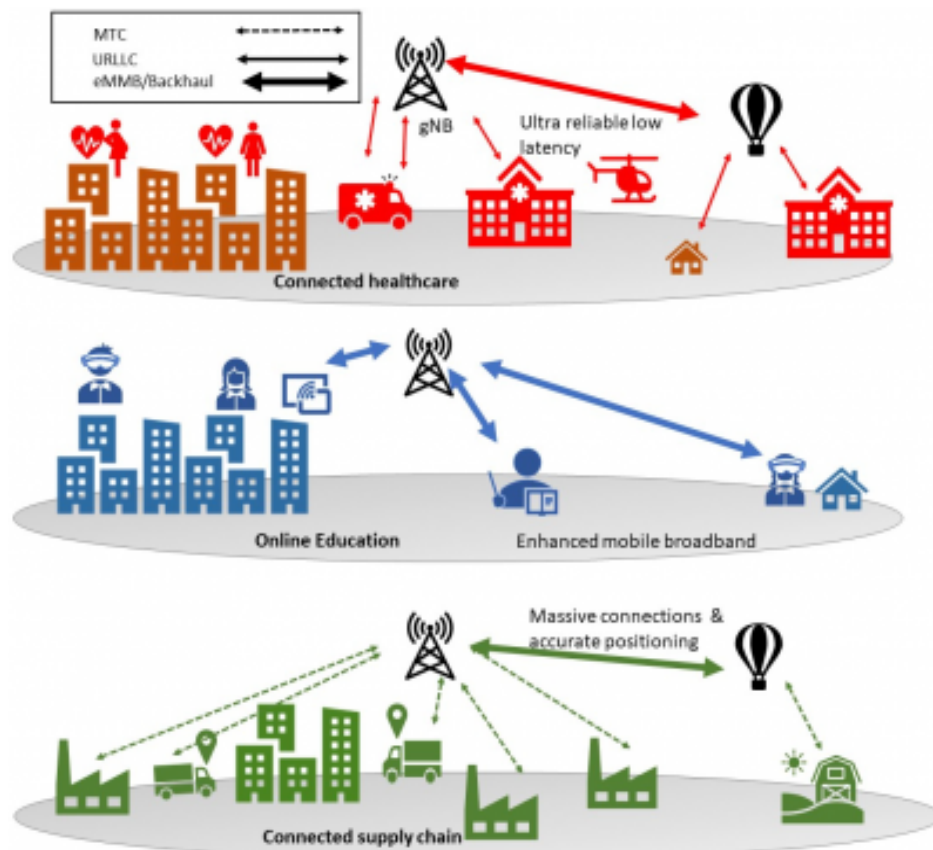
Figure 1.4 Potential Roles of 5G Technology (Ahmadi et al., 2020)

This surge in wireless network usage and demand has caused network interference jumps. According to JENDELA (2021), as shown in Figure 1.5, despite having 91.8% 4G coverage across Malaysia, the main complaint is poor 4G LTE coverage.
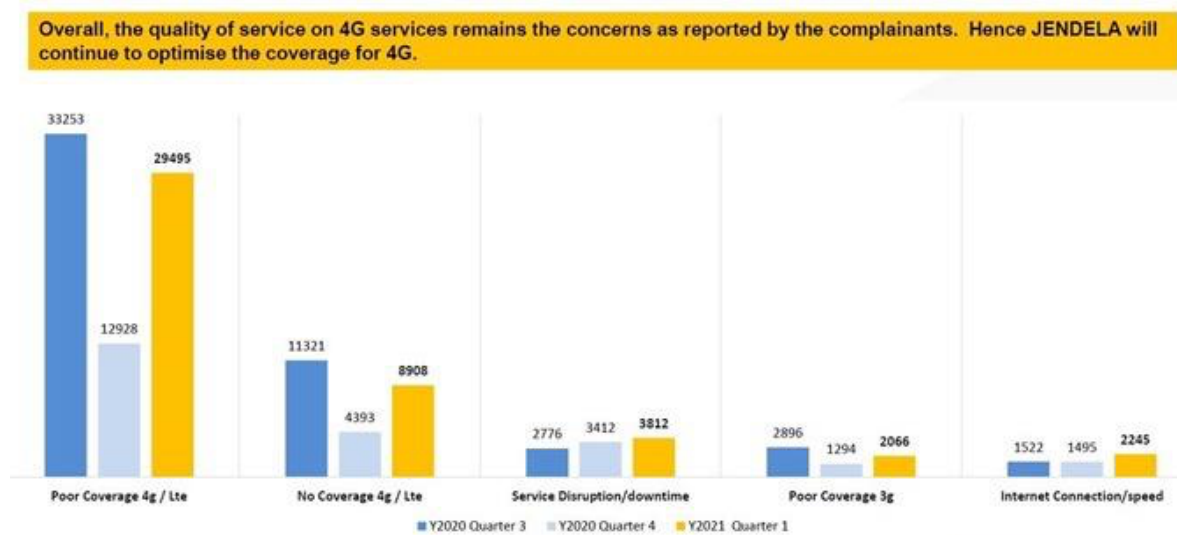
Figure 1.5 Network Complaints by Category (January – March 2021) (JENDELA, 2021)

In addressing this issue, there must be a comprehensive plan to address the needs and demands for better quality and total coverage for the users. 5G network is expected to have a higher number of deployments of low-power nodes such as picocells, femtocells, and device-to-device (D2D) machines which will produce a denser network configuration as compared to 4G's network configuration. Thus, this will promote better spectral efficiency, improved power consumption, and maximized capacity, provided that the interference within the system is managed well.

However, according to Siddiqui et al. (2021), denser networks will have higher chances of interference occurrences due to the continuous transmission and reception of signals between base stations and their user devices. For example, in a small cell setup such as femto- and pico-cells, the base stations are often installed in a scattered manner, which can result in serious co-channel interference, as claimed by Haroon et al. (2020). To ensure the best quality of experience for 5G users, the two most important aspects to be taken into account are the multiplexing method and the spectrum allocation technique to be implemented into the 5G network configuration.

Previously, multiplexing methods such as Orthogonal Frequency Division Multiplexing (OFDM) (Ismail, et al., 2019), Windowed-OFDM (W-OFDM) (Sarowa, Kumar and Singh, 2020), and Multicarrier Code Division Multiple Access (MC-CDMA) (Kumar and Venkatesan, 2019) have been extensively studied for 4G. OFDM, according to previous studies, is claimed to have the ability to reduce multipath interference with more robustness and less complexity than CDMA. In addition, equalisation can be done on a carrier-by-carrier basis, resulting in improved spectral efficiency with MIMO than with CDMA. However, to establish the successful handling of various traffic that would occur in a multi-tier heterogeneous network, an appropriate strategy must be chosen for 5G. Research done by Oughton et al. (2019) claimed that the 5G spectrum bands should provide an average per-user traffic capacity improvement of approximately 40% in comparison with the existing LTE capacity. Besides that, based on a study conducted by Kebede, et al. (2022), the high out-of-band (OOB) emissions produced by OFDM, W-OFDM and MC-CDMA caused difficulties in fully exploit the fragmentation resources between the used frequency bands. Hence, this will result in severe interference occurrence in the system.

In addition, based on a review done by Siddiqui et al. (2021), 5G H-Nets have had some issues due to immense interference. As a result, implementing an effective interference mitigation mechanism for 5G is critical. Kamel et al. (2018) have already begun investigating several interferences reduction approaches. The approaches are namely the advanced receiver method studied by Chalaliya and Dave (2018), distributed cell association and power control (CAPC) in Danh and Gulliver (2020), and the joint scheduling technique discussed by Anand, de Veciana and Shakkottai (2020). A load balancing and control mitigation technique studied by Shami et al. (2019) can improve the average user throughput from 0.59 to 0.72 Mbps (22%). However, these methods produced a large processing burden and lacked appropriate backhaul, which will affect the overall throughput of the network, as mentioned by Choudhary, Kim and Sharma (2019). There is indeed an impending requirement for a practical mitigation technique by achieving at least 100 times increment in throughput for 5G, as stated by Alam et al. (2023).

1.3 RESEARCH OBJECTIVES

The study aims to achieve the following objectives:

1- To design a new 5G configuration using Filter Bank Multicarrier (FBMC) to address low out-of-band emissions (OOB) as an improved multiplexing method.

2- To develop an enhanced Dynamic Spectrum Allocation (E-DSA) algorithm capable of mitigating cross-tier and co-tier interferences maximizing the throughput.

3- To analyse the power spectral density (PSD) performance of the 5G FBMC configuration with hardware implementation using National Instrument Universal Peripheral Universal Software Radio Peripheral (NI-USRP) for validation.

1.4 RESEARCH QUESTIONS

1- What are the limitations of the current 4G multiplexing method?

2- What are the types of multiplexing methods suitable for 5G?

3- Why are the interference mitigation methods important for the 5G network?

4- How to determine the effectiveness of an enhanced DSA (E-DSA)?

1.5 RESEARCH HYPOTHESES

The enhanced dynamic spectrum allocation was identified as the proposed method (E-DSA). It has its foundations in the dynamic spectrum access (also known as dynamic spectrum management or DSM) theory. In order to enhance the performance of a communication network as a whole, DSM entails a set of strategies built on theoretical ideas from network information theory and game theory (Jun, Hui, Peng and Liqi, 2012), (Suzan, Khaled, Ali and Ameen, 2010). The idea of the dynamic spectrum assignment in this study is based on ideas from cross-layer optimization, artificial intelligence, and machine learning. The hypothesis is that the E-DSA method is expected to have the potential to significantly increase both the spectrum efficiency and throughput of 5G networks. Software-defined radio (SDR) combined with a powerful processor platform (i7), both at the servers and the terminals, can enable observational research of E-

DSA. A technique called E-DSA uses collaborative optimization. The capability of the new 5G configuration can be tested, and the efficiency can be assessed using the E-DSA algorithm due to the use of LabVIEW Communications software (LV Comm) and the National Instrument Universal Peripheral Universal Software Radio Peripheral (NI-USRP) hardware platforms. The conventional DSA has previously been used to enhance the public switch telephone network's (PSTN's) copper loop-based digital subscriber line (DSL) performance. As a result, it is also anticipated that E-DSA could be implemented in wireless 5G system applications.

1.6 RESEARCH METHODOLOGY

The following methodologies were adopted to achieve the objectives stated above:

1- A literature review to compare 4G and 5G multiplexing methods, challenges and applications of 5G network's interference mitigation techniques, 5G's dynamic spectrum allocation techniques, software-defined radio previous applications on a wireless network configuration, including software and hardware together with throughput analysis on the wireless network. This literature review will inform the design of 5G-FBMC with the E-DSA method developed for 5G configuration.

2- Acquiring the related software. A GNU Radio-based platform simulation will be established and used for preliminary studies involving the 4G DSA technique. MATLAB's simulations are implemented for theoretical analysis, and LabVIEW Communications software is used for designing the 4G OFDM and 5G FBMC configurations. This will be followed by the use of NI USRP RIO in the hardware implementation.

3- Designing, proposing and analyzing the 4G and proposed 5G (FBMC) configurations using power spectral density (PSD) analysis.

4- The proposed E-DSA with the implementation of the 5G FBMC design is analysed based on the recorded BER values with increasing noise levels. The throughputs will also be calculated and recorded.

5- NI USRP RIO is used as a full duplex system to test the performance of OFDM and FBMC at the transceivers.

Figure 1.6 below illustrates the basic flow of the research approach used in this study.
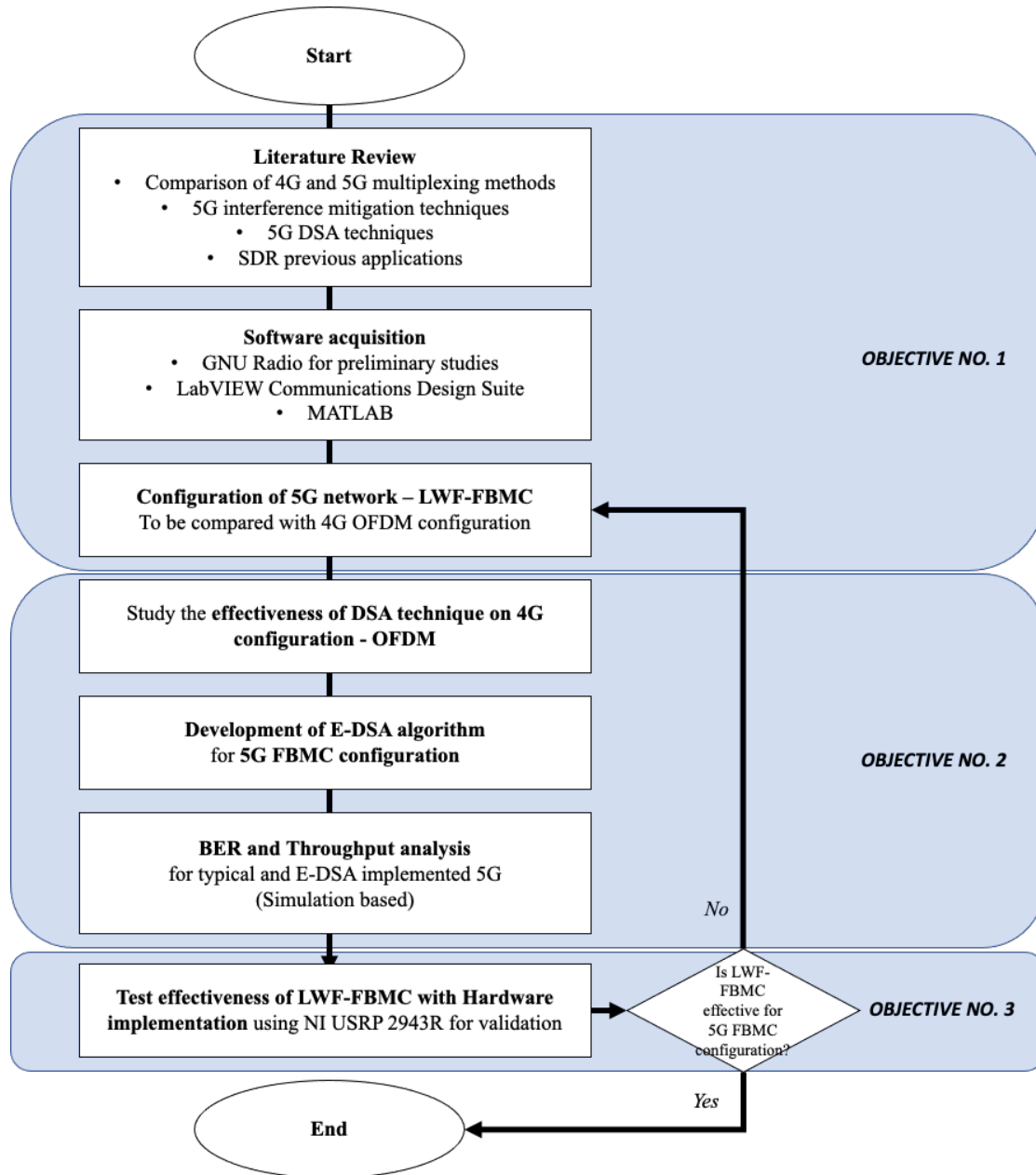
Figure 1.6 The Flow Chart of the Methodology

1.7   RESEARCH SCOPE

The research scope of this project focuses on the heterogeneous network setup for both 4G OFDM and 5G FBMC designs. Thus, both macrocell and microcell base stations and users, as well as urban environment specifications, are considered. MATLAB, GNU Radio and LabVIEW Communications (LV Comm) software are used to simulate the E-DSA technique in a 5G FBMC network configuration. A system configuration limited to 20 MHz of bandwidth, Quadrature Phase Shift Keying (QPSK) modulation, 128 subcarriers and up to 6 GHz of frequency are also utilized for the design.

For hardware implementation, many types of software-defined hardware can be used to test the effectiveness of the simulated design in real-time. However, in this research, only one NI USRP RIO transceiver is used to integrate with the simulation setup. This is because the LV Comm's version used is compatible with the transceiver. Hence, a more comprehensive output can be produced.

1.8   THESIS ORGANIZATION

The topic of this study is introduced in the first chapter of this thesis. It outlines the problem statements, together with their importance, goals, study technique, and research scope. Additional discussion on 5G multiplexing strategies, 5G interference mitigation methods, the E-DSA idea and its implementation difficulties, software-defined radio and its applications, and other topics are covered in Chapter 2. The methodologies used in this study are covered in depth in Chapter 3. It comprises the hardware design utilising the NI USRP 2943R and the design setup for the simulation in LabVIEW Communications (LV Comm). Chapter 4 presents the findings and outputs of the study. Discussions are made based on the bit error rates, throughput analysis, and power spectral density (PSD) analysis on 4G OFDM and 5G FBMC configurations, with and without the proposed E-DSA implementation. Finally, the conclusion and future recommended work of this study are presented in Chapter 5. The chapter also highlights the impact and significance of the research findings.

CHAPTER TWO

LITERATURE REVIEW

2.1 INTRODUCTION

The goal of this study is to demonstrate how the enhanced dynamic spectrum allocation (E-DSA) and augmented multiplexing can reduce interference in a 5G heterogeneous network. It is important to first comprehend the typical interference scenarios that take place in a heterogeneous network, including the underlying causes of the interference and its effects on user devices. The investigation of various multiplexing techniques for 5G is also crucial for the efficient use of a medium bandwidth. Additionally, research on various interference mitigation strategies is necessary to comprehend why the dynamic spectrum allocation method was selected for use in this project. As the core method for the creation of E-DSA, Nash Bargaining Solution (NBS) and Game Theory (GT) studies were also conducted. The definitions of the performance metrics for this research were also outlined, such as the bit error rate (BER), throughput (TP), and power spectral density (PSD). Finally, the software-defined radios and hardware used for this research are also explained. Therefore, this chapter presents the following subjects that are essential in this research:

1- Interference scenarios on 5G heterogeneous network

2- 5G multiplexing methods

3- 5G interference mitigation techniques

4- 5G dynamic spectrum allocation (DSA) techniques

5- Nash Bargaining Solution (NBS) game theory for the E-DSA algorithm

6- BER, TP, and PSD analysis definitions

7- Software-defined radio (SDR) and hardware acquisition

2.2 INTERFERENCE SCENARIOS IN 5G HETEROGENEOUS NETWORK

The 5G network configuration is an incorporation of diverse systems, including a Heterogeneous Network (H-Net), internet of things, relay node, millimetre-wave, and

device-to-device communication, as mentioned by Siddiqui et al. (2021), which creates a multi-tier H-Net.

According to Haroon et al. (2020), each tier requires the least amount of energy and power for transmission. If the inter-tier and intra-tier interferences are adequately handled, the use of several tiers in cellular network architecture will result in superior performance in terms of capacity, coverage, spectral efficiency, and overall power consumption, as explained by Al-Amodi and Datta (2020). A study conducted by Han et al. (2015) reported that different transmission powers are frequently used by base stations at different tiers. Thus, the 5G network must be able to provide a satisfactory quality of service, especially when users are travelling at high speeds (Bogale and Le, 2016).

In the H-Net environment, co-tier and cross-tier interferences are driven by the concurrent functioning of numerous small cells, and within these cells, multiple machine kinds or small devices or smartphones connect with one another (Hassan and Gao, 2015). These interferences are typically seen in large settings when high throughput is required by many people, such as during internet browsing, heavy data applications, downloading and uploading of images and videos, etc. The following interferences are specifically present in the multi-tier heterogeneous structure of mobile networks:

a) Co-Tier Interference

When both users are located in the same network tier, co-tier interference can occur. In this instance, interference to nearby "femto base stations" could be caused by an uplink transmission of a "femto user" from one cell. The short-area coverage of a femtocell is about 50 metres. Consequently, the need for several femto-base stations and a large number of users to use the same link was unavoidable (Hasan et al., 2015).

b) Cross-Tier Interference

Users in this scenario are from various network tiers. A macro user in the femto access point interferes with the uplink to the femto base station in some way. The coverage areas of the two base stations overlap similarly when a user is in the femto base station's coverage area. A macro base station experiences cross-tier interference from the femto user. The interference typically occurs in the cross-tier downlink when the macro base station, which is close to the femto access point but far from the macro user, receives interference (Nasser et al., 2019). Due to the low power of the macro base station and the close proximity to the

nearest femto base station, the macro user will experience significant downlink interference.

2.3 5G MULTIPLEXING METHODS

2.3.1 Definition of Multiplexing Methods

According to Sangdeh and Zeng (2019), multiplexing is a technique for merging multiple signals into a single signal so that each user can extract their required data after receiving the multiplexed signal. De-multiplexing is the reversible procedure that extracts multiple channels from a single signal, and it is implemented at the end of a multiplexer or receiver. This is made feasible via a de-multiplexer, which is also known as demux. Demuxing divides a signal into its constituent components. As a result, it only has one input and several outputs. Figure 2.2 shows the types of multiplexing techniques.
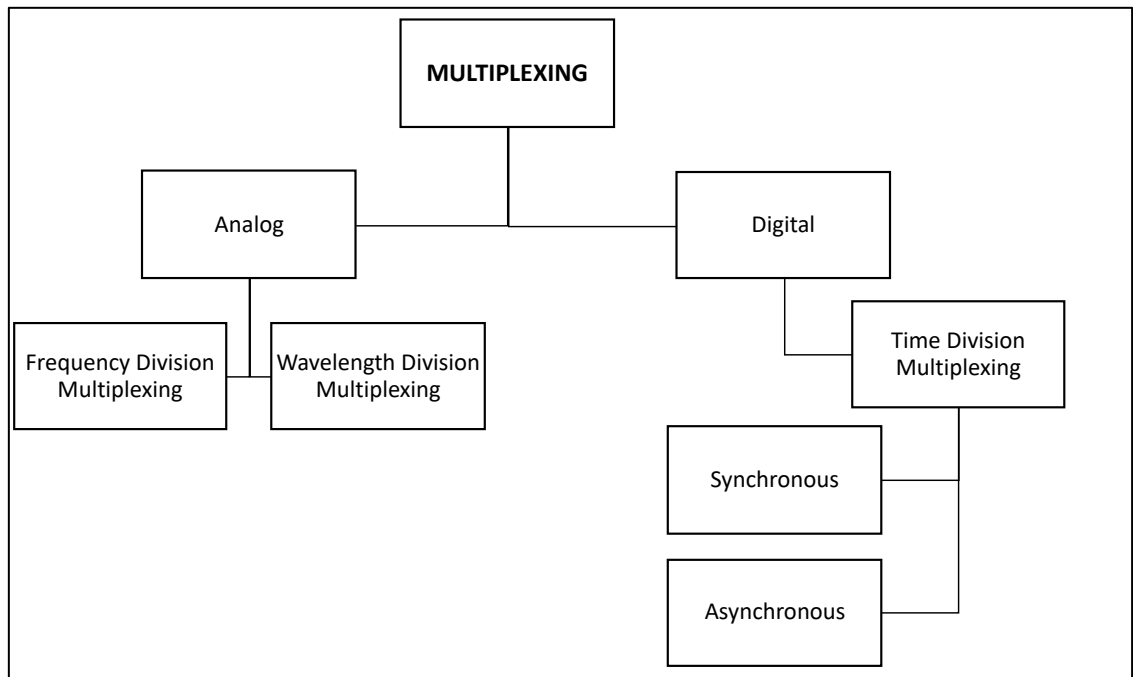
Figure 2.1 Multiplexing Techniques (Shaik, 2022)

According to Shaik (2022), multiplexing can be separated into two categories, namely analogue multiplexing and digital multiplexing, as depicted in Figure 2.1. The process of combining multiple analogue signals into one signal is known as analogue

multiplexing. The multiplexing of analogue signals depends on the frequency or wavelength of the signals. The two analogue multiplexing techniques are frequency division multiplexing (FDM) and wavelength division multiplexing (WDM). Digital multiplexing is the process of combining many digital signals into a single signal. The most popular method of digital multiplexing is Time Division Multiplexing (TDM). The two types of time division multiplexing are synchronous and asynchronous. The contrast between FDM, WDM, and TDM is shown in Table 2.1.

Table 2.1 Comparison between FDM, WDM, and TDM.

Properties	FDM	WDM	TDM
Communication channel	Divided by frequency	Divided by wavelength	Divided by time
Multiplexing technique	Analog	Analog	Digital
Synchronization	Not required	Required	Required
Circuitry complexity	Complex circuitry at the transmitter and receiver	Complex circuitry at the transmitter and receiver	Does not require complex circuitry
Bandwidth consumption	Effectively used	Effectively used	Not used effectively

2.3.2 Challenges of 4G Multiplexing Techniques

Orthogonal Frequency Division Multiplexing (OFDM) is the multiplexing technique utilized for the current 4G LTE network. A digital multi-carrier modulation technology called OFDM uses frequency-division multiplexing (FDM). Data is transmitted via numerous parallel data streams or channels using closely spaced orthogonal sub-carrier signals. Each sub-carrier is modulated with a standard modulation technique at a modest symbol rate to maintain total data speeds comparable to typical single-carrier modulation schemes contained within a similar bandwidth. The capacity of OFDM can handle challenging channel conditions, eliminate Inter-Symbol Interference (ISI) via cyclic prefixes, and optimise spectrum consumption is its main advantage over single-carrier

schemes. Due to this, OFDM has become the norm in wideband digital communication applications, including wireless networks and long-term development (LTE).
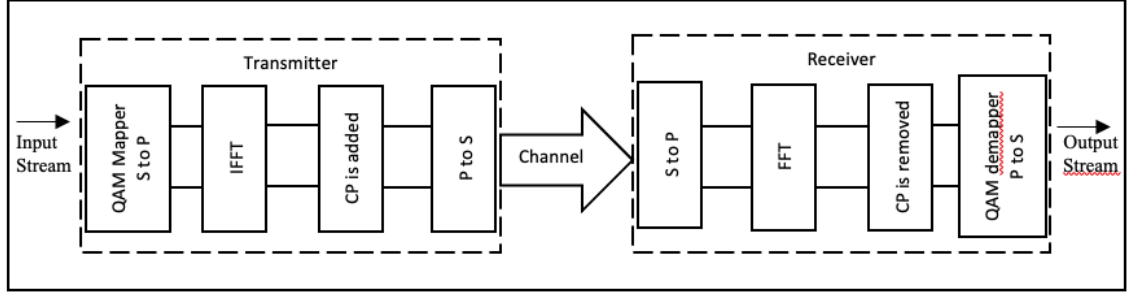
Figure 2.2 Basic OFDM Structure (Ramadan, 2022)

The general block diagram of an OFDM system is shown in Figure 2.2. The incoming high-rate data is divided into numerous parallel sub-streams at the transmitter. Typical modulators such as Quadrature Amplitude Modulation (QPSK), 16-Quadrature Amplitude Modulation (16QAM), and more sophisticated form vectors connected with guard intervals are used to modulate each stream. After that, using the inverse fast Fourier transform, the pre-OFDM symbols are modulated onto a number of orthogonal sub-carriers (IFFT). Following that, an OFDM symbol is created by multiplexing the mapped sub-carriers. The symbol description is changed from the frequency domain to the time domain through the parallel-serial technique. Additionally, by lengthening symbols, cyclic prefix insertion reduces the chance of Inter-Symbol Interference (ISI). At the receiver, the reverse procedure is performed to recover the transmitted data. In the discrete time-domain, the baseband OFDM modulation is presented as Equation 2.1,

$$s(k) = \sum_{n=-\infty}^{+\infty} \prod(k - nM) \sum_{m=0}^{M-1} c_n(m)e^{\frac{j2\pi mk}{M}} \qquad (2.1)$$

where $s(k)$ is the OFDM modulation's complex output, $c_n(m)$ is the complex data from a QAM constellation at subcarrier index m and block index n, M represents the overall number of subcarriers, and Π represents the rectangular function as written in Equation 2.2,

$$\prod(t) = \begin{cases} 1 & if\ 0 \leq k \leq M - 1 \\ 0 & elsewhere \end{cases} \qquad (2.2)$$

17

A more compressed expression can be written as Equation 2.3,

$$s_n(k) = \sum_{m=0}^{M-1} c_n(m) e^{\frac{j2\pi mk}{M}}$$
(2.3)

where $s_n(k)$ is the OFDM modulation's complex output sample at block index n and sample index k.

However, an appropriate strategy must be adopted for 5G to establish successful handling of various traffic that would occur in a multi-tier heterogeneous network.

2.3.3 Candidates for 5G Multiplexing Techniques

Ramadan (2022) outlined a thorough analysis and description of the waveform candidates for 5G, including OFDM, Filtered-OFDM (F-OFDM), Universal Filtered Multicarrier (UFMC), and Filter Bank Multicarrier (FBMC).

In f-OFDM, the subcarriers are filtered to provide substantially lower out-of-band (OOB) leakage while retaining stringent signal separation in the time domain and complex field orthogonality. According to Al-Jawhar et al. (2020), f-OFDM has a quick roll-off rate and the ability to adapt to diverse 5G requirements with flexible filter design choices where good frequency localization is required. Roessler (2019) stated that UFMC is also a method that combines the benefits of orthogonality OFDM and filter bank in FBMC. Instead of filtering each carrier individually, as in FBMC, a sub-band of subcarriers is filtered. The number of carriers per sub-band and the filter settings are usually the same, which prevents aliasing. As a result, UFMC can be thought of as a middle ground between OFDM and FBMC.

Finally, the FBMC stands for Filter Bank Multicarrier (FBMC), which is designed to eliminate the Cyclic Prefix (CP) effect and is compatible with other physical layers enhancement techniques such as Millimeter Waves (mm-wave) and Massive Multiple-Input Multiple-Output (M-MIMO), as explained by Yang et al. (2021).

In this study, FBMC was chosen as the multiplexing method for 5G as it promotes the best spectral efficiency due to the absence of cyclic prefixes. It also has the lowest OOB emissions resulting in very low sidelobes. However, to minimize the circuitry complexity, an improved design of the prototype filter must be implemented.

The summary of the contributions and limitations of the multiplexing techniques in 5G is presented in Table 2.2.

Table 2.2 5G Multiplexing Methods

Author and year	Method	Contributions	Limitations
Ismail, A. N. et al. (2019)	OFDM	• ISI elimination with the CP insertion. • Reduced receiver's implementation complexity. • Robust channel delays. • Simple MIMO integration It's simple to integrate MIMO.	• Low spectral efficiency due to the high OOB emissions. • High power consumption due to the strict requirements of synchronization. • High Peak-to-Average Power Ratio (PAPR).
Al-Jawhar, Y. A. et al. (2020)	f-OFDM	• ISI elimination with the CP insertion. • Flexible filtering. • Well-adapted to various channel conditions. • Shorter filter length than FBMC. • High data rate transmission.	• Higher receiver complexity than OFDM.
Roessler, A. (2019)	UFMC	• Good frequency location. • MIMO-compatible.	• High ISI. • Higher receiver complexity due to a large FFT size • PAPR is high.

		• Well-adapted to various channel conditions.		
Yang, F. et al. (2021)	FBMC	• Best spectral efficiency due to the absence of CP. • Excellent frequency location. • Low OOB emissions. • Low power consumption for IoT applications. • Optimal BER. • Combat doppler effects. • High data rates during transmission. • Offset QAM (OQAM) modulation.	• Low ISI immunity • The high complexity of implementation due to Orthogonal QAM (OQAM) modulation. • The filter is longer than the symbol duration.	

2.3.4 FBMC as the Multiplexing Method for 5G

2.3.4.1 FBMC Transceiver

The transceiver block diagram of the typical FBMC multiplexing method is illustrated in Figure 2.3, which was adapted from a study by Franzin and Lopes (2017). The key modification is the substitution of OFDM with a multi-carrier system with the implementation of filter banks. The prototype filters (PF) in the filter banks need to be carefully designed to obtain a more enhanced spectral shaping of subcarriers as compared to OFDM.
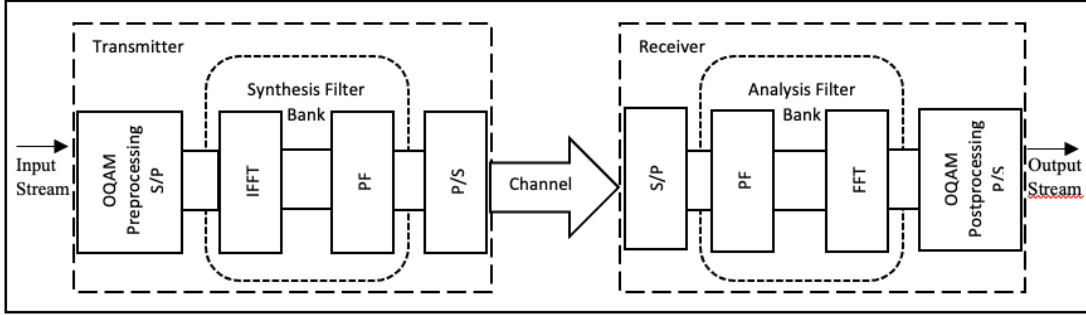
Figure 2.3 Block Diagram of FBMC (Franzin and Lopes, 2017)

2.3.4.2 OQAM Pre-processing

The OQAM pre-processing block in FBMC, as shown in Figure 2.4, employs the conversion between QAM and OQAM symbols (Kansal and Shankhwar, 2017).
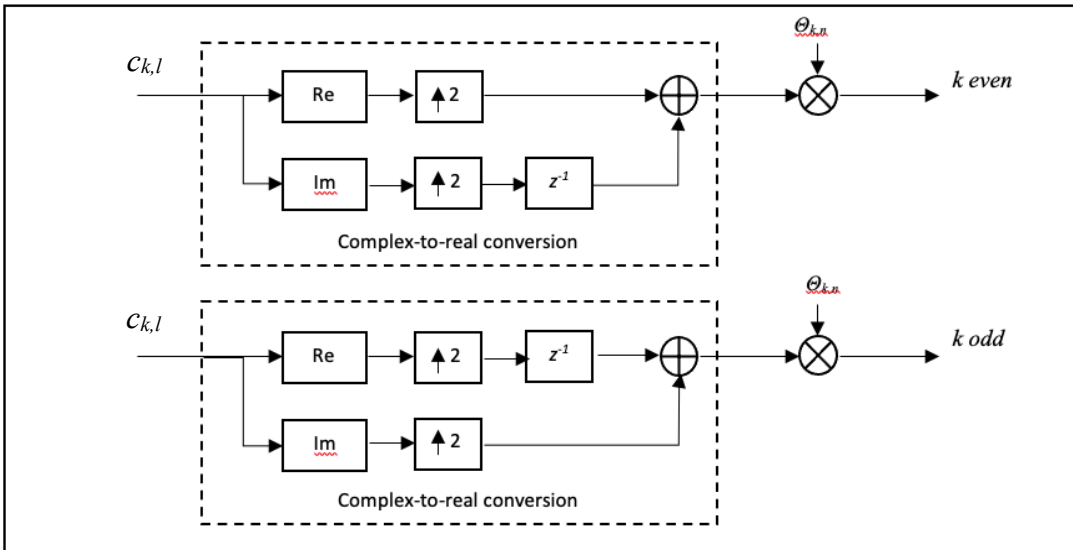
Figure 2.4 OQAM Pre-processing Block in FBMC (Kansal and Shankhwar, 2017)

The first step is known as the staggering, which is a complex-to-real conversion in which the real and imaginary portions of a complex-valued symbol $c_{k,l}$ are extracted to produce $d_{k,2l}$ and $d_{k,2l+1}$ symbols. The conversion also depends on the even or odd-numbered subchannels. Then the sampling rate is up-sampled by a factor of 2, followed by the multiplication by $\Theta_{k,n}$ sequence (FP7-ICT Future Networks Project No. ICT – 211887, 2010) as written in Equation 2.4,

21

$$\theta_{k,n} = j^{(k+n)} \qquad (2.4)$$

Nevertheless, it must be understood that the $\theta_{k,n}$ sequence can be either a positive or negative sign, but the organization of the samples must obey the stated definition. For instance, a substitute sequence will be as follows,

$$\theta_{k,n} = \begin{cases} 1, j, 1, j \ldots & even\ k \\ j, 1, j, 1 \ldots & odd\ k \end{cases}$$

The input signals are purely real or imaginary-valued once the OQAM pre-processing is completed.

2.3.4.3 OQAM Post-processing
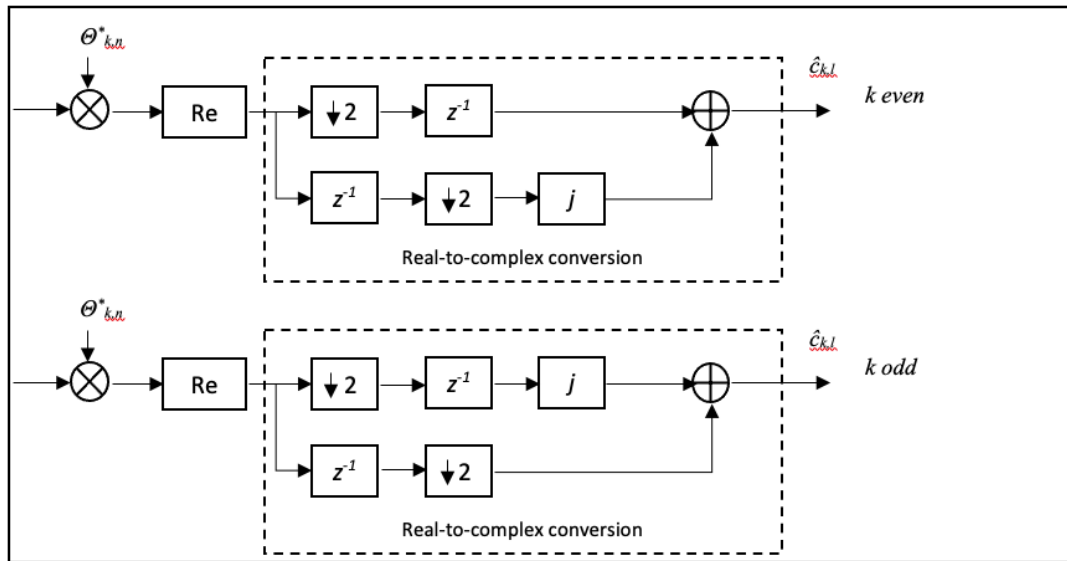
Figure 2.5 OQAM Post-processing Block in FBMC (Kansal and Shankhwar, 2017)

The OQAM post-processing block diagram, depicted in Figure 2.5, operates by multiplying the incoming signal by $\Theta^{*}_{k,n}$ sequence and extracting the real portion. The de-staggering process occurs afterwards with two real-valued symbols where one is multiplied by j to form a complex-valued symbol, $\hat{c}_{k,n}$. It is also called a real-to-complex conversion. Finally, the sample rate of the conversion is then reduced by a factor of two.

Until today, OFDM is the most advanced multiplexing technique which can support data rates between 100 and 200 Mbps. However, the high Peak Average Power Ratio (PAPR) factor and the high consumptions of Cyclic Prefix (CP) consume much of the system bandwidth (Kumar and Bharti, 2017). Due to the signal's high peak-to-average power ratio (PAPR), the high-power amplifier (HPA) will be driven into the nonlinear area, which results in in-band noise and out-of-band (OOB) radiation. The second source of OOB radiation is the transmission signal's high inherent sidelobes, which are brought on by the time domain window of the OFDM symbols. Due to those factors, the OFDM limitations should be mitigated in the future 5G technology. This can be achieved by deploying the FBMC technique. FBMC is considered to be one of the best choices for 5G communications because of its low out-of-band (OOB) radiation. By carefully designing the prototype filter, FBMC can produce a better spectral shaping of subcarriers as compared to OFDM. In addition to that, the prototype filter also promises efficient spectral utilization by lessening interference among subcarriers. Apart from that, the transmission bandwidth's maximum capacity also can be achieved in FBMC configuration by implementing Offset Quadrature Amplitude Modulation (OQAM). Therefore, the comparison between OFDM and FBMC for 5G systems is among the main highlight of the study. Table 2.3 summarizes the main differences between OFDM and FBMC techniques.

Table 2.3 Main Differences between OFDM and FBMC

Property	OFDM (4G)	FBMC (5G)
Spectrum Sensing	Low spectrum sensing performance due to spectral leakage	High spectrum sensing
Side lobes	Big interfering side lobes	Small side lobes
Doppler Effect	Easily affected by carrier frequency offset (CFO)	Not easily affected by CFO
MIMO Systems	More flexible to MIMO	Less flexible to MIMO

Synchronization	Multiple access interference (MAI) withdrawal must be performed at the receiver for accurate detection.	MAI is suppressed because of the good frequency localization of the sub-carriers
Computational Complexity	Not too complex	Very complex
Cyclic Prefix	The cyclic prefix is essential, and bandwidth is sacrificed	The cyclic prefix is not required, and bandwidth is conserved

2.3.4.4 Prototype Filter Design

The prototype filters (PF) in the filter banks need to be carefully designed to obtain a more enhanced spectral shaping of subcarriers as compared to OFDM. This section compares three prototype filters in terms of their spectral shaping capabilities.

2.3.4.4.1 Rectangular filter

The prototype filter for the traditional OFDM transmission method is the rectangle function. This filter evenly distributes the energy that a symbol carries through the time domain. In order to successfully resist inter-symbol and inter-carrier interference in the time-invariant multi-path channels, its duration might be increased at the transmitter. Bracewell (1986) depicted its analytical expression, which is shown in Equation 2.5,

$$h_{rect}(t) = \begin{cases} 1 & |t| < \frac{1}{2} \\ 0 & elsewhere \end{cases} \qquad (2.5)$$

Any segment of any function can be chosen by multiplying with an appropriate displaced rectangle function. The resulting frequency response of the OFDM system is significantly influenced by the properties of the rectangular filter. In particular, the signal is smoothed by the convolution with the rectangle function (Proakis and Dimitris, 2013). A rectangular filter's Fourier transform is as follows:

24

$$H_{rect}(\omega) = \frac{1}{\sqrt{2\pi}} \frac{\sin(\frac{\omega}{2})}{\frac{\omega}{2}} \tag{2.6}$$

with $\omega = 2\pi f$. Even after truncation, the implementation of a long-duration rectangular filter can be substantial. A reasonable baseline for comparison is a rectangular filter.

2.3.4.4.2 *Root Raised Cosine (RRC) Filter*

The transmitted signal in data communication systems needs to stay inside a specific bandwidth. The regulations or system design limitations may be responsible for this (Gentile, 2007). Since time interference must still be cancelled, the filter selection must reduce the effective bandwidth. Raised cosine response is frequently accomplished using two identical filters, one at the emitter side and the other at the receiver side. The reaction then takes the form of a square-root increased cosine. Equation 2.7 illustrates the transfer function of Joost's (2010) root-raised cosine filter.

$$H(\omega) = \begin{cases} B & |\omega| < \omega_1 \\ \frac{B}{\sqrt{2}}\sqrt{1 + \cos(\pi \frac{|\omega|-\omega_1}{r\omega_c})} & \omega_1 \leq |\omega| \leq \omega_2 \\ 0 & |\omega| > \omega_2 \end{cases} \tag{2.7}$$

with $B = \sqrt{T_c}$

2.3.4.4.3 *PHYDYAS Filter*

The PHYDYAS prototype filter's design is based on the frequency sampling method. According to the Nyquist theory, the transmission filter's impulse response must cross the zero axis at each integer multiple of the symbol period. This leads to a symmetry constraint about the cut-off frequency in the frequency domain. As a result, the design is built on imposing symmetry constraints while taking into account the frequency coefficients (Bellanger et al., 2010). Based on the interpolation algorithm provided in Equation 2.8, the frequency response of the prototype filter is calculated using the frequency coefficients.

$$H(f) = \sum_{k=-K+1}^{K-1} H_k \frac{\sin(\pi(f-\frac{k}{MK})MK)}{MK\sin(\pi(f-\frac{k}{MK}))} \tag{2.8}$$

In this study, there is a need to design a prototype filter that can enhance the spectral shaping of subcarriers. The design should also be able to produce very low OOB emissions so that spectral efficiency can be maximized.

2.4 REVIEW OF 5G INTERFERENCE MITIGATION TECHNIQUES

The 5G network comprises numerous network tiers with various sizes, various transmission powers, and numerous intelligent devices. This leads to the emergence of the co-tier and cross-tier interference problem. These have an impact on macro users in lower tiers. Users from the same tier are also impacted by co-tier interference. Therefore, in the context of 5G, interference mitigation presents a significant challenge to resource allocation. Various sophisticated interference mitigation strategies are discussed in the following subsections.

2.4.1 Advanced receiver

The method that aids in interference mitigation is the advanced interference management at the receiver, or "an advanced receiver." In order to detect and decode interference signal symbols within the modulation constellation, coding scheme, channel, and resource allocation, the receiver will use the structure of interference signals. The interference signal can then be rebuilt and subtracted from the intended signal using the output from the detector and decoder. Advanced receivers feature intra-cell interference control, like in the case of massive MIMO, in addition to aiding in the mitigation of inter-cell interference at the cell boundaries.

2.4.2 Distributed cell association and power control (CAPC) methods for multi-tier network

To facilitate the simultaneous association of users to numerous base stations in the 5G multi-tier network, the current CAPC schemes that allow each user to associate with a single base station should be upgraded. Thus, an effective distributed CAPC method is required for interference management in 5G networks. It is also necessary to implement a prioritised power control strategy that allows users in various tiers to have varied channel access priority. The future generation of wireless communication will feature resource-aware cell association techniques, which allow users to connect with the best cell to

maximize their performance. Given that the amount of this summary information is typically extremely modest, distributed techniques are typically advantageous when the cluster size is very large. The distributed methods frequently involve iteration and experience significant delays.

2.4.3 Joint Scheduling

In order to maximize the utility function of a cluster, which is a collection of many Transmission Points (TPs), collaborative scheduling is used to jointly decide on serving UEs and transmission techniques. Depending on the specific scheme, the joint scheduling might be carried out either centrally or decentralized. In the centralized scenario, the central controller receives all the necessary data from the cluster's TPs before making all the necessary calculations and sending the associated scheduling information to each TP. Although centralized systems frequently perform better than distributed systems, they have a poor backhaul and a high processing burden. On the other hand, in the distributed example, each TP does its own calculation and communicates with the others to coordinate the overall process in exchange for a tiny quantity of summary data. As a result, the next-generation systems must include more specific information about collaborative scheduling.

2.4.4 Enhanced inter-cell interference coordination (eICIC)

ICIC is a frequency domain approach that reduces inter-cell interference by sub-banding the frequency. But heterogeneous networks cannot use it. The eICIC approaches, which are based on the time domain for co-frequency inter-cell interference coordination, are successfully employed to manage the interference in an H-NeT. In the eICIC, time is taken into account, and certain user equipment (UE) from various cells is orthogonal to another in the time domain. Not only does it help in lowering interference of the traffic channels but also that of the control channels in various cells. In eICIC, there are two basic methods. One is known as Cell Range Expansion, while the other is known as Almost Blank Subframe (ABS) (CRE).

2.4.5 Coordinated multipoint (CoMP) for interference management

CoMP offers the potential of sending data in a coordinated manner from several network points in the direction of users who are closer to the cell edge and hence more susceptible to interferences. With regard to CoMP specifically, a number of transmission stations offer coordinated transmission in the downlink, and a number of receiver points offer coordinated reception in the uplink. The ideal transmission point can be chosen easily, but other operation modes have also been suggested, such as collaborative transmission from several network sites, coordinated scheduling, and beamforming methods.

2.4.6 Dynamic Spectrum Allocation Technique (DSA) for Interference Mitigation

The DSA produces capacity enhancement by selecting or aggregating different Random Access Technologies (RATs) on various spectrum license regimes. They can be referred to as licensed, unlicensed (mainly 5 GHz) and lightly licensed spectrum. TV White Space (TVWS) and Licensed Shared Access (LSA) bands are two examples of lightly licenced frequencies (2.3 GHz, 3.5 GHz). Examples of major DSA use-cases include interference reduction on a cluster of small cells by offloading traffic on the non-licensed spectrum, capacity increase using a supplemental carrier on a non-licensed spectrum using any RAT, and extended Licensed-Assisted Access (LAA) (coordinated or autonomous manner). According to the kind of traffic and interference circumstances, these use-cases depend on the capability to dynamically choose an appropriate channel from a list of options (cognitive radio concept).

By utilizing Dynamic Channel Selection, Channel Segregation techniques, Load balancing among a group of neighbouring cells / small cells, co-locating Wireless Fidelity (WiFi) access points, sharing site-lease agreements, and backhaul, the proposed solutions will take advantage of the advantage of flexible waveforms and interference management schemes. Advanced interference mitigation strategies are compared in Table 2.4.

Table 2.4 Comparison of Advanced Interference Mitigation Techniques.

Author name and year	Method	Contribution	Strengths	Limitations
Chalaliya, H. A. et al., 2018	Advanced Receiver	The receiver makes use of the interference signal's structure to identify and decode the symbols. The unwanted signal can then be rebuilt and subtracted from the desired signal.	Manages intra-cell interference as in the case of large MIMO and minimizes inter-cell interference at the cell boundaries.	More mature inclusion of advanced receiver technologies would be required in the next-generation specifications.
Danh and Gulliver, 2020	Distributed cell association and power control (CAPC) methods	Cell association schemes that allow users to connect with the best cells to maximize their performance	Supports user association with numerous base stations simultaneously in a 5G multi-tier network	Distributed systems are iterative and have significant delays
Anand et al., 2020	Joint Scheduling	Calculates serving UEs and transmission plans jointly for a cluster, which is a collection of many	The overall utility function of the cluster is optimized.	Suffer from a heavy processing load and proper backhaul.

		Transmission Points (TPs)		
Altay and Koca, 2019	Enhanced inter-cell interference coordination (eICIC)	Based on time domain for co-frequency inter-cell interference coordination.	Reduces interference of traffic channels and reduces interference of control channels in different cells	Not suitable for heterogeneous network
Irram et al., 2020	Coordinated multipoint (CoMP)	Introduces the potential for coordinated transmissions from various network points to consumers who are closer to the cell edge and more susceptible to interferences	Helps in interference management	Does not highlight network capacity enhancement
Zhang et al., 2020	Dynamic spectrum allocation	Depending on the type of traffic and the circumstances of any interference, dynamically choose a suitable channel from a list of alternatives	Increases capacity and takes advantage of adjustable waveforms and interference control techniques	Not focused on a heterogeneous network

		(cognitive radio concept)		

2.5 REVIEW OF 5G DYNAMIC SPECTRUM ALLOCATION TECHNIQUES

The dynamic spectrum allocation (DSA) technique has been widely researched for various types of implementations.

2.5.1 Double Auction Method

Devi M. et al. (2021) suggested a double auction method where a double auction design for spectrum allocation explicitly decouples the buyer-side and seller-side auction design while achieving truthfulness, individual rationality, and budget balance. The researchers combine spectrum allocation results from different subgraphs and resolve potential conflicts. Though the proposed method promotes high efficiency, revenue, and utilization, it is not well adapted to a cooperative environment and lacks interaction between users.

2.5.2 Semi-Hidden Markov Model

The semi-hidden Markov model was put out by Koley, Bepari, and Mitra (2018) to forecast temporal correlations in primary users' (PUs) spectral activity under a non-geometric distribution of state durations. They optimised the number of secondary users (SUs) that can be allocated by statistically modelling the frequency of free channels. In terms of reduced PU interference, less spectrum handoff needs, and improved spectrum usage efficiency, the suggested approach was found to beat the traditional sensing-based dynamic spectrum allocation (DSA). However, this approach also lacks user engagement and is poorly suited to a cooperative environment.

2.5.3 Multi-Agent System (MAS)

In a multi-agent system, Xie (2018) talked about how to train agents to cooperate in order to rescue injured people and remove impediments. The outcomes also demonstrated that by allocating rewards according to participation level and situation, it was possible to develop the capacity for cooperative activities for the most effective injured rescue and

obstacle clearance. This technique is still judged unsuitable for a heterogeneous network even though it includes a cooperative mechanism.

2.5.4 Game Theoretic Power Control and Spectrum Sharing Method

A game-theoretic method for spectrum sharing and power regulation in cognitive radio (CR) networks was put forth by Naseer et al. in 2021. The suggested algorithm reduces utility, which lowers total cost and maximizes the global function. In CRs, cost dominance plays a key role in fostering collaboration and effective power distribution. The reduction in power consumption as a result of better resource management for cognitive radio is demonstrated by simulation results.

The 5G Dynamic Spectrum Allocation Techniques are summarized in Table 2.5 below:

Table 2.5 Summary of the 5G Dynamic Spectrum Allocation Techniques

Author name and year	Method	Contribution	Strengths	Limitations
Devi, M., et. al. (2021)	Double auction method	Achieved truthfulness, individual rationality, and budget balance while explicitly separating the buyer-side and seller-side auction designs.	Higher efficiency, revenue, and utilization	Not cooperative
Koley, Bepari and	Semi-Hidden Markov Model	A model was used to predict the likelihood of free channels; the	Reduced PU interference, fewer handoff needs for the spectrum, and	Not cooperative

Mitra (2018)		number of secondary users (SUs) that can be provided was optimized.	improved spectrum efficiency	
Xie (2018)	Multi-Agent System (MAS)	Acquired cooperative behaviour in a multi-agent system to rescue the injured and remove impediments in accordance with the injured's triage	The ability for cooperative activities for the most effective injured rescue and obstacle removal might be acquired through the distribution of rewards.	Not suitable for a heterogeneous network
Naseer et. al. (2021)	Game theoretic power control and spectrum sharing	Showed lower aggregate cost and demonstrated global function maximization by inhibiting utility	In cognitive radios, cost dominance is a key facilitator of collaboration that leads to effective power distribution.	Did not consider the heterogeneity aspect

Based on the reviews, it can be said that the game theoretic power control and spectrum sharing method is the best method to be implemented in E-DSA. This is because, out of all the methods, it promotes the best technique for a cooperative system. However, for this study, the game theory implemented should be suitable for the heterogenetic aspect of the 5G network.

2.6 NASH BARGAINING SOLUTION (NBS) GAME THEORY FOR E-DSA ALGORITHM

Although all locations in the rate area are permitted by information theoretical considerations, it might be claimed that the interference channel creates a conflict between

the interfering links. In a generic interference game, each link is regarded as a player. It has been demonstrated that non-cooperative approaches, such as iterative water-filling, result in effective MAC and broadcast channel solutions (Yu et al., 2004). However, in situations including interference channels, non-cooperative solutions may be seriously suboptimal. There are various methods that might be used to address the problem. Utilizing competitive methods in repeated games is one that has grown in popularity in recent years. The methodology used in this study is fundamentally different and is based on Nash's general bargaining theory (1950).

Two N-player game solution concepts are discussed in this section. The Nash equilibrium (NE) is the first idea, and the Nash bargaining solution is the second (NBS). Only the Gaussian interference game is concentrated on in order to simplify the notation. Every time a non-cooperative zero-sum game is played, Nash equilibrium results. However, compared to a cooperative strategy in the non-zero-sum scenario, where players can collaborate, they can result in a significant loss for all players. The term "prisoner's dilemma" refers to this circumstance. In this light, the primary concerns are that rates can be accomplished by cooperation in this instance and how to do so in a stable manner,

The underlying structure for Nash bargaining in an N players game is a set of outcomes of the bargaining process S which is compact and convex. S can be considered as a set of possible joint strategies or states, a designated disagreement outcome d (which represents the agreement to disagree and solve the problem competitively), and a multiuser utility function $U : S \cup \{d\} \to \mathcal{R}^N$. The Nash bargaining presents a function, F, which assigns to each pair- $(S \cup \{d\}, U)$ as shown above, and an element of $S \cup \{d\}$. As the Nash solution is unique, to obtain the solution, Nash assumed four axioms:

1. **Linearity**. The solution is adjusted correspondingly If the same linear transformations are applied to the utilities of all players.

2. **Independence of irrelevant alternatives.** According to this axiom, the bargaining solution of a large game $T \cup \{d\}$ assigns the same solution to the smaller game if it is found in a small set S. The negotiating process in TS is unaffected by the irrelevant alternatives.

3. **Symmetry**. If two players are identical, changing their names will not affect the result, and they will receive the same utility.

4. If s is the outcome of the bargaining, then no other state t exists such that $U(s) < U(t)$ (coordinate-wise).
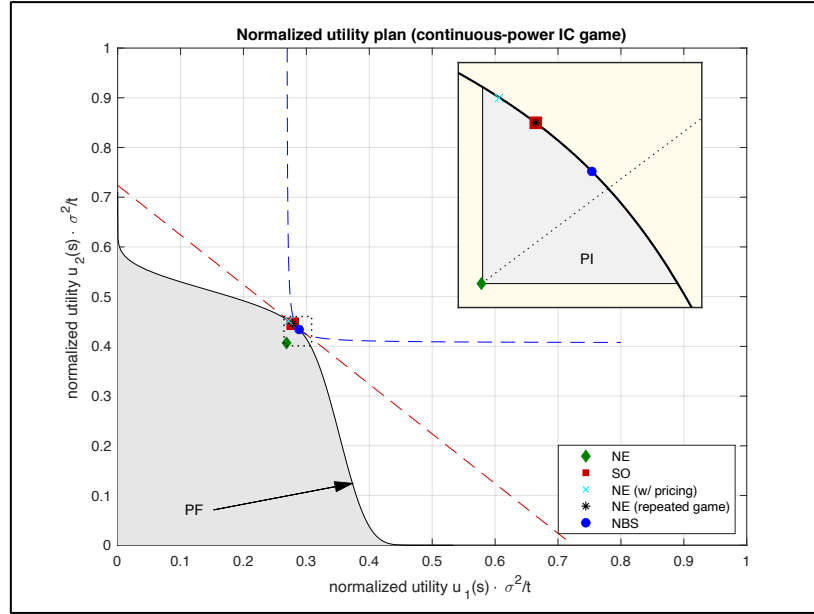
Figure 2.6 Graphical Interpretation of the NBS

The graphical interpretation of the NBS is shown in Figure 2.6. The NBS corresponds to the profile such that $(u_1(s), u_2(s))$ is the point of tangency between the Pareto frontier (PF) and the hyperbola with the vertex in $x = u_1(s)$ and $y = u_2(s)$. Therefore, as shown in Figure 2.7 by a blue dot, the point of tangency is, by definition, located in the Pareto improvement region. Again, the greater channel condition of player 2 makes it stronger in negotiations, which is why the NBS is lopsided in favour of player 2.

2.7 BIT ERROR RATE (BER), THROUGHPUT (TP), AND POWER SPECTRAL DENSITY (PSD) ANALYSIS

In this study, the three key performance metrics to be determined and analyzed are the BER, TP and spectral efficiency using PSD analysis.

First of all, the bit error rate (BER), as defined by Panwar and Kumar (2012), is the frequency at which errors occur in a transmission system. Systems that transmit digital data from one location to another must be evaluated using BER. The system may experience issues while data link transfer is carried out. If this occurs, the system's efficacy can be

questioned. As a result, it is crucial to evaluate the system's performance, and BER makes sure that this is possible. BER examines a system's complete end-to-end performance, including the performance of the transmitter, receiver, and communication medium. It can be seen from using the energy per bit to noise power spectral density ratio (E_b / N_o) that the bit error rate, BER, can be affected by a number of factors. It is feasible to optimize a system to deliver the necessary performance levels by changing the factors that can be controlled. Typically, this is done during the design phase of a data transmission system so that the performance parameters can be changed at the preliminary design concept stages. The interference levels that exist in a system are often determined by outside variables and cannot be altered by the design of the system. However, the system's bandwidth can be modified. The bandwidth can be decreased to lower the interference. But lowering the bandwidth restrictions will result in lower data throughput.

In addition, the TP, in accordance with Bithas and Lopez-Martinez (2021), establishes the volume of information units that a system can process in a given period of time. It is widely used in a wide range of computer and network systems, organizations, and other systems. The speed at which several tasks can be completed is one of the related measurements of system productivity. The response time measures how long it takes to respond to a single interactive user request.

Thirdly, according to Rani (2016), the PSD is also a measure of the power per unit area that may be used to represent the strength of a signal in a particular area. The PSD is also known as the total of the signal's power across frequency. PSD is measured in terms of energy per frequency (width), and energy within a certain frequency range can be derived by integrating PSD within that frequency range. The FFT method, which involves computing the autocorrelation function and then converting it, is used to calculate PSD directly.

2.8 SOFTWARE-DEFINED RADIO (SDR) AND HARDWARE ACQUISITION

People are expecting to easily get high-speed network service, given the growing demand for wireless communication networks in the modern world. Additionally, the improved technology design of the communication system's chips and gadgets has resulted in much lower prices than in the past. To be cemented in a particular system, each component in

various communication systems is modified. The software-defined radio was developed to address the lack of flexibility.

Due to poor chip manufacture many years ago, the functionality of the personal computer was severely constrained. The central processing unit (CPU), for instance, is utilized to manage all commands and calculations. As a result, the CPU's low upper limit only has a little work to do. A personal computer can handle a greater workload when CPU and other chip development accelerates dramatically. As a result, processing signals in communication systems is simpler.

In this study, three types of SDRs were used to simulate the design and analyze the results. Firstly, the LabVIEW Communications System Design Suite (LV Comm) was used for the construction of the modulation and demodulation for both OFDM and proposed FBMC techniques. Then, the GNU Radio. Finally, MATLAB software was used for the preliminary investigations of the whole research.

2.8.1   LabVIEW Communications System Design Suite (LV Comm)

The LabVIEW Communications System Design Suite (LV Comm) combines LabVIEW NXG with tools made especially to speed up the wireless communications system prototyping. In the same environment, LV Comm also supports the design, development, and deployment of wireless communication systems to a variety of hardware targets, including general-purpose CPUs, Linux Real-Time Operating Systems from National Instruments, and Field Programmable Gate Arrays (FPGAs). Using a unified graphical programming approach, the ability to directly call code created using The MathWorks, Inc. MATLAB® software, and the import of customized Very High-Speed Integrated Circuit (VHSIC) Hardware Description Language (VHDL) code, wireless design and prototype teams can reduce the time it takes to validate wireless algorithms with over-the-air (OTA) signals.

2.8.2   GNU Radio

The foundation for computer-based signal processing is GNU Radio. The system can function more cost-effectively and with greater flexibility if programmes are created to process signals. Personal computers can process digital signals in a way that is defined by

specific programmes simply by applying algorithms or schemes. One of the wireless communication revolutions is GNU Radio because of its versatility. Another program, OpenBTS, uses the entire mobile communication system and implements the second-generation (2G) mobile communication standard.

2.8.3   MATLAB

The MathWorks company created the proprietary multi-paradigm programming language and computer environment known as MATLAB. Matrix manipulation, function and data visualization, algorithm implementation, user interface building, and connecting with other programming languages are all possible with MATLAB. Although MATLAB is primarily designed for numeric computation, symbolic computation capabilities are accessible through an optional toolbox that uses the MuPAD symbolic engine. Graphical multi-domain simulation and model-based design for embedded and dynamic systems are added via an additional programme called Simulink.

2.8.4   National Instrument's Universal Software Radio Peripheral reconfigurable I/O (NI USRP RIO) hardware

A game-changing SDR, the NI USRP RIO offers wireless communications designers an affordable SDR with unbelievable performance for creating 5G wireless communication systems. USRP Software Defined Radio Devices like USRP-294x and USRP-295 feature an FPGA and are referred to as "USRP RIOs". These devices have a cutting-edge 2x2 MIMO RF transceiver with a LabVIEW programmable Kintex 7 FPGA that is DSP-focused. Researchers working on wireless communications may prototype more quickly and drastically reduce the time it takes to get findings, thanks to LabVIEW's unified design flow. The NI USRP RIO expands the USRP platform by offering a better user experience and giving the ideal performance and software tool flow balance, making SDR prototyping more approachable. It is perfect for many different kinds of applications, such as huge MIMO, spectrum monitoring, 5G wireless communications, and many more. RF front ends, FPGAs, and processors—on board or on the computer—are frequently seen in SDR architectures. For the purpose of providing an excellent SDR prototype solution for

educational laboratories and communications research, USRP and LabVIEW offer flexibility, versatility, and affordability.
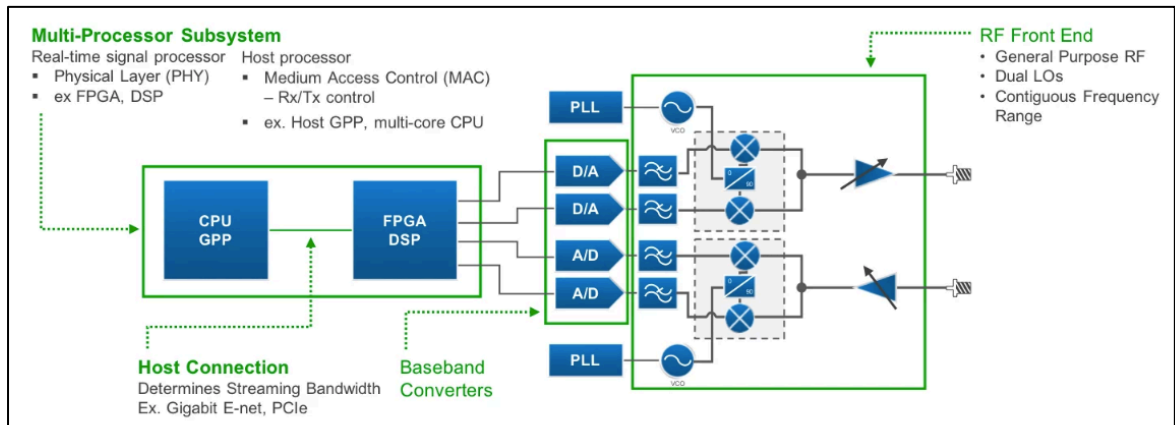
Figure 2.7 Typical Architecture of an SDR (National Instruments, 2022)

2.9 CHAPTER SUMMARY

Throughout this chapter, the literature reviews of 5G interference heterogeneous network scenarios, 5G multiplexing methods, dynamic spectrum allocation (DSA) techniques, NBS game theory, and software, as well as hardware acquisitions, have been presented and discussed in terms of their definitions and importance.

CHAPTER THREE

RESEARCH METHODOLOGY

3.1 INTRODUCTION

This chapter first describes in detail the experimental setups for the construction of the typical 4G OFDM and 5G FBMC configurations using LV Comm software. This software was used because it can compare the performance between 4G and 5G configurations' multiplexing methods for both simulation and hardware basis. The results were also analysed based on the PSD analysis.

Second, for the development of the E-DSA algorithm, a preliminary study was first conducted. This involved comparing the typical 4G LTE and DSA 4G LTE configurations entailing the downlink and uplink communication using GNU Radio software. Python language was used as the programming language. The DSA techniques implemented were depicted in a study by Othman (2018) to prove the effectiveness of the DSA method's implementation on 4G's configuration. Once the effectiveness of the DSA method was proven, the DSA technique was then used to enhance the 5G FBMC configuration. With this, an enhanced dynamic spectrum allocation (E-DSA) algorithm was developed. The validity of the algorithm was first tested, then followed by the BER and TP analysis. In this study, the considered 5G scenarios were the urban macrocell and microcell configurations.

Third, the hardware implementation setup using the NI USRP RIO was designed to validate the 4G OFDM and 5G FBMC configurations by running the simulation designs. The PSD results were recorded and compared.

3.2 5G FBMC AS AN IMPROVED MULTIPLEXING METHOD

Figure 3.1 shows the steps to achieve the first objective of this research.

1ST OBJECTIVE

Design of enhanced FBMC to reduce out-of-band emissions as an improved multiplexing method for 5G

STEPS

1. Determine the best prototype filter for enhanced FBMC using MATLAB software
2. Design OFDM (4G) and FBMC (5G) configurations using LV Comm software

ANALYSIS

1. Comparison of the frequency responses and PSD performance of 3 types of prototype filters
   a) Rectangular filter for OFDM
   b) Root raised cosine (RRC) filter for f-OFDM
   c) Lowpass Hamming windowed FIR filter (LWF-Hamming) for LWF-FBMC

2. Comparison of PSD performance for 4G OFDM and 5G FBMC

Figure 3.1 Methodology to Achieve the First Objective of this Research

In designing the FBMC as the multiplexing method for 5G, the prototype filter must first be chosen to be implemented in the FBMC design, as depicted in Figure 2.3 from sub-section 2.3.4.1. Three types of filters were designed, and their PSDs were compared and analysed to determine the best prototype filter. These prototype filters are the Rectangular filter for OFDM, Root raised cosine (RRC) filter for f-OFDM, and Lowpass Hamming windowed FIR filter (LWF-Hamming) for FBMC.

Next, after determining the prototype filter for FBMC, the designs for both OFDM and FBMC configurations were constructed using LV Comm. The PSD outputs for both configurations were compared and analysed.

These two steps resulted in the PSD outputs that explained the OOB emissions' comparison between the OFDM and FBMC designs.

3.2.1 Proposed Prototype Filter for FBMC

According to Nissel et al. (2017), the transmitted signal *s(t)* of a multi-carrier system in the time domain can be mathematically described as given in Equation 3.1,

$$s_{TX}(t) = \sum_{k=0}^{K-1} \sum_{l=0}^{L-1} g_{TX(l,k)}(t) \varkappa_{TX(l,k)} \qquad (3.1)$$

where the transmitted symbol at subcarrier position l and time-position k is indicated by $\varkappa_{TX(l,k)}$. Besides that, the transmitted basis pulse $g_{TX(l,k)}$, is essentially a time and frequency-shifted version of the prototype filter $\rho(t)$ and is defined as in Equation 3.2,

$$g_{TX(l,k)}(t) = \rho(t - kT)e^{j2\pi lF(t-kT)}e^{j\theta_{l,k}} \qquad (3.2)$$

where T represents the time spacing, and F represents the frequency spacing (subcarrier spacing). After transmission over a channel, the received symbols are decoded by projecting the received signal *r(t)* onto the basis pulses $g_{l,k}(t)$, that is, in Equation 3.4,

$$y_{l,k} = \langle r(t), g_{l,k}(t) \rangle = \int_{-\infty}^{\infty} r(t) g_{l,k}^*(t) dt \qquad (3.4)$$

The Balian-Low theorem (Feichtinger and Strohmer, 2012), which implies that it is theoretically impossible for the following required attributes to all be met at the same time, suggests that there are certain basic restrictions for multicarrier systems. These involve the maximum symbol density, *TF* needs to be set equal to 1, the time-localization, $\varphi_t < \infty$, the frequency-localization $\varphi_f < \infty$ and orthogonality, $\langle g_{l_1,k_1}(t), g_{l_2,k_2}(t) \rangle = \gamma_{(l_2-l_1),(k_2-k_1)}$, with γ representing the Kronecker gamma function. The localization measures φ_t and φ_f are defined as:

$$\varphi_t = \sqrt{\int_{-\infty}^{\infty} (t - \bar{\bar{t}})^2 |\rho(t)|^2 dt} \qquad (3.5)$$

$$\varphi_f = \sqrt{\int_{-\infty}^{\infty} (f - \bar{\bar{f}})^2 |P(t)|^2 df} \qquad (3.6)$$

where the pulse $\rho(t)$ is normalized to have unit energy, $\bar{t} = \int_{-\infty}^{\infty} t|\rho(t)|^2 dt$ represents the average time and $\bar{f} = \int_{-\infty}^{\infty} f|P(f)|^2 df$, the mean frequency of the pulse. Such that localization measures can be interpreted as standard deviation with $|\rho(t)|^2$ and $|P(f)|^2$ representing the probability density function (PDF).

The less stringent real orthogonality criterion is used in place of the complex orthogonality condition to fulfil the Balian-Low theorem: $\mathbb{R}\{g_{l_1,k_1}(t), g_{l_2,k_2}(t)\} = \gamma_{(l_2-l_1),(k_2-k_1)}$. For FBMC, the expression for prototype filter $\rho(t) = \rho(-t)$ is orthogonal for a time spacing of $T = T0$ and a frequency spacing of $F = 2/T0$, leading to $TF = 2$. The orthogonal T-F spacing is then reduced by a factor of two each, that is, $T = T0/2$ and $F = 1/T0$, which leads to TF becoming 0.5.

The only information symbols that may be conveyed in this fashion are real-valued ones; hence the equivalent time-frequency spacing for complex symbols is $TF = 1$. Offset-QAM gets its name from the frequent mapping of a complex symbol's real and imaginary parts to the first and the second time slots, respectively.

In this study, the proposed FBMC design implemented the lowpass Hamming windowed FIR filter (LWF-Hamming) as its filter (LWF-FBMC). The impression of a windowing-based scheme was to estimate the anticipated filtering characteristics by using a digital FIR filter. The impulse response was denoted as $h_f(n)$ by assuming the anticipated filter frequency response function is $H_f(e^{j\omega})$.

Assuming the low-pass FIR filter is in the linear phase, the general selection of $H_f(e^{j\omega})$ will be as follows,

$$H_f(e^{j\omega}) = \begin{cases} e^{-j\omega\tau} & |\omega| \leq \omega_c, \\ 0 & \omega_c \leq |\omega| \leq \pi, \end{cases}$$

where τ is a constant. The inverse discrete Fourier transform (IDFT) is used to calculate the $h_d(n)$ in Equation 3.7,

$$h_d(n) = \frac{1}{2\pi} \int_{-\omega_c}^{\omega_c} H_d(e^{j\omega}) e^{j\omega n} d\omega = \frac{\sin[\omega_c(n-\tau)]}{\pi(n-\tau)} \tag{3.7}$$

By multiplying a specific window $w(n)$, the impulse response $h(n)$ of the linear phase FIR filter is written as Equation 3.8 below,

$$h(n) = h_d(n)w(n) \tag{3.8}$$

Therefore, the corresponding $H(e^{j\omega})$ is obtained by discrete Fourier transform (DFT). The minimum stopband attenuation of a filter generated using the Hamming window is 53 dB, which is enough for the majority of digital filter implementations. The Hamming window (Suhaib et al., 2014) is defined by Equation 3.9,

$$w(n) = 0.54 - 0.46 \cos\left(\frac{2\pi n}{M-1}\right) \qquad ; 0 \le n \le M - 1$$

or

$$w(n) = 0.54 - 0.46 \cos\left(\frac{\pi n}{2}\right) \qquad ; 0 \le n \le 4 \tag{3.9}$$

where M is the filter order.

Table 3.1 Parameter Values of $h_d(n)$ and $w(n)$

n	Impulse response, *h(n)*	h_d(n)	w(n)
0	0.01273	0.15901	0.08
1	0.12149	0.224984	0.54
2	0.25	0.25	1
3	0.12149	0.224984	0.54
4	0.01273	0.159091	0.08

Table 3.1 shows the parameter values of $h_d(n)$ and $w(n)$ to calculate the value of impulse response **h(n)**. It was assumed that M is an odd number. Thus the frequency response function becomes,

$$H(\omega) = e^{-j\omega\left(\frac{M-1}{2}\right)}\left\{h\left(\frac{M-1}{2}\right) + 2\sum_{n=0}^{\frac{M-3}{2}} h(n)\cos\omega\left(n - \frac{M-1}{2}\right)\right\} \tag{3.10}$$

By assuming that *M=5* and substituting it into Equation 3.11,

44

$$H(\omega) = e^{-j2\omega}\{h(2) + 2\sum_{n=0}^{1} h(n)\cos\omega(n-2)\} \tag{3.11}$$

$$H(\omega) = e^{-j2\omega}[0.25 + (2 \times 0.01273 \cos 2\omega) + (2 \times 0.12149 \cos \omega)] \tag{3.12}$$

$$H(\omega) = e^{-j2\omega}[0.25 + 0.02546 \cos 2\omega) + (0.243 \cos \omega)] \tag{3.13}$$

By substituting $\omega = \frac{\pi}{4} rad/s$ into Equation 3.13, the frequency response function for the proposed lowpass Hamming windowed FIR filter (LWF-Hamming) becomes,

$$H_{LWF-Hamm}(\omega) = e^{-j\frac{\pi}{2}}\left[0.25 + \left(0.02546 \cos\frac{\pi}{2}\right) + \left(0.243 \cos\frac{\pi}{4}\right)\right] \tag{3.14}$$

The frequency responses and PSD outputs for the LWF-Hamming filter were compared with the rectangular filter for OFDM and RRC filter for f-OFDM. The frequency response functions were mentioned in Subsections 2.3.4.4.1 and 2.3.4.4.2.

3.2.2 Design of 4G OFDM and 5G FBMC Configurations Using LV Comm

3.2.2.1 OFDM Transmitter Configuration

Figure 3.2 shows the proposed configuration for the OFDM transmitter using LV Comm.
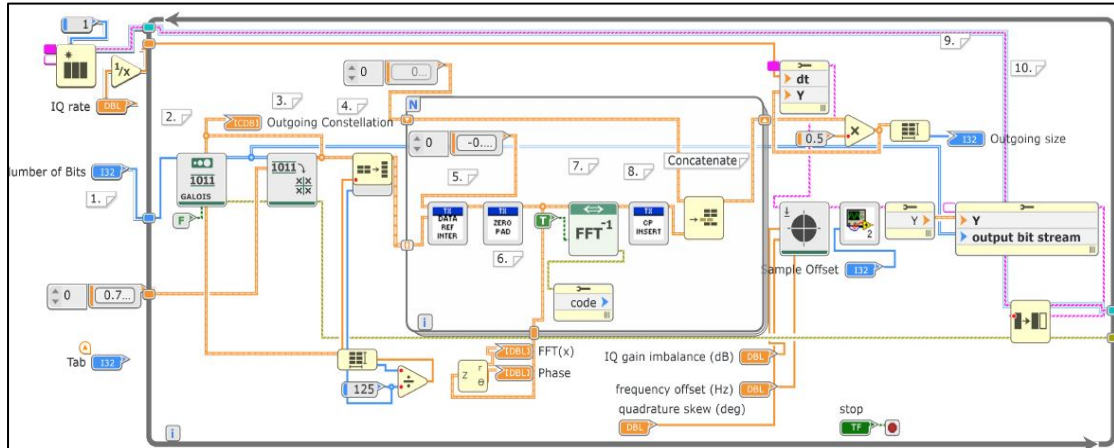
Figure 3.2 OFDM Transmitter Configuration Using LV Comm

The number of bits was first initialized along with the locations of the Quadrature Amplitude Modulation (QAM) map. Then, random data bits were generated using a Pseudo Noise (PN) sequence of 9. At this stage, there were a total of 125 bits. Then, the bits were mapped into symbols, and the symbols arrays were divided into 5 sets of 125-point data sets, which formed OFDM symbols. Then, 25 reference symbols after the sixth data symbol were inserted, followed by the insertion of 53 zeroes at the edges of the passband. After that, an inverse fast Fourier transform (IFFT) process was performed for the frequency-to-time domain conversion of the signal. A 64-sized cyclic prefix was then inserted by duplicating the last 64 points of the array at the beginning. The five time-domain waveforms were then scaled to a complex magnitude typically below 0.7 for each of the in-phase and quadrature (IQ) components. Finally, the transmission of data to the receiver was completed via the data queue block.

3.2.2.2 OFDM Receiver Configuration

Figure 3.3 shows the proposed configuration for the OFDM receiver using LV Comm.
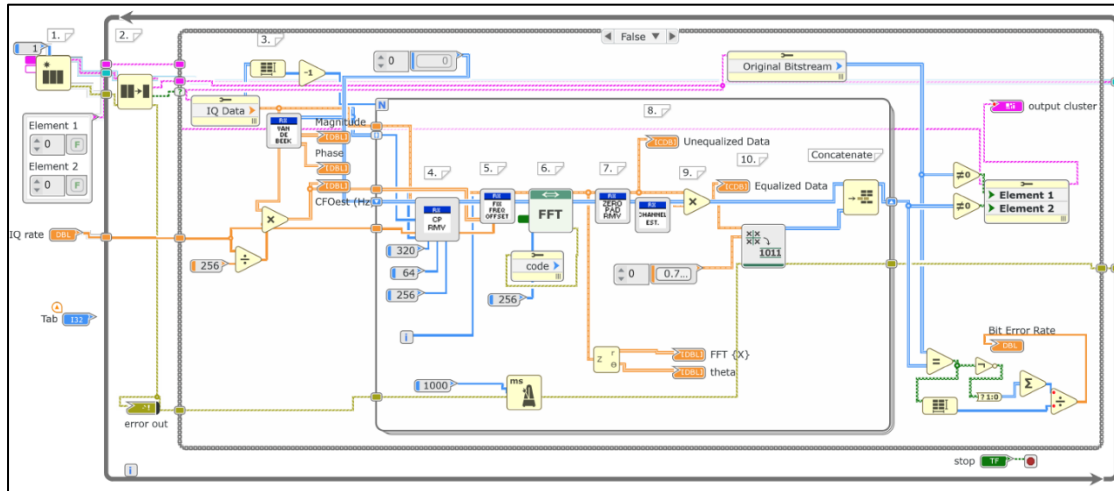
Figure 3.3 OFDM Receiver Configuration Using LV Comm

The QUEUE was initialized, and the IQ data was dequeued. Then, the Van De Beek algorithm was implemented to detect the cyclic prefix's locations for synchronization and to estimate the frequency offset. After that, the cyclic prefix and frequency offset were removed from the incoming signal.

The fast Fourier transform (FFT) was then computed to convert the time domain OFDM symbol to the frequency domain. After that, the data and reference bits were separated, and the zero padder was removed. The linear fit equalization of coefficients was computed for both the in-phase and quadrature components corresponding to the reference symbols. In addition, the data symbols were also implemented in the equalization process, and finally, the mapping of symbols to bits was then performed.

3.2.2.3 FBMC Transmitter configuration

The transmitter configuration for FBMC is similar to that of OFDM, except that there are additional programmed blocks added into the configuration, namely the orthogonal QAM (OQAM) pre-processing and the Synthesis Filter Bank (SFB) blocks, as shown in Figure 3.4. Other than that, there was no cyclic prefix block being added.

47
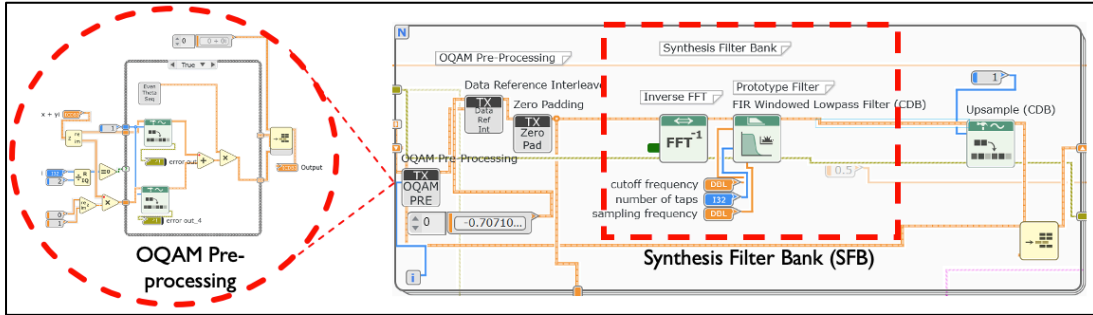
Figure 3.4 FBMC Transmitter Configuration Using LV Comm

3.2.2.3.1 *OQAM Pre-Processing*

Figure 3.5 shows the proposed OQAM Pre-processing using LV Comm.
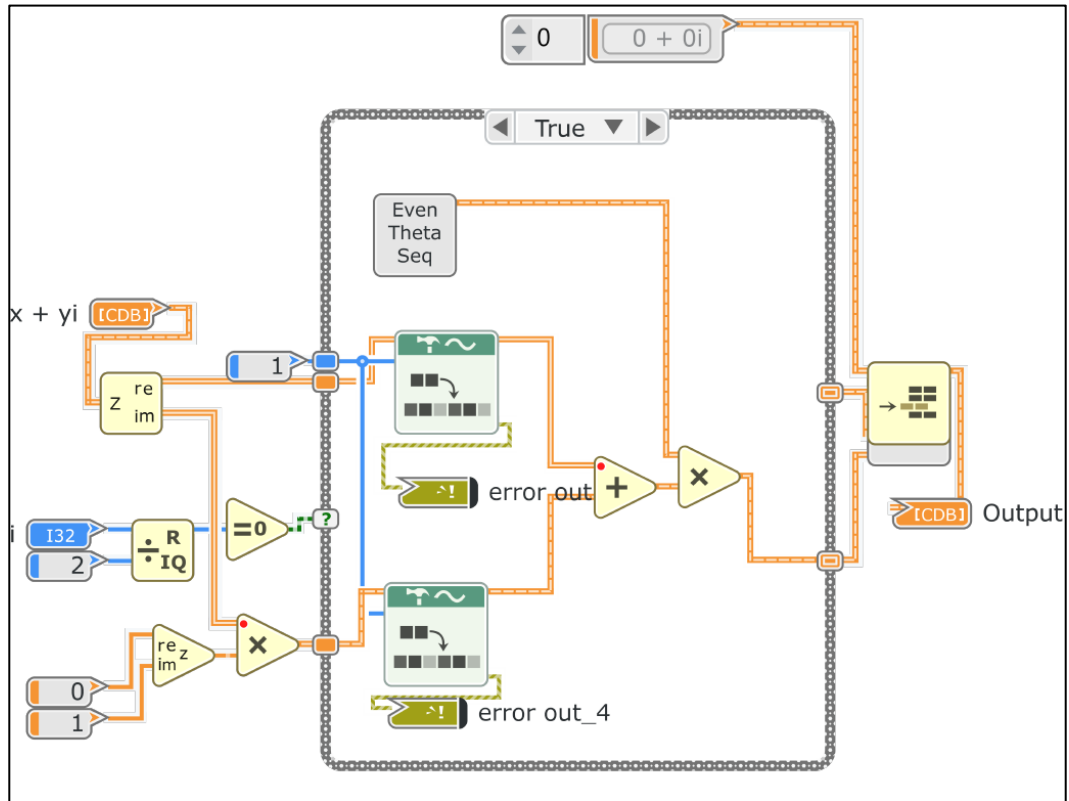
Figure 3.5 OQAM Pre-processing Configuration Using LV Comm

Firstly, the staggering operation was performed and followed by upsampling the sample rate by 1 and multiplying it by odd or even $\Theta_{k,n}$ sequences. The signal was then passed to the IFFT block for the conversion to the time domain from the frequency domain.

3.2.2.3.2 *Synthesis Filter Bank (SFB)*

Figure 3.6 shows the proposed Synthesis Filter Bank configuration using LV Comm.
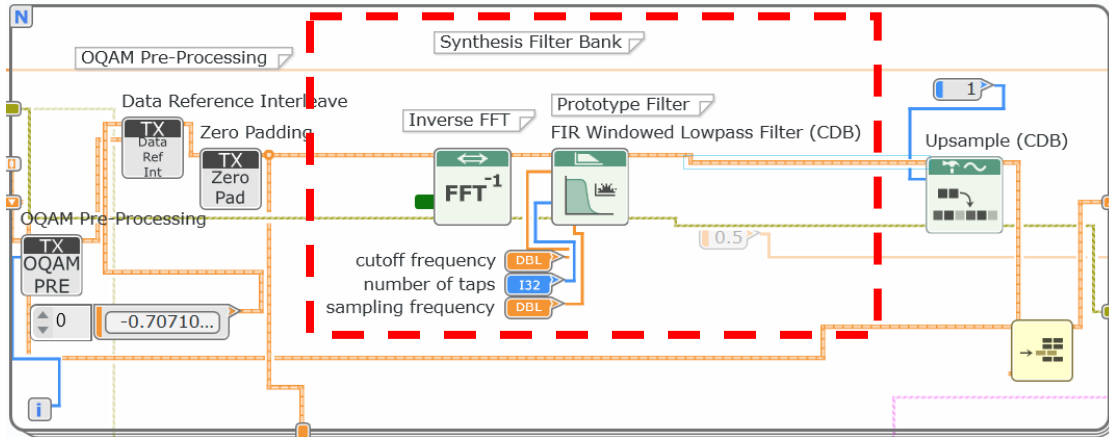
Figure 3.6 Synthesis Filter Bank (SFB) Configuration Using LV Comm

After passing through the IFFT block, the signal was then transmitted to the Synthesis Filter bank block, where the FIR windowed lowpass filter was implemented as the prototype filter with scalable parameters such as the sampling frequency, number of taps, and cut-off frequency. After that, the signal was upsampled by 1 and transferred to the queue to be transmitted to the receiver.

3.2.2.4 *FBMC* Receiver configuration

The receiver configuration for LWF-FBMC is similar to that of OFDM, except that there were additional blocks added into the configuration, namely the Analysis Filter Bank (AFB) and OQAM post-processing blocks, as shown in Figure 3.7. Besides that, the cyclic prefix removal block was removed.
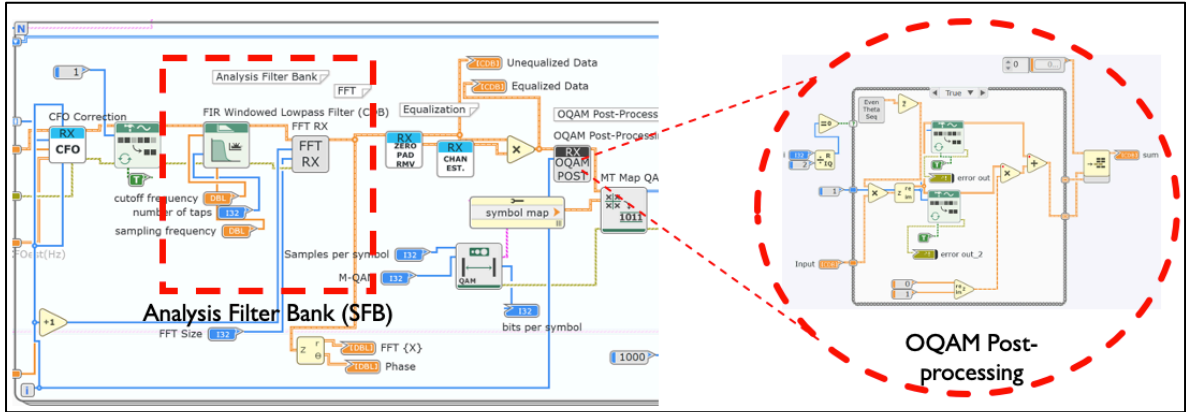
Figure 3.7 FBMC Receiver Configuration Using LV Comm

3.2.2.4.1 *Analysis Filter Bank (AFB)*

Figure 3.8 shows the proposed Analysis Filter Bank (AFB) configuration using LV Comm.
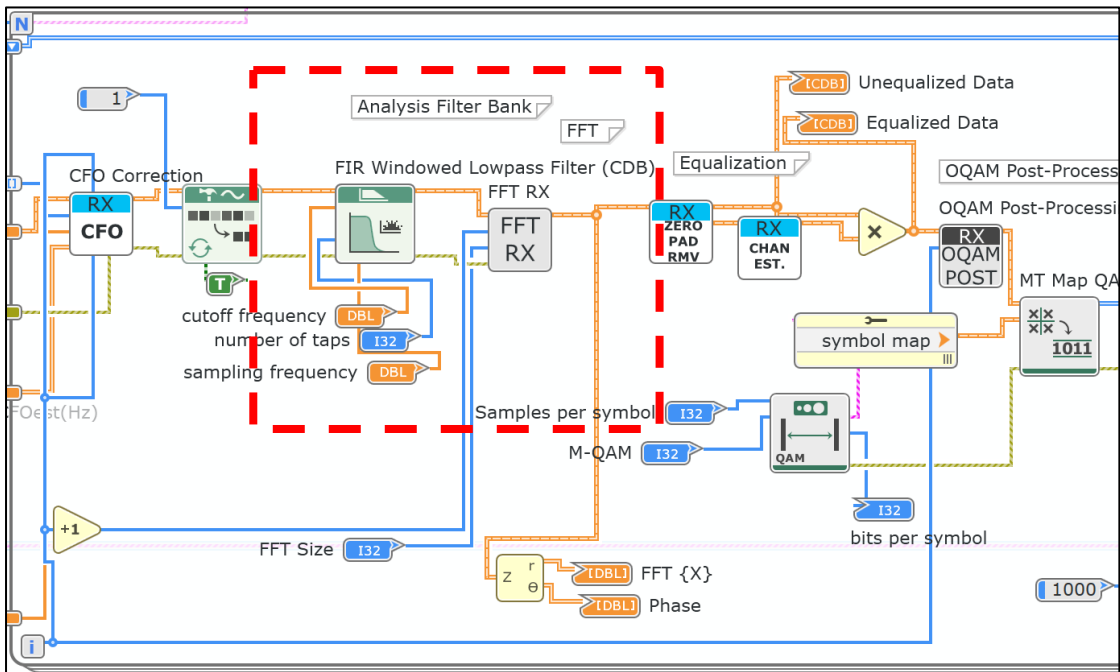
Figure 3.8. Analysis Filter Bank (AFB) Configuration Using LV Comm

The signal passed through the AFB before it was passed to the FFT block for FFT computation. Figure 3.8 shows that the filter used for AFB is similar to that used in SFB. However, the signal was first decimated before passing through the filter.

3.2.2.4.2   OQAM Post-processing

Figure 3.9 shows the proposed OQAM post-processing configuration using LV Comm.
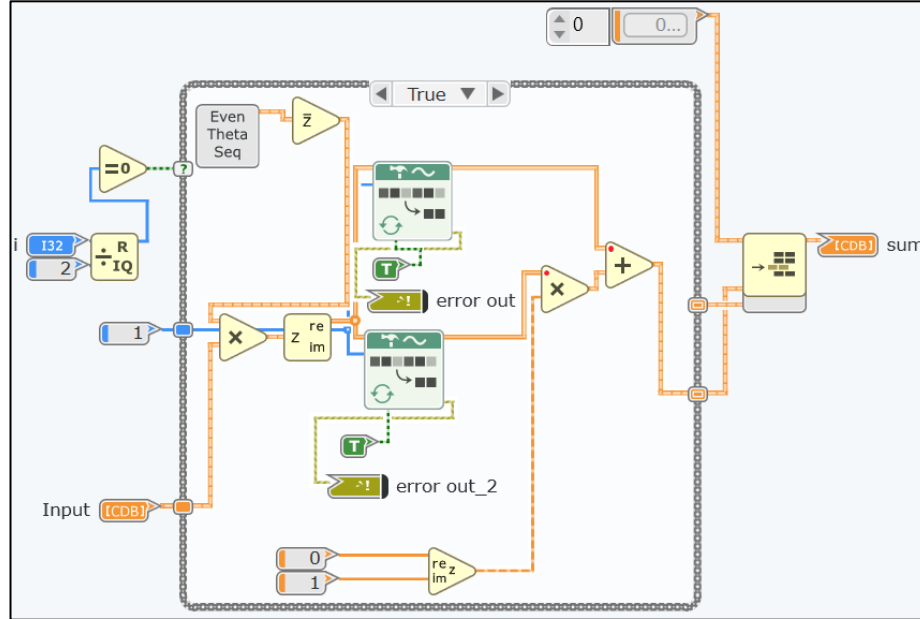
Figure 3.9 OQAM Post-processing Configuration Using LV Comm

After the FFT computation, the signal was passed through the equalizer and then through the OQAM post-processing blocks. Here, the signal was multiplied with different odd or even $\Theta^*_{k,n}$ sequences depending on the odd or even condition of the incoming signal. Then, the real part of the signal was extracted, and a de-staggering operation was performed to produce a complex symbol. Then, the downsampling of the sample rate took place.

3.2.2.5 Interference Channel Model Configuration

This study used the Rayleigh flat fading (Jakes Model), with the addition of additive white Gaussian noise (AWGN) as the interference channel model for OFDM and LWF-FBMC systems. This model, proposed by Jakes (1974), is a commonly accepted model of a multipath fading environment (Raghavan, 2005), which is suitable for both 4G and 5G heterogeneous networks.

3.2.2.5.1   Flat-Fading Rayleigh Channel (Jakes Model)

The Rayleigh Distribution equation was depicted and adapted from the NI official website on the LabVIEW NXG section (https://www.ni.com/docs/en-US/bundle/labview-nxg-feature/page/manual-overview.html). The Rayleigh distribution defines a flat-fading channel categorized by a single-tap impulse response with a time-varying Rayleigh-distributed envelope. This model explains the statistical time-varying criteria of the envelope at the receiver of a flat fading channel or the envelope of an individual multipath element.

The equation for the probability density function (PDF) for the Rayleigh distribution is as shown in Equation 3.15,

$$p(R) = \frac{R}{\sigma^2} exp\left(-\frac{R^2}{2\sigma^2}\right) u(R) \tag{3.15}$$

where R is the specified fading variance.

Besides that, a deterministic method such as the Jakes model simulates Rayleigh fading waveforms which is time-correlated. According to Liu (2011), it is an ideal simulation model of small-scale Rayleigh flat fading channels where it can be produced by the implementation of low-frequency oscillators (LFO). It is assumed that N rays that are equal in strength are received at a moving receiver's arrival angles that are uniformly distributed, in which ray n is affected by a Doppler shift, which can be defined by the following Equations 3.16, 3.17, and 3.18,

$$\omega_n = \omega_m cos(\alpha_n) \tag{3.16}$$

where

$$\omega_n = 2\pi f_m \tag{3.17}$$

and

$$a_m = 2\pi \frac{(n-0.5)}{N} \tag{3.18}$$

represents the arrival angle of the ray n.

An AWGN channel is the most common model of a communication system. The value N_s is the amount of noise power P_N per unit bandwidth B.

$$N_s = \frac{P_N}{B} \tag{3.19}$$

For real sampling, $B = F_s/2$ can be inserted into the above equation, and the noise power in a sampled band-limited system is given as,

$$P_N = N_s \times \frac{F_s}{2} \tag{3.20}$$

Therefore, the noise power is directly proportional to the bandwidth at the sampling stage. The channel model configuration design using LV Comm in this study is shown in Figure 3.10.
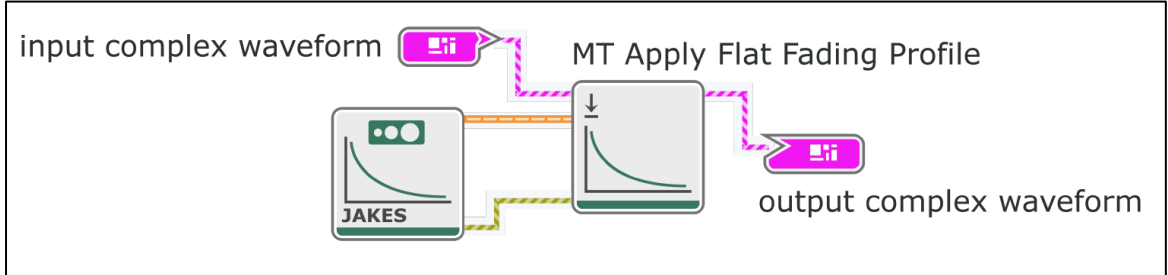
Figure 3.10 Channel Model Configuration of Rayleigh Flat Fading (Jakes Model) Using LV Comm

Table 3.3 shows the parameters used in this study for both OFDM (Ismail, A. N. et al., 2019) and LWF-FBMC configurations.

Table 3.3 System Parameters for 4G OFDM and 5G LWF-FBMC

Property	OFDM (4G)	LWF-FBMC (5G)
Overlapping Factor, K	1	4
Prototype Filter	None	Lowpass Windowed FIR

| | | Number of taps: 2 |
		Window: Hamming
Cyclic prefix size	64	None
Modulation type	QAM	OQAM
IQ rate (Hz)	5M	
Bandwidth	20M	
Number of bits	1250	
QAM order	4	
Samples per symbol	32	
IQ gain imbalance	0	
Frequency offset (Hz)	250	
Quadrature skew	1	
Sample Offset	4	
FFT size	256	
Number of subcarriers	128	
Channel Estimation	Linear mean square	
Channel Model	Flat Fading Rayleigh, Jakes Model Profile length: 1000 Doppler spread: 0.01 Fading variance: 1	
AWGN, Eb/n0 (dB)	40	

The simulation designs were initiated after the 4G OFDM and the 5G FBMC configurations were constructed using LV Comm. Their FFT waveform, phase, and equalized as well as unequalized data plots in the receiver were then recorded and compared with their transmitted output plots. The comparison results are presented in Subsection 4.2.2 in Chapter 4. Then, after the validity was proven, the PSD outputs of the configurations were then recorded and analyzed. The outputs were analyzed based on the

type of prototype filter used for OFDM and FBMC that affects the spectral shaping of the configurations. The PSD analyses' results are presented in section 4.2 in Chapter 4.

3.3 DEVELOPMENT OF E-DSA

Figure 3.11 shows the steps to achieve the second objective of this research.

2ND OBJECTIVE

Development of E-DSA algorithm

STEPS

1. Design 4G configuration for OFDM with DSA algorithm implementation using GNU Radio
2. Design a 5G system model that includes E-DSA using NBS algorithm and FBMC implementation

ANALYSIS

1. Comparison of the BER and throughput performances between 4G OFDM with DSA and 5G FBMC with E-DSA
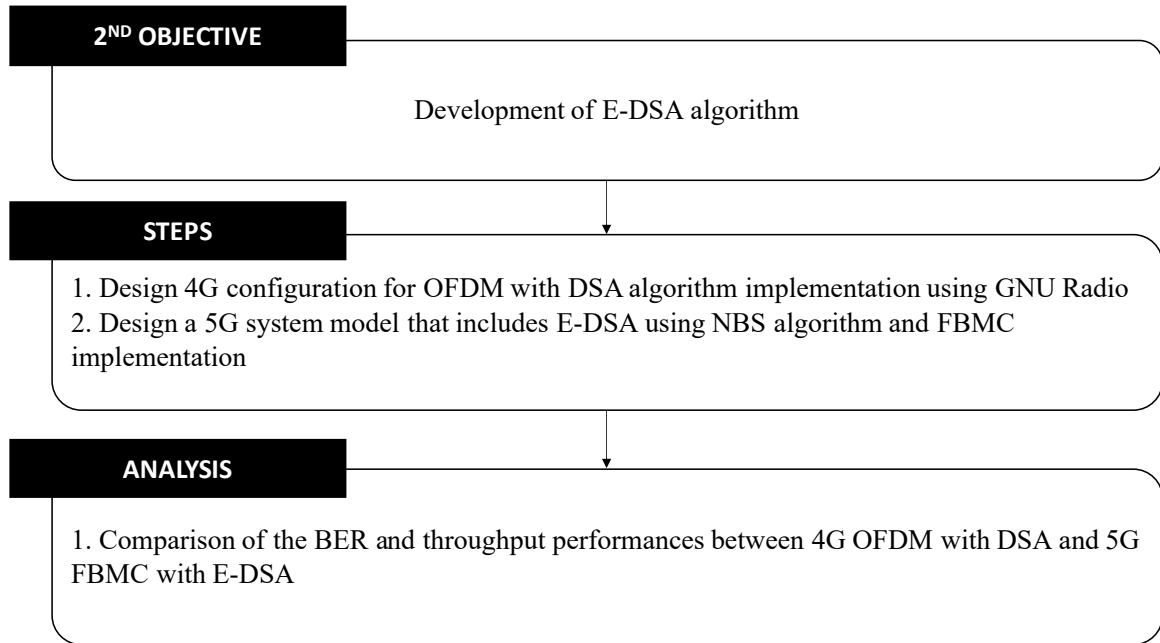
Figure 3.11 Methodology to Achieve the Second Objective of this Research

First, a conventional DSA algorithm derived by Othman (2018) was implemented on a 4G OFDM configuration using GNU Radio software. The purpose of this experiment was to prove that the DSA implementation can improve the throughput of the current 4G configuration when compared with the typical 4G configuration without DSA implementation.

Then, an enhanced dynamic spectrum allocation (E-DSA) technique was developed by enhancing the conventional DSA algorithm. A 5G system model was created that implemented an E-DSA algorithm using NBS game theory together with the LWF-FBMC as the multiplexing method.

Lastly, the comparison between OFDM DSA for 4G and FBMC E-DSA for 5G were analyzed based on their BER and throughputs.

3.3.1 DSA algorithm for 4G OFDM Using GNU Radio

The DSA algorithm for 4G OFDM is outlined in Table 3.4 below,

Table 3.4 DSA Algorithm for 4G

1. Initialization
i.   Set $R_i = 0$ and $\Omega_i = \emptyset$ for all $i = 1, 2, \ldots, K$.   ii.   Set $S = \{1, 2, \ldots, N\}$ and $U = \{1, 2, \ldots, K\}$.
2. While $U \neq \emptyset$
i.   Find (i, a) which satisfies $\left\lvert G_{i,a}\right\rvert \geq G_{i,j}$ for all $i \in U$ and $j \in S$.   ii.   For the found i,   If $R_i \leq R_{i,min}$, then $\Omega_i = \Omega_i \cup \{a\}, S = S - \{a\}$, $R_i = R_i + C(G_{i,a})$ else $B = B - \{i\}$
3. While S$\neq \emptyset$
i.   Find i satisfying $\dfrac{G_{i,a}}{\sum G_{i,j}} \geq \dfrac{G_{m,n}}{G_{m,j}}$ for all $m = [1, K]$ and $a \in S$.   ii.   For the found i, find a satisfying $\left\lvert G_{i,a}\right\rvert \geq G_{i,k}$ for all $k \in S$ iii.   Update R_i, S and Ω_i for found a: $R_i = R_i + C(G_{i,a})$, $S = S - \{a\}$ and $\Omega_i = \Omega_i \cup \{a\}$.
4. Power allocation: water fill power for each Ω_i.

First, the highest channel gain for each user was determined, and then the corresponding subcarrier was allocated to it. A minimum rate was chosen for each user. In the case where the current usage rate is lesser than the minimum rate, the algorithm would keep on searching for the second largest channel gain, and one more subcarrier would be allocated to the user until the minimum rate was achieved. The allocation logic would move to the next step once all the users achieved the minimum rate. This step would continue to

iterate until all the subcarriers are occupied. Table 3.5 outlines the parameters used for the DSA 4G configuration.

Table 3.5 Parameters Used for Preliminary Study on DSA for 4G Using GNU Radio

Parameters	Typical 4G configuration	Proposed improved 4G configuration (With DSA)
Source of data	Random source block	Base station core block
FFT length	64 bytes	
CP length	16 bytes	
Bandwidth (Hz)	10M	
Multiplexing method	OFDM (downlink)	
Modulation scheme	QPSK	
Noise source	Gaussian with Amplitude = 1 – 10	

For the 4G configuration with OFDM using GNU Radio, the flow graph of the modulator is shown in Figure 3.12 and the demodulator in Figure 3.13.
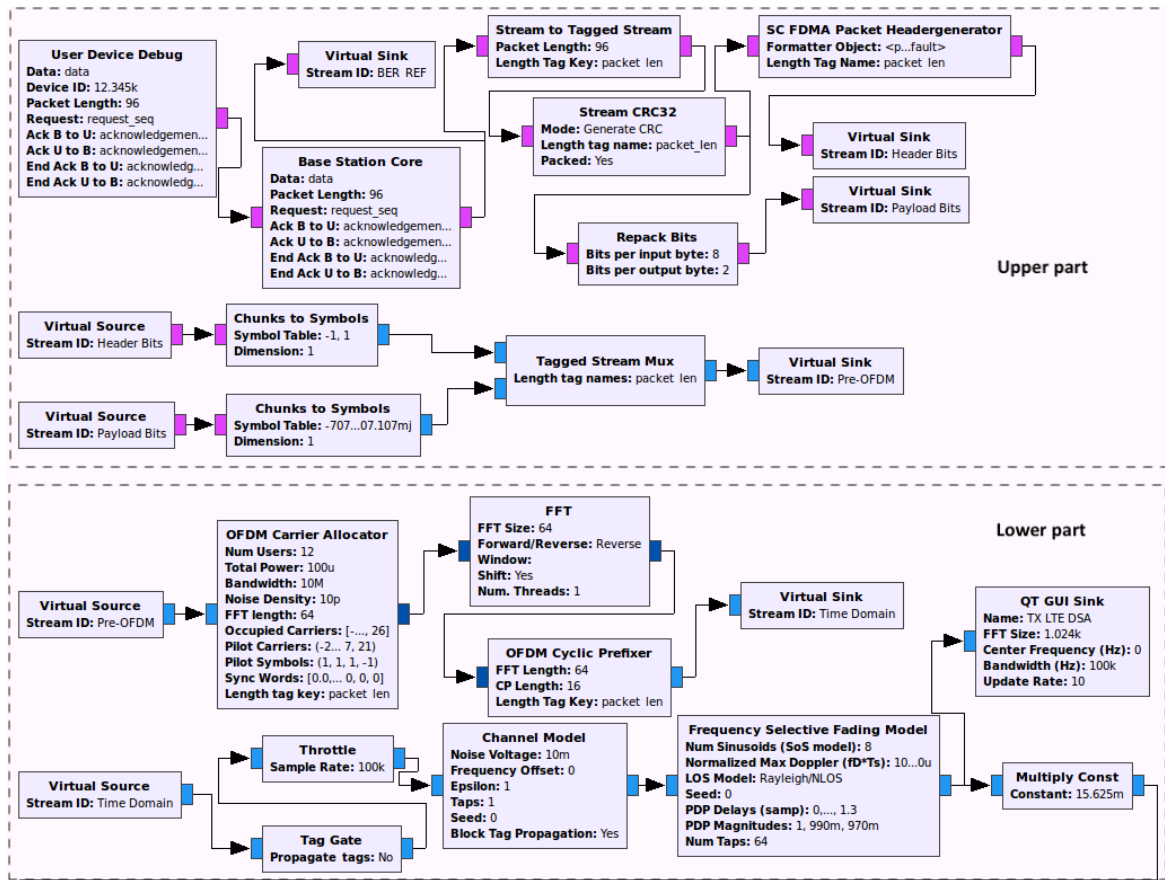
Figure 3.12 Flow Graph of 4G Configuration with DSA Implementation OFDM

Modulator (Downlink)

As shown in Figure 3.12, the upper part represents the mapping of data in packets for transmission, and the lower part shows the implementation of OFDM and transmission. Appropriate blocks were configured in the assembly of the transmission. The random set of data was generated from the Random Source block and sent to the stream blocks, in which the data were converted to stream data. After that, the data were grouped separately into header and payload bits. The header and payload bits were then transmitted through the Chunks to Symbols blocks to be converted to symbols.

The lower part was constructed to consist of a carrier allocator block. Pre-OFDM symbols pass through this OFDM Carrier Allocator block, where the packets are grouped into distinct device IDs and allocated to specific subcarriers. They would then pass through to the Cyclic Prefixer block to remove the Inter Symbol Interference (ISI).
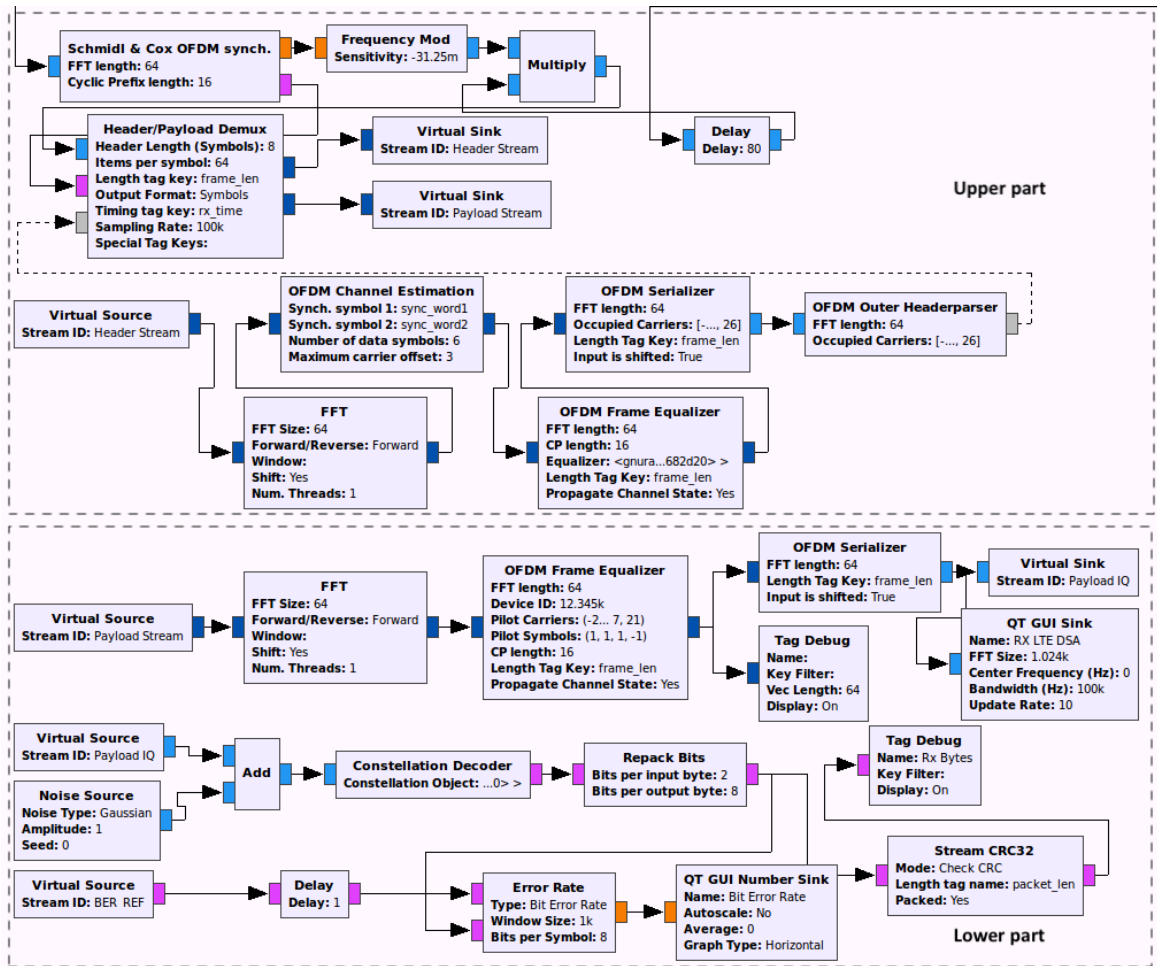
Figure 3.13 Flow Graph of 4G Configuration with DSA Implementation OFDM Demodulator (Downlink)

The demodulator was assembled as shown in Figure 3.13. The upper part of the flow graph shows the Schmidl and Cox (SC) OFDM Sync block that implements the SC algorithm to obtain the timing metric and frequency offset. After the timing metric was calculated, the trigger was sent to notify the subsequent block regarding the start symbol of a packet. The Header / Payload demux block was involved in the received data processing. The Channel Estimator block calculated the initial channel taps and sent them to the rest of the blocks by tags. The other blocks, such as the OFDM Frame Equalizer, OFDM Serializer, and Packet Header Parser, were also used in the reception and equalization process of the reception stage.

The lower part that represented the end step of the demodulation process was put together, in which the Payload stream was converted to Payload IQ by passing through the FFT, OFDM Frame Equalizer, and OFDM Serializer blocks. Finally, a Noise Source block was used to generate Gaussian noise with certain amplitude levels so that the configuration could be triggered by its presence. The Error Rate block was then used to calculate the bit error rate of the configuration.

Based on the methodology presented, the BER values generated from the downlink configuration were then inserted into the throughput calculation to analyze the throughput enhancement between a typical 4G OFDM design with the one incorporating DSA. The results are presented in Subsection 4.3.1 in Chapter 4.

3.3.2 Development of the E-DSA Algorithm for 5G FBMC

3.3.2.1 The Validity of the E-DSA Algorithm for 5G FBMC
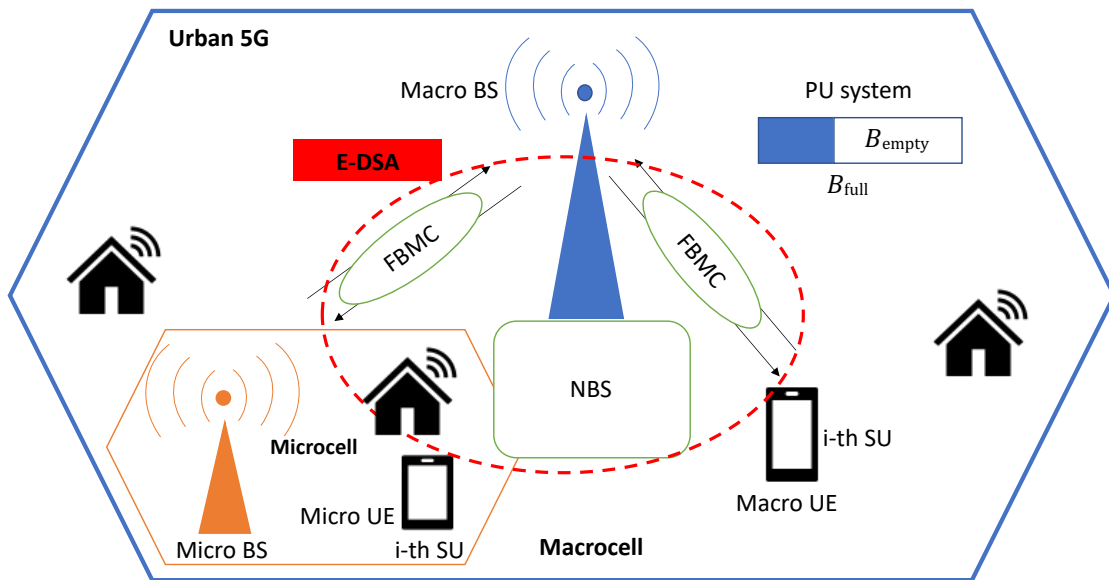
Figure 3.14 Proposed System Model for E-DSA 5G FBMC Network

The proposed system model for this research is shown in Figure 3.14. It was assumed that one primary user (PU) system and N SUs were incorporated into the spectrum distribution system. The SUs' base stations and the total spectrum of the PU system are denoted by

B_{full}. To obtain additional revenue, the PU system auctions free spectrum resources to the *i-th* SU at unit bandwidth price p_i, which is a function of the spectrum price. It is worth noting that the size of spectrum B_{empty} ($B_{\text{empty}} \leq B_{\text{full}}$) provided by the PU for SUs varied from time to time. Firstly, the SUs obtained the available spectrum information of the PU through spectrum sensing, including the spectrum quality and the available spectrum size, and transmitted it to the base station. Then, under the guidance of the base station, the SUs obtained the spectrum through the E-DSA algorithm using the Nash bargaining method to meet the communication requirements and maximize the total revenue of the SU system.

According to Han et al. (2018), the description of spectrum allocation using the Nash bargaining scheme is outlined in Table 3.6 below:

Table 3.6 Description of Spectrum Allocation Using Nash Bargaining Scheme

Item	Description	Remarks
N	Set of secondary users (SUs)	$\{1, 2,..., N\}$
A	Set of allocations where SUs cooperate with each other	Revenue received by the ith SU $< A$ - No cooperation for i-th SU
$U_{i,min}$	Minimum revenue that the i-th SU is required to gain	$U_i > 0$. $(U_{1,min}, U_{2,min}, ..., U_{N,min})$
(A, U_{min})	N-person bargaining game problem	$\{U \in A \mid U \geq U_{min}, \forall i \in N\}$ is a non-empty bounded set

In this study, the following optimal solution (Anand et al., 2020) is shown in Equation 3.29,

$$\max_{U_i \in, U_i \geq U_{i,min}, \forall i} \sum_{i=1}^{N}(U_i - U_{i,min}) \tag{3.29}$$

When the revenue of each SU satisfies $U_i \geq U_{i,min}$, the SUs will cooperate. Therefore, it was assumed that $U_{i,min} = 0$, that is $U_i > 0$. To obtain spectrum from the primary user (PU) system, the SUs were required to pay the cost to the PU through bargaining. Thus, this study contained two sections to define the utility function- the revenue $Y_i(b_i) = \emptyset_i \eta_i b_i$ determined once the i-th SU has been allocated to spectrum b_i and

the payment of the cost $Z_i(b_i) = p_i b_i$ that the i-th SU is responsible for, the utility function is defined as follows:

$$U_i(b_i) = Y_i(\emptyset_i, b_i) - Z(p_i b_i) = \emptyset_i \eta_i b_i - p_i b_i \qquad (3.30)$$

where $\eta_i = \log_2(1 + K\gamma_i)$ is the spectrum efficiency function of the i-th SU, $K = \frac{1.5}{\ln\left(\frac{0.2}{\varepsilon}\right)}$, and $\emptyset_i$ is the revenue factor of the unit transmission rate of the i-th SU. $\emptyset_i$ is inversely proportional to the bandwidth request size, which results in $\emptyset_i = x + y\left(\frac{1}{b_i}\right)$ where x and y are constants. Furthermore, $\eta_i b_i$ is the throughput, ε is the target BER, and γ_i is the SINR of the *i-th* SU. Therefore, the SUs' utility function is formulated as follows:

$$U_i(b_i) = b_i \eta_i \left(x + y\left(\frac{1}{b_i}\right)\right) - c_i b_i (\textstyle\sum_{i=1}^N b_i) \qquad (3.31)$$

Equation 3.31 can be optimized by solving the model under the following constraints:

$$\max_{b=(b_1, b_2, \ldots, b_N)} U = \textstyle\sum_{i=1}^N U_i \qquad (3.32)$$

$$\begin{cases} b_i \eta_i \geq r_{i,min} \\ \displaystyle\sum_{i=1}^N b_i \leq B_{empty} \end{cases} \quad \forall i = 1,2,\ldots,N$$

where b_i is the bandwidth size obtained in the solution, η_i is the spectrum efficiency, and $b_i \eta_i$ is the obtained throughput. The constrained optimization problem of Equation 3.32 can be solved by using the Lagrange multiplier extremum method according to Kuhn-Tucke's theory. The Lagrange function M is formulated in Equation 3.33,

$$M = \textstyle\sum_{i=1}^N (b_i \eta_i (x + \frac{y}{b_i}) - c_i b_i (\textstyle\sum_{i=1}^N b_i)) - \mu(\textstyle\sum_{i=1}^N b_i - B_{idle}) + \textstyle\sum_{i=1}^N \varsigma_i (b_i \eta_i -$$

$$r_{i,min}) (3.33)$$

The E-DSA solution of the *i-th* SU can be solved via a series of the Lagrange multipliers' iterations. Equation 3.34 defines the solution of the spectrum request strategy. b_i,

$$b_i^{(T+1)} = \frac{x\eta_i - c_i(\sum_{j\neq i}^{N} b_j) - \sum_{j\neq i}^{N} c_j b_j - \mu^{(T)} + \eta_i \varsigma_i^{(T)}}{2c_i}$$

(3.34)

The assumed parameters of the E-DSA algorithm are listed in Table 3.7.

Table 3.7 Assumed Parameters for E-DSA Algorithm

Parameters	Description
Total spectrum of PU, B_{full}	20 MHz, $0 \leq B_{empty} \leq B_{full}$
x, y	5, 1
Minimum rate requirement, $r_{i,min}$	0.2 Mbps, $\forall i$
Initial value of Lagrange multipliers	$\mu^{(0)} = 10$, $\varsigma_i^{(0)} = 5$, $\forall i$
Price weight factors, $c_1 = c_2$	1, 2

The algorithm flow of the proposed E-DSA is summarized in Figure 3.15 below,
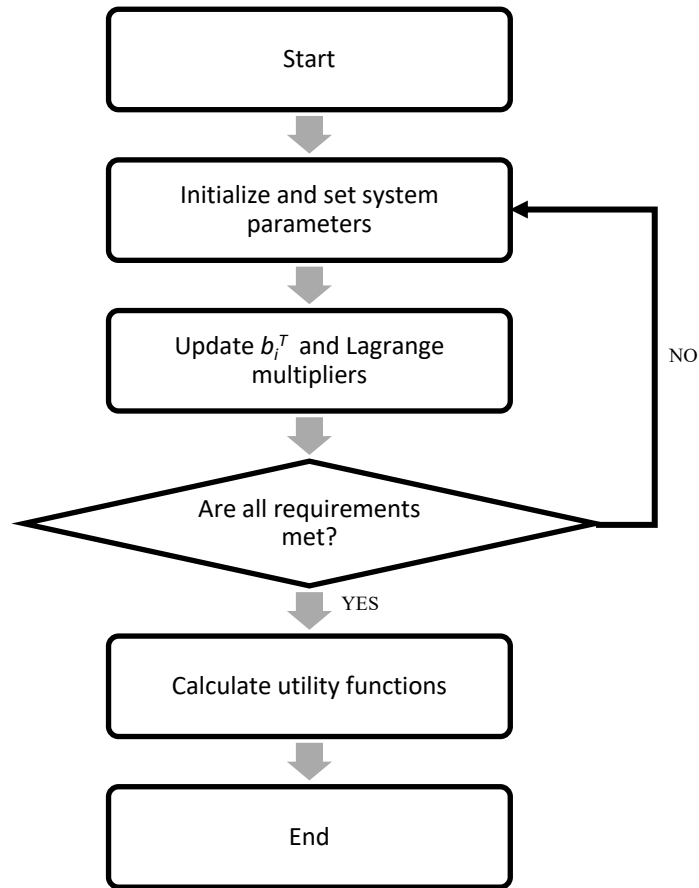
Figure 3.15 E-DSA Algorithm Flowchart

The results on the validity of the E-DSA algorithm are presented in Subsection 4.3.2 in Chapter 4.

3.3.2.2 Proposed Theoretical Bit Error Rate (T-BER) and Throughput Calculations for 5G Urban Macro and Micro configurations

After developing the E-DSA algorithm for the 5G FBMC and testing its validity, the algorithm was implemented into the 5G urban macro and micro scenarios to test its effectiveness on a heterogeneous network via throughput analysis.
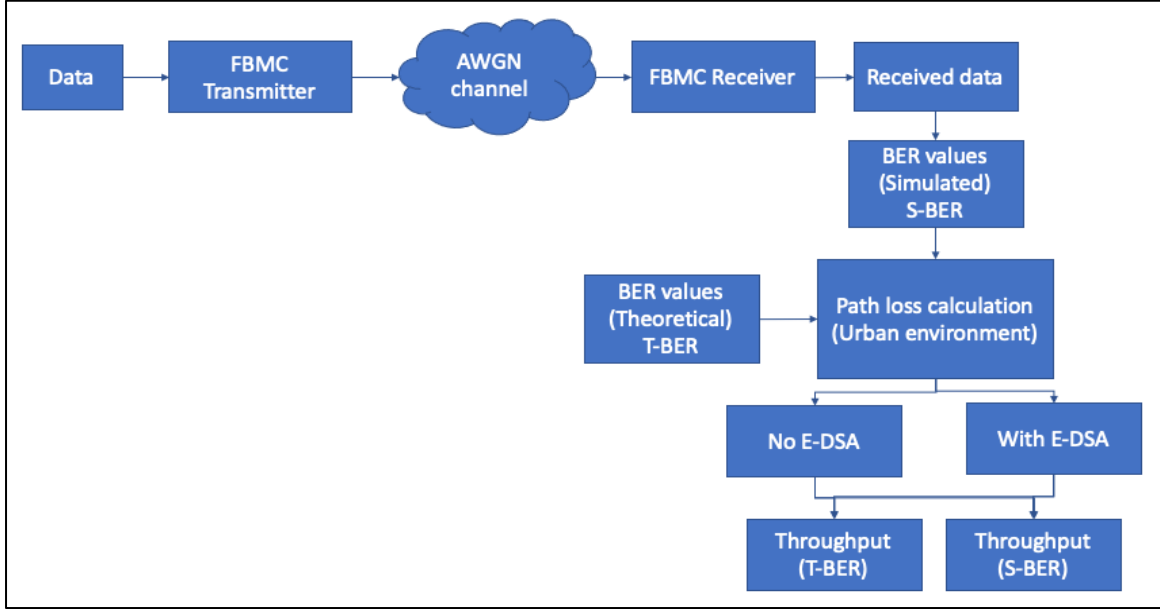
Figure 3.16 Steps for Throughput Calculation

Figure 3.16 shows the steps to calculate the throughput. The formula implemented from the 3GPP technical report by ETSI 5G (2016) to calculate the throughput of 5G FBMC configuration with and without E-DSA implementation is put together in this section. Table 3.8 lists the assumptions for the parameters for the throughput calculation.

Table 3.8 Assumed Parameters for Throughput Calculation

Parameter	Values
Distance between transmitter (Macrocell base station) and receiver (Macrocell users) $d_{ma,ma}$ (km)	0.1 – 0.35
Distance between transmitter (Macrocell base station) and receiver (Microcell users) $d_{ma,mi}$ (km)	0.15 – 0.40
Distance between transmitter (Microcell base station) and receiver (Macrocell users) $d_{mi,ma}$ (km)	0.01 – 0.13
Distance between transmitter (Microcell base station) and receiver (Microcell users) $d_{mi,mi}$ (km)	0.005 – 0.029
Carrier frequency, f_c (Hz)	1 G
Bandwidth (Hz)	10 M

The path loss between macrocell users and macrocell base station is denoted by PL_{ma}. It is formulated as shown in Equation 3.21 below,

$$PL_{ma} = 28.0 + 22\log_{10}(d_{ma}) + 20\log_{10}(f_c) \tag{3.21}$$

where d_{ma} is the distance between the transmitter and receiver for the macrocell network.Moreover, the path loss of the microcell network, denoted by PL_{mi}, is formulated as in Equation 3.22 below,

$$PL_{mi} = 32.4 + 21\log_{10}(d_{mi}) + 20\log_{10}(f_c) \tag{3.22}$$

Next, the channel gain for both macrocell and microcell is formulated as in Equation 3.23 below,

$$G = 10^{\frac{-PL}{10}} \tag{3.23}$$

After that, the signal-to-interference plus noise ratio (SINR), γ_{ma} for macrocell network is as shown in Equation 3.24,

$$\gamma_{ma} = \frac{G_{ma,ma} \times P_{ma}}{\sigma^2 + (\sum_{neig(ma)} G_{ma,ma} \times P_{ma}) + (G_{ma,mi} \times P_{mi})} \tag{3.24}$$

where P_{ma} is the transmit power of the microcell base station, $G_{ma,ma}$ is the channel gain between the macrocell user and the microcell base station and lastly σ^2 is the power of the AWGN. Furthermore, the γ_{mi} for the microcell network when considering the interference caused by neighboring cells as in Equation 3.25,

$$\gamma_{mi} = \frac{G_{mi,mi} \times P_{mi}}{\sigma^2 + (\sum_{neig(mi)} G_{mi,mi} \times P_{mi}) + (G_{mi,ma} \times P_{ma})} \tag{3.25}$$

Then before calculating the throughput, the total capacity of users is formulated as in Equation 3.26,

$$C = \Delta f \times \log_2(1 + \alpha\gamma) \tag{3.26}$$

where Δf is the subcarrier spacing and α = -1.5*ln(5ε) relates to the bit error rate (BER), ε. The theoretical BER (T-BER) expression used for OFDM modulation in this paper was chosen from a study conducted by Nissel and Rupp (2017). For the same bandwidth, Kamel et al. (2016) also implied that the SINR of OFDM is $\gamma_{typ-OFDM} = \frac{1}{2}(\gamma_{typ-FBMC})$ because FBMC only experiences half the noise power. Thus, the BER expression of FBMC becomes the expression in Equation 3.27,

$$\varepsilon_{typ-FBMC} = \frac{1}{2}\left(1 - \frac{1}{\sqrt{1+\frac{1}{\gamma}}}\right) \quad (3.27)$$

For a typical 5G FBMC configuration without E-DSA implementation, the throughput of a serving macrocell is formulated as in Equation 3.28,

$$TP_{typ} = \sum(\beta \times C) \quad (3.28)$$

where β is the subcarrier assignment and is set to 1.

The throughput expression for 5G FBMC with E-DSA implementation is expressed in Equation 3.29 below,

$$TP_{E-DSA} = b_i \eta_i \quad (3.29)$$

The throughput results are presented in Subsection 4.3.1 in Chapter 4.

3.4 HARDWARE IMPLEMENTATION USING NI USRP RIO TRANSCEIVER FOR 4G OFDM AND 5G LWF-FBMC DESIGNS

Figure 3.17 shows the steps to achieve the third objective of this research.

3RD OBJECTIVE

Hardware implementation for PSD analysis between OFDM and LWF-FBMC configurations using NI USRP

STEPS

1. Hardware setup
2. Simulation setup using LV Comm

ANALYSIS

1. Comparison of the PSD outputs between OFDM and FBMC with hardware implementation
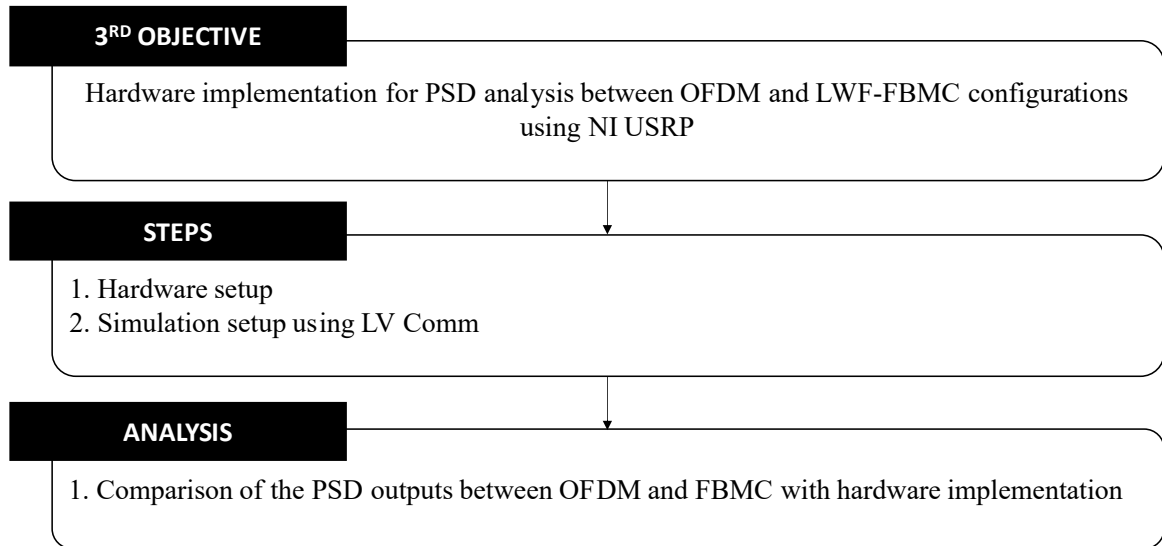
Figure 3.17 Methodology to achieve the third objective of this research

First, the hardware components, as well as their functions used for the experimental setup in this research, were outlined. This was followed by constructing the simulation set-up for the integration between the LV Comm software and the NI USRP hardware to generate the PSD waveforms for both the OFDM and LWF-FBMC designs. The PSD analysis was then carried out based on the PSD outputs for OFDM and LWF-FBMC configurations.

3.4.1   Experimental Hardware Setup

This section describes the experimental setup for the real-time analysis using NI USRP RIO. The list of components used for this experiment is outlined in Table 3.9 below:

Table 3.9 List of Hardware Components and Their Functions

No	Component	Function	Description
1	Personal computer (PC)	• Host computer • Comes with LV Comm software, which offers a single design pipeline to help wireless communications researchers prototype more quickly and get findings rapidly.	Model: Dell XPS 8930 Desktop Processor: 8th Generation Intel(R) Core(TM) i7-8700 (6-Core, 12M Cache, up to 4.6 GHz)
2	NI USRP RIO	• Act as a transceiver for a full-duplex system. • Deliver the optimum balance of performance and streamlined software tool flow.	Model: NI USRP 2943R Bandwidth: 120MHz Frequency: 1.2 GHz to 6GHz
3	Peripheral component interconnect express (PCIe) – MXI Express	• A computer having a PCI Express slot that acts as a remote controller for systems or devices connected via PCI. • Because of this link's transparency to software programmes and drivers, linked devices can be controlled by computers and servers without the need for further programming.	PCIe 8371 Interface Kit for USRP RIO
4	Two (2) Vertical Antennas	• Omnidirectional antennas that receive signals equally from all directions.	Model: Vert2450 Frequency: 2.4 to 2.48 GHz, 4.9 to 5.9 GHz

			Gain: 3dBi
			Pattern: Omni
5	PCIe extender	• Provides separate power for the graphics card and lessens the load on the motherboard when utilizing several graphics cards.	PCI-E 1x to 16x powered riser adapter card with multi-layer shielded wire

Figure 3.18 PC with LV Comm Software and NI USRP 2943R Transceiver

Figure 3.18 shows the PC and NI USRP 2943R used for this research. The LV Comm software was installed on the PC for the simulation's design and analysis purposes.
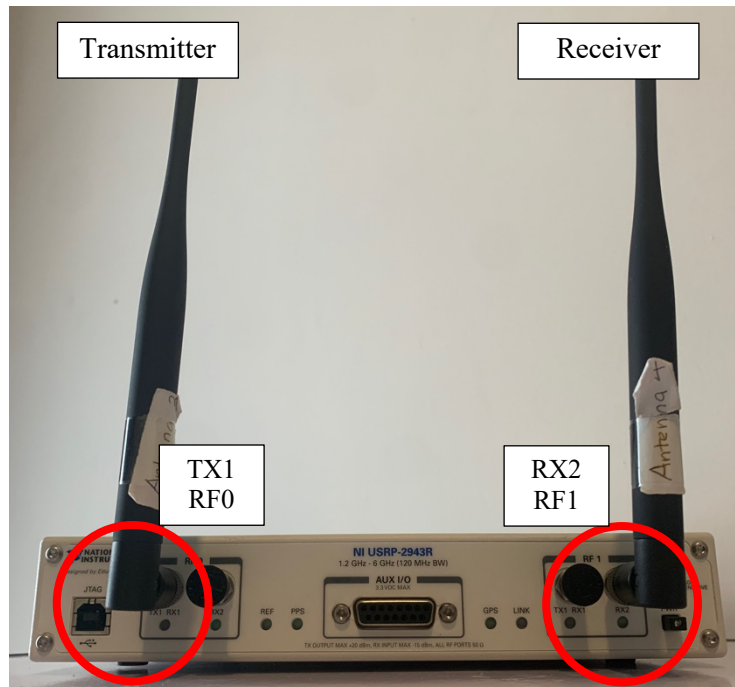
Figure 3.19 Two Vert2450 Vertical Antennas for Transmitter and Receiver

Figure 3.19 shows the connection of the two Vert2450 Vertical Antennas to the NI USRP 2943R's channel slots. The first antenna acts as a transmitter and is connected to the TX1 slot at channel RF0. The second antenna acts as a receiver and is connected to the RX2 slot at channel RF1. The TX1's LED indicator will light up in red to ensure that the NI USRP 2943R successfully transmits the data. Furthermore, the RX2's LED indicator will light up in green to indicate a successful reception of data.

Figure 3.20 PCIe Extender and PCIe – MXI Express (PCIe 8371)

Figure 3.20 shows the connection of the PCIe – MXI Express to the PCIe Extender. This was to lessen the motherboard from overprocessing when the NI USRP RIO is operating.

Figure 3.21 PCIe Slot in CPU

Figure 3.21 shows the PCIe cable that was connected to the PCIe slot in the CPU. After this stage, the NI USRP 2943R was switched on prior to switching on the PC.

3.4.2 Simulation setup for OFDM and LWF-FBMC Using LV Comm

Based on Figure 3.19, the NI-USRP programming blocks (inside red boxes) were used to define the transmitter and receiver's IQ rates, the channels' carrier frequencies, the channels' gains, and the active antennas. The functions of the NI-USRP programming blocks were explained in Subsection 2.8 in Chapter 2.
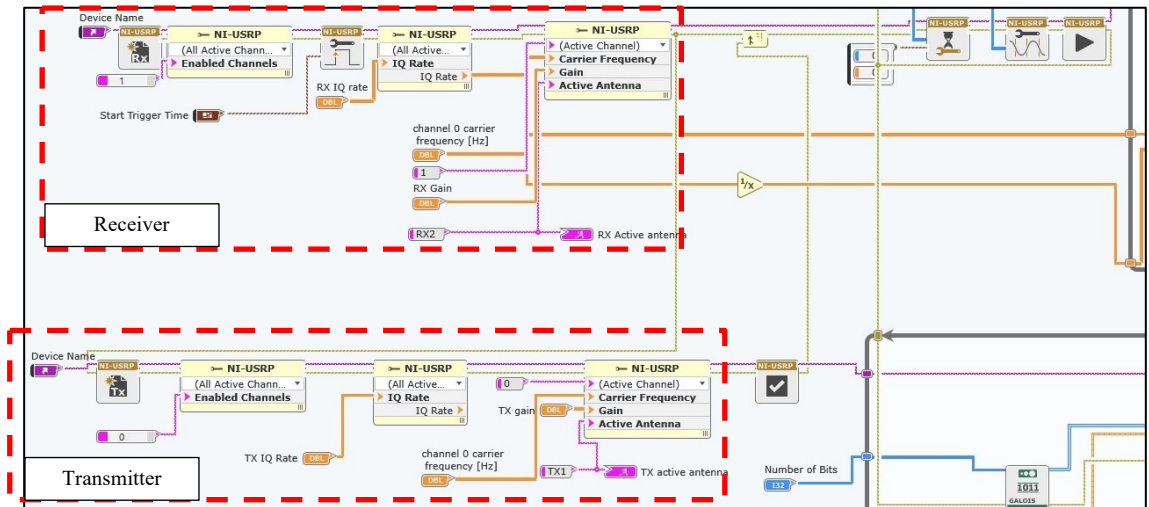
Figure 3.22 NI-USRP Programming Blocks for Transmitter and Receiver

The additional parameters used in the designs are outlined in Table 3.10 below:

Table 3.10 Additional Parameters for Hardware Validation

Parameters	OFDM	LWF-FBMC
Presence of OQAM	No	Yes
Presence of Cyclic Prefix	Yes	No
Type of Prototype filter	Rectangular	LWF-Hamming
Carrier Frequency (Hz)	2G	
IQ rate (bit/s)	5M	
Channel gain (dB)	25	

3.4.3 OFDM Transceiver Design Using LV Comm

Figure 3.23 shows the transceiver design for the OFDM configuration using LV Comm. The flow of data for the modulation and demodulation of the OFDM configuration is similar to that explained in Subsection 3.2.2 in this chapter.
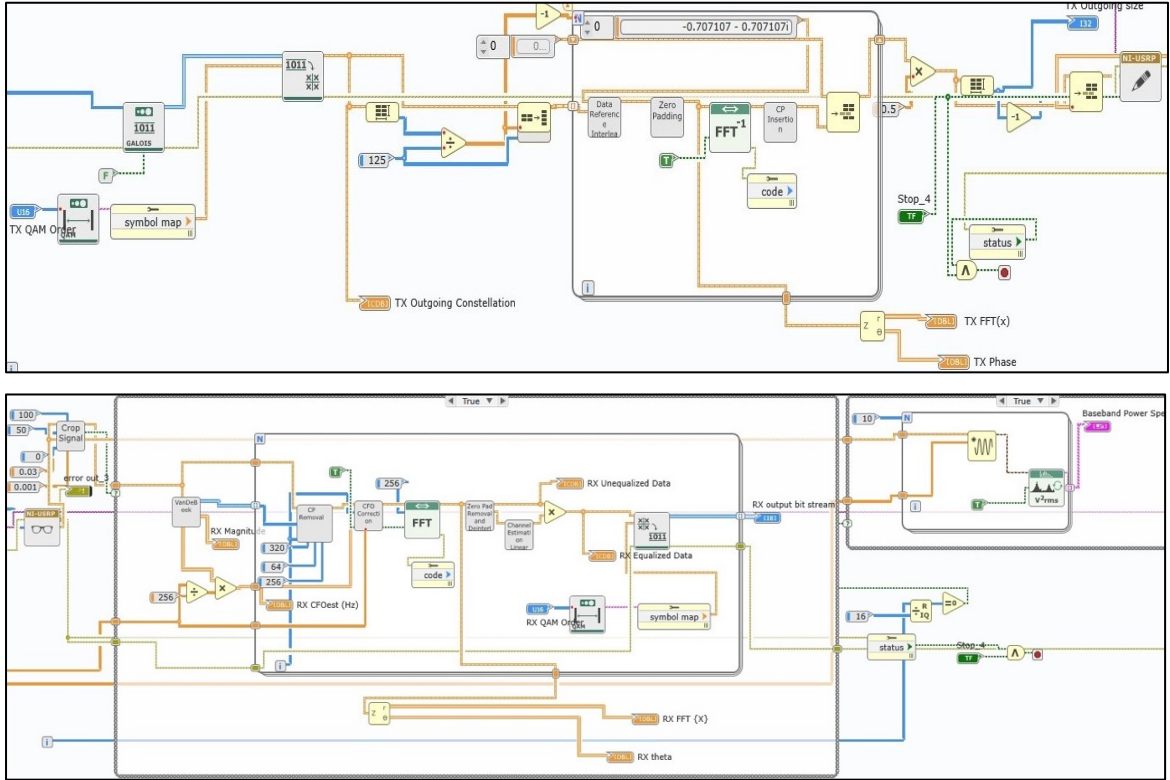
Figure 3.23 Transceiver Design for OFDM

At the transmitter, the Quadrature Amplitude Modulation (QAM) maps positions and the quantity of initial bits were initialised together. Then, a 9-bit Pseudo Noise (PN) sequence was used to create random data bits. There were 125 bits in total at this point. The symbols were then separated into 5 sets of 125-point data sets, creating the OFDM symbols after the bits had been converted to symbols. Following the sixth data symbol, 25 reference symbols were added, and then 53 zeros were added to the passband's edges. After that, the signal's frequency to time domain conversion was carried out using an inverse fast Fourier transform (IFFT). Then, by duplicating the array's first 64 points, a 64-sized cyclic prefix was inserted. The five time-domain waveforms were subsequently scaled to a complex magnitude for each of the in-phase and quadrature (IQ) components that is normally less than 0.7. Finally, the data queue block enabled the completion of the data transmission to the receiver.

The Van De Beek algorithm was used on the receiver side to find the sites of the cyclic prefix for synchronisation and to calculate the frequency offset. Afterwards, the incoming signal was free of the frequency offset and cyclic prefix.

Next, the time domain OFDM symbol was transformed into the frequency domain using the fast Fourier transform (FFT). The zero padder was then removed after separating the data and reference bits. Then, the in-phase and quadrature components that correspond to the reference symbols had their linear fit equalisation coefficients determined. The equalisation process also included the implementation of the data symbols, and after that, the mapping of symbols to bits was carried out.

3.4.4   LWF-FBMC Transceiver Design Using LV Comm

Figure 3.24 shows the transceiver design for LWF-FBMC using LV Comm. The flow of data for the modulation and demodulation of the LWF-FBMC configuration is similar to that explained in Subsection 3.2.3 in this chapter.
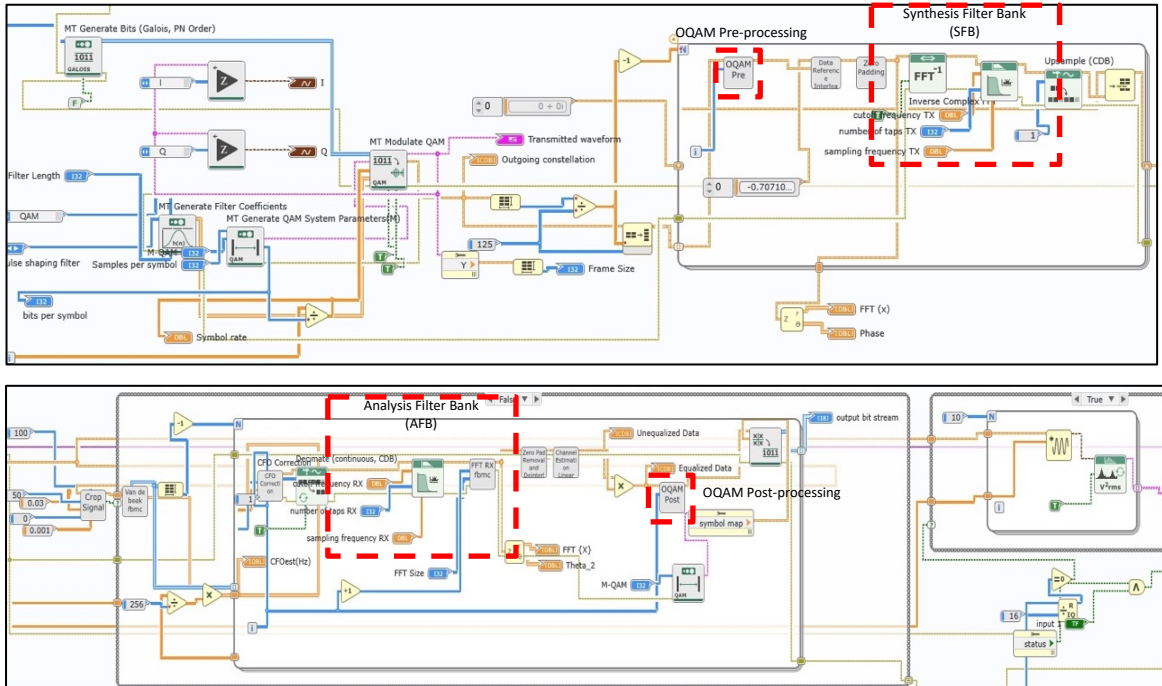
Figure 3.24 Transceiver Design for LWF-FBMC

Since orthogonal QAM (OQAM) pre-processing and the Synthesis Filter Bank (SFB) blocks are programmed, the transmitter design for FBMC is similar to that of OFDM, as was previously said. There were no other cyclic prefix blocks being added aside from that.

The staggering procedure was initially carried out at the OQAM pre-processing block, and then the sample rate was upsampled by 1 and multiplied by odd or even $\Theta_{k,n}$ sequences. After that, the signal was sent to the IFFT block to be converted from the frequency domain to the time domain.

The signal was sent to the Synthesis Filter bank block after passing through the IFFT block, where the FIR windowed lowpass filter was created as a prototype filter with scalable parameters, including the sampling frequency, number of taps, and cut-off frequency. The signal was then upsampled by 1 and added to the queue before being sent to the receiver.

The receiver setup for LWF-FBMC then resembles that of OFDM, with the exception that new blocks, such as the Analysis Filter Bank (AFB) and OQAM post-

processing blocks, were added to the design, as illustrated in Figure 3.5. The cyclic prefix removal block was also taken out.

The signal initially passes through the AFB before being sent to the FFT block for FFT computation. The filter employed for AFB and SFB is comparable, as can be seen in Figure 3.8. However, before going through the filter, the signal was first reduced in size.

The signal was routed via an equaliser after the FFT calculation and then OQAM post-processing blocks. Depending on whether the incoming signal was odd or even, the signal was multiplied here using various odd or even $\Theta^*_{k,n}$ sequences. Following the extraction of the signal's real component, a de-staggering process was carried out to create a complex symbol. The sample rate was subsequently down-sampled after that.

The PSD analysis results for both 4G OFDM and 5G LWF-FBMC configurations are presented in Subsection 4.4.2 in Chapter 4.

3.5 CHAPTER SUMMARY

Throughout this chapter, the steps for designing the enhanced FBMC configuration using LV Comm, developing an enhanced dynamic spectrum allocation (E-DSA) algorithm and analysing the performance between OFDM and FBMC configurations using the NI USRP RIO were outlined. Besides that, the mathematical expressions used for the calculation of throughputs were also presented.

CHAPTER FOUR

RESULTS AND DISCUSSIONS

4.1 INTRODUCTION

This chapter firstly presents the results concerning the PSD analysis of the 5G FBMC configuration's performance as compared to 4G OFDM's using GNU Radio and LV Comm software. The simulation results based on the methodology explained for GNU Radio were outlined in Subsection 3.2.1 in Chapter 3 and the LV Comm in Subsection 3.2.2, respectively. The validations of the PSD analysis using the LV Comm by testing the performance of the prototype filter used for FBMC, are also presented in this chapter.

Secondly, for the development of an enhanced DSA (E-DSA) algorithm, the result of the preliminary study on the implementation of DSA on 4G using GNU Radio is also presented. For this part, the throughputs performance for both the downlink and uplink configurations were taken into account. This is followed by the validation of the newly developed E-DSA algorithm. Subsequently, the results of the throughput analysis for the E-DSA implementation algorithm are also shown.

Lastly, for the simulation-hardware integration part, the result for the successfulness of the transceiver design is presented after running the simulation design for both OFDM and LWF-FBMC configurations. This is shown by the validation output of the LED lights seen at both the transmitter and receiver of the NI USRP 2943R hardware. Then, the results for the PSD analyses on the validation of the OFDM and LWF-FBMC's simulation designs are presented.

4.2 5G FBMC AS AN IMPROVED MULTIPLEXING METHOD

4.2.1   PSD Analysis on Prototype Filters

As per described in Chapter 3, one of the factors affecting the OOB emissions is the usage of prototype filters. In this research, three different types of prototype filters were examined. The Root-raised cosine (RRC) filters were utilized by filtered-OFDM (f-OFDM), rectangle filters by OFDM, and Lowpass Windowed FIR (Hamming) filters (LWF-Hamming) by FBMC.
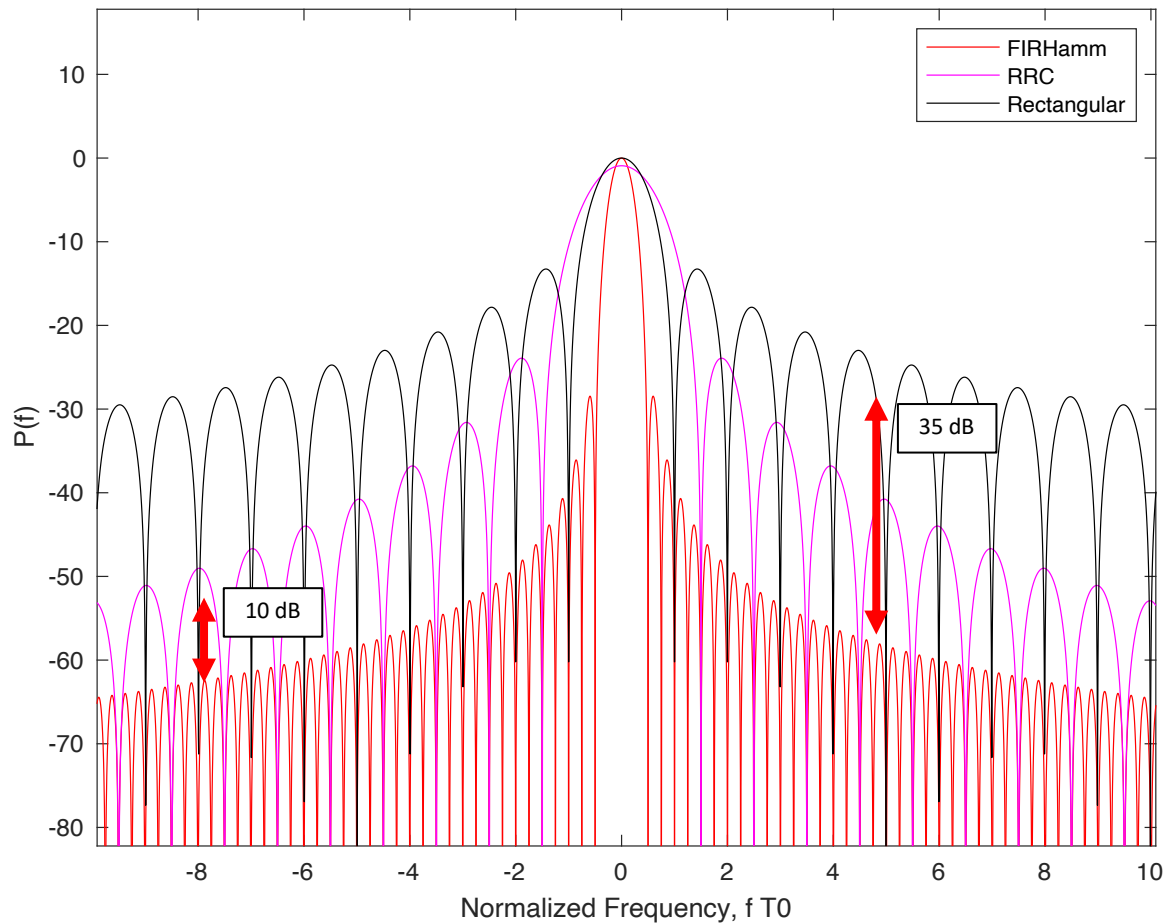
Figure 4.1 Frequency Responses of Proposed LWF-Hamming, RRC, and Rectangular Prototype Filters

The frequency responses of the prototype filters are shown in Figure 4.1. In addition to having low sidelobes and a rapid spectrum decay, the frequency responses of RRC filters, rectangle filters, and LWF-Hamming are extremely different from one another. When compared to the LWF-Hamming filter, the RRC and rectangle filters, in particular, showed a very expressive spectrum degradation, where RRC was seen to have a 10 dB higher PSD than LWF-Hamming, and the rectangle filters to have a 35 dB higher PSD than LWF-Hamming.

Both systems produce a substantial amount of OOB interference which may disrupt communications in adjacent wireless channels. Conventional disabling of the set of OFDM subcarriers on the left and right side of its spectrum sometimes is not sufficient to avoid interference. Table 4.1 shows the stop-band energy of different filters.

Table 4.1 Stop-band Energy of Different Filters

Prototype Filter	RRC for f-OFDM	Rectangular for OFDM	Proposed FIR-Hamming for FBMC
Stop-band Energy	-55 dB	-30 dB	-65 dB

Since the proposed filter is designed using the FIR filter, not only the influence of noise is considered to guarantee the effectiveness of the method. The desired power is also increased as the interference power decreases.

It can be concluded that the proposed LWF-Hamming filter obtained a superior spectrum decay with minimal sidelobes by encouraging a comparison among all the prototype filters. The MATLAB codes for the comparison of the frequency responses of the prototype filters are presented in Appendix I.
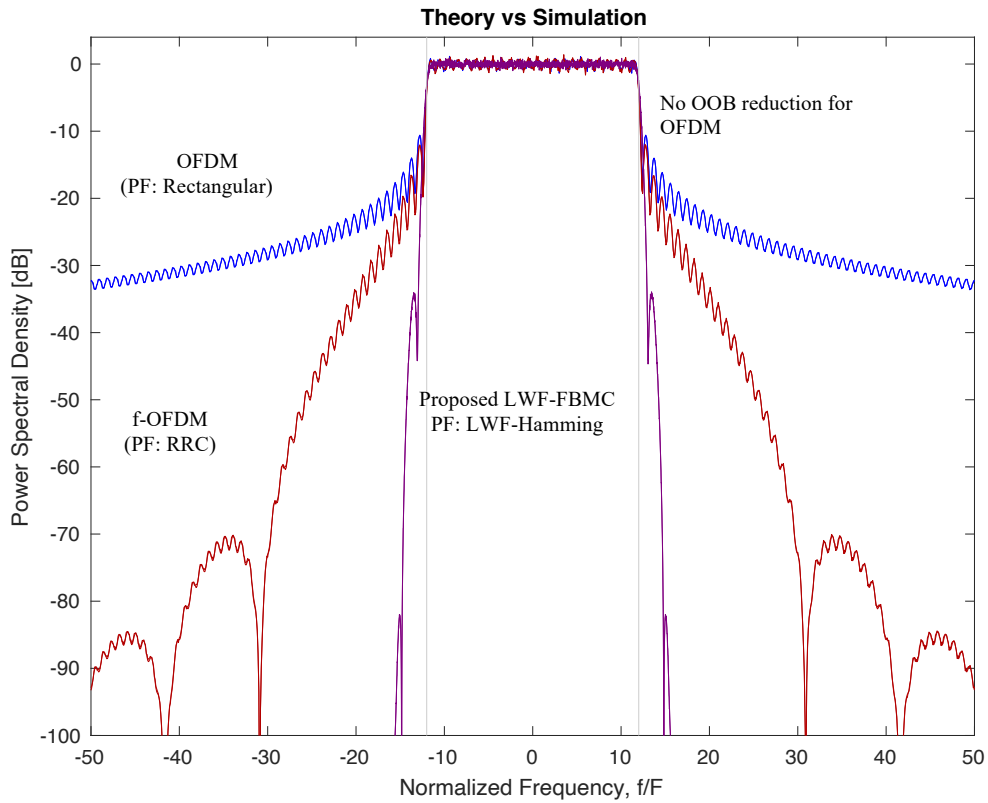
Figure 4.2 PSD of OFDM, f-OFDM and LWF-FBMC

As can be observed from Figure 4.2, the LWF-FBMC and f-OFDM designs have substantially better spectrum characteristics than OFDM. Nevertheless, LWF-FBMC still performs significantly better, as its normalized frequency is closer to 0 by 50% as compared to f-OFDM. Because OFDM used rectangular transmit and receive pulses, the computing complexity was significantly reduced.

Additionally, the cyclic prefix suggested that the transmit and receive pulses were marginally offset, preserving orthogonality in frequency-selective channels. Due to the rectangular pulse's unfortunate lack of frequency domain localization, there were a lot of out-of-band (OOB) emissions. The MATLAB codes for the PSD comparison for OFDM, f-OFDM and LWF-FBMC are presented in Appendix II.

4.2.2 PSD Analysis on 4G OFDM and 5G FBMC Configuration

For the construction of 4G OFDM and 5G FBMC using LV Comm software, to check whether the configurations of 4G OFDM and 5G FBMC can successfully transmit and receive data, the unequalized and equalized data plots at the receiver's side were recorded and analyzed. Figure 4.3 shows the plots from the receiver's side of both OFDM and FBMC configurations using LV Comm.
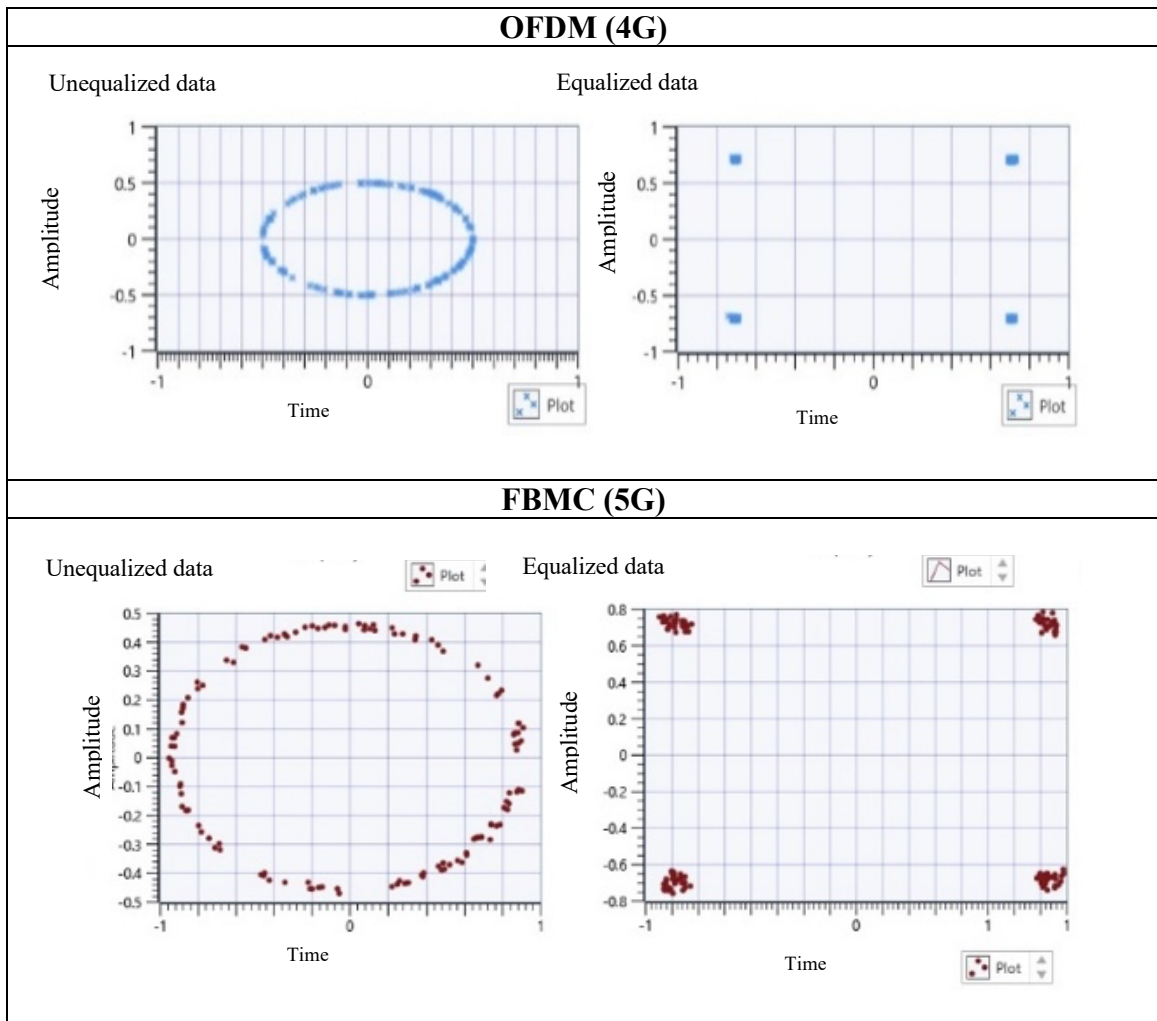
Figure 4.3 Receiver Plots for Both LWF-FBMC and OFDM Configurations

The unequalized data plot shows the result before the data goes through the channel estimation, whereas the equalized data plot shows the result after going through the channel estimation. Based on the receiver plot, the unequalized and equalized data sketches show that the signal can be generated at any point, and the receiver can receive the exact value of the QAM constellation points from the transmitter in the absence of noise.

Besides that, it can also be understood that the equalizer is successful in combating Inter-symbol Interference (ISI) based on the accuracy of the constellation diagram at the receiver. Thus, it can be said that both the OFDM and LWF-FBMC configurations can transmit and receive data successfully.

The next step was the analysis involving the spectral efficiency when both configurations were submitted to the Rayleigh flat fading channel that acts as a multicarrier channel. This section discusses the spectrum efficiencies of OFDM and FBMC configurations by analysing the power spectral density graphs that were recorded using LV Comm. Figure 4.4 shows the baseband power spectrum (BPS) for both FBMC and OFDM configurations.

OFDM (4G)	LWF-FBMC (5G)
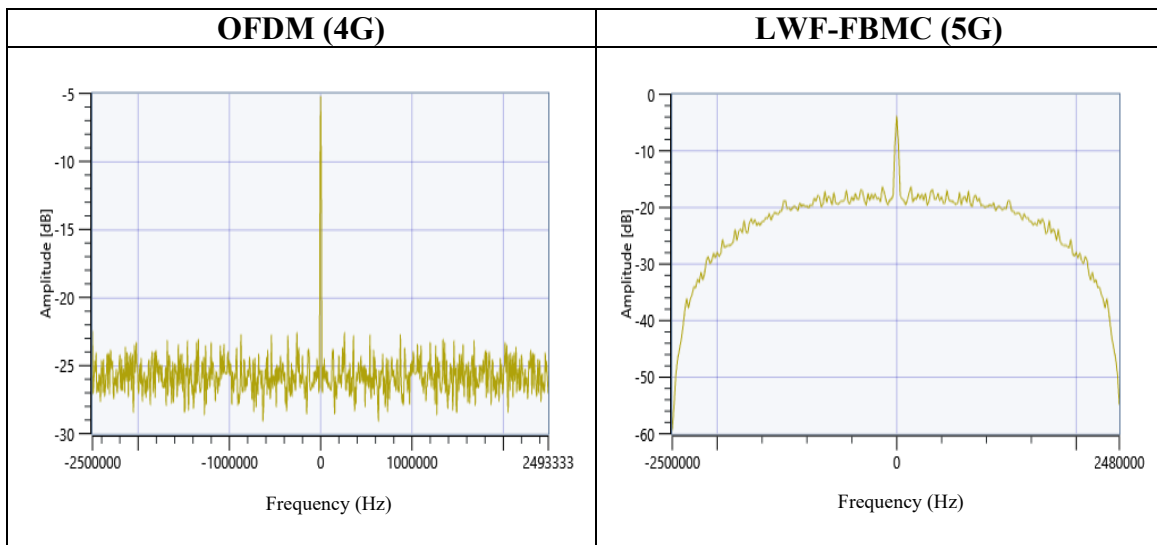
Figure 4.4 Baseband Power Spectrum (BPS) for Both FBMC and OFDM Configurations

The baseband power spectrum indicates which frequencies contain the power of the signal, which is claimed to be the average of the signal's energy. As seen in the figure, FBMC's graph shows that the received signal has less noise than OFDM's received signal due to the effect of the implementation of the windowed FIR prototype filter in the filter banks for FBMC. Figure 4.5 shows the power spectral density (PSD) for both proposed OFDM and FBMC configurations.

OFDM (4G)	LWF-FBMC (5G)
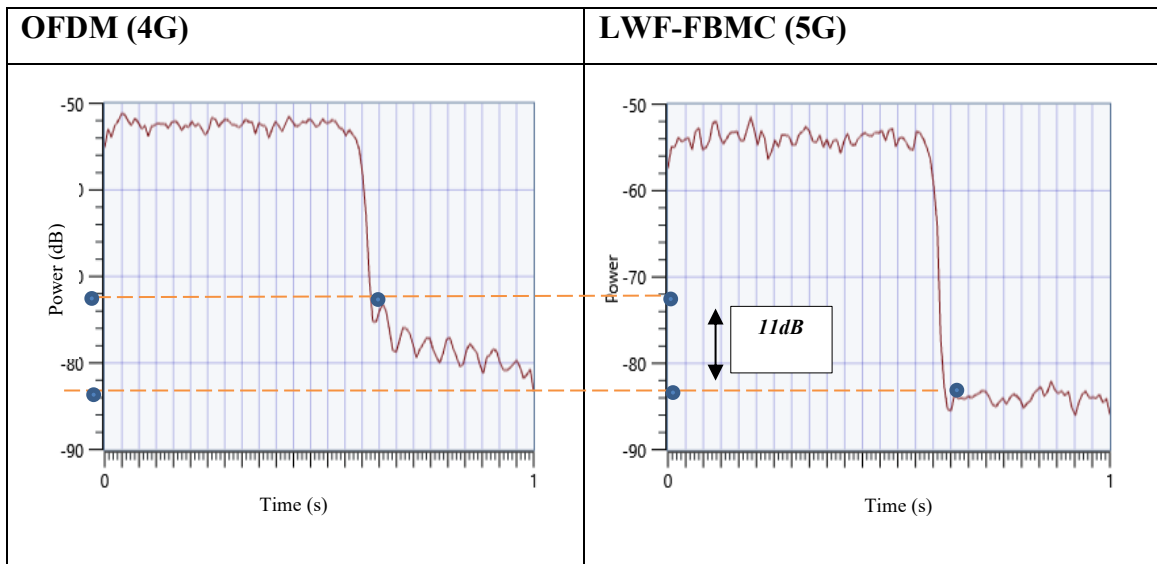
Figure 4.5 Power Spectral density (PSD) for Both LWF-FBMC and OFDM configurations

The PSD is the total of the signal's power over frequency. It can be explained that the waveform of OFDM sub-carriers has higher amplitude lobes than FBMC, where a difference of 11 dB of power was recorded. In other words, FBMC's amplitude is 15.4% lower than that of OFDM.

This shows that OFDM has a greater out-of-band (OOB) leakage where each sub-carrier affects the global spectrum shape. In the case of a non-perfect synchronization, the secondary lobe of the neighbouring sub-carrier will produce more inter-channel interference (ICI) in the case of OFDM.

Table 4.2 outlines the PSD comparison between OFDM (4G) and LWF-FBMC (5G) configurations.

Table 4.2 PSD Comparison between OFDM (4G) and LWF-FBMC (5G) Configurations

Item	PSD	
	OFDM	Proposed LWF-FBMC
Power	-75 dB	-86 dB
Improvement	15.4%	

4.3 DEVELOPMENT OF E-DSA ALGORITHM FOR 5G FBMC NETWORK

4.3.1 The Effectiveness of DSA Algorithm for 4G Configuration Using GNU Radio Software

The graph of the throughput comparison between the standard 4G configuration and the 4G configuration with DSA implementation for downlink communication is shown in Figure 4.6. It can be seen that the 4G configuration containing DSA consistently has greater throughputs than the standard 4G configuration.

Additionally, it is evident that the throughput falls as the noise amplitude rises. It can be observed that the throughputs for the 4G configuration incorporating DSA are always higher than that of the typical 4G configuration. Besides that, it can also be seen that as the noise amplitude increases, the throughput decreases.

The throughput of the DSA-implemented 4G setup is 50.2% higher than the standard 4G configuration when the noise amplitude is set to 1. The percentage difference then grows and becomes 67.2% when the noise level is raised to 2. However, the percentage difference grows significantly when the noise amplitude is adjusted to 5, compared to 3 and 4, respectively. Future studies will do additional research to examine the impact of noise amplitude.
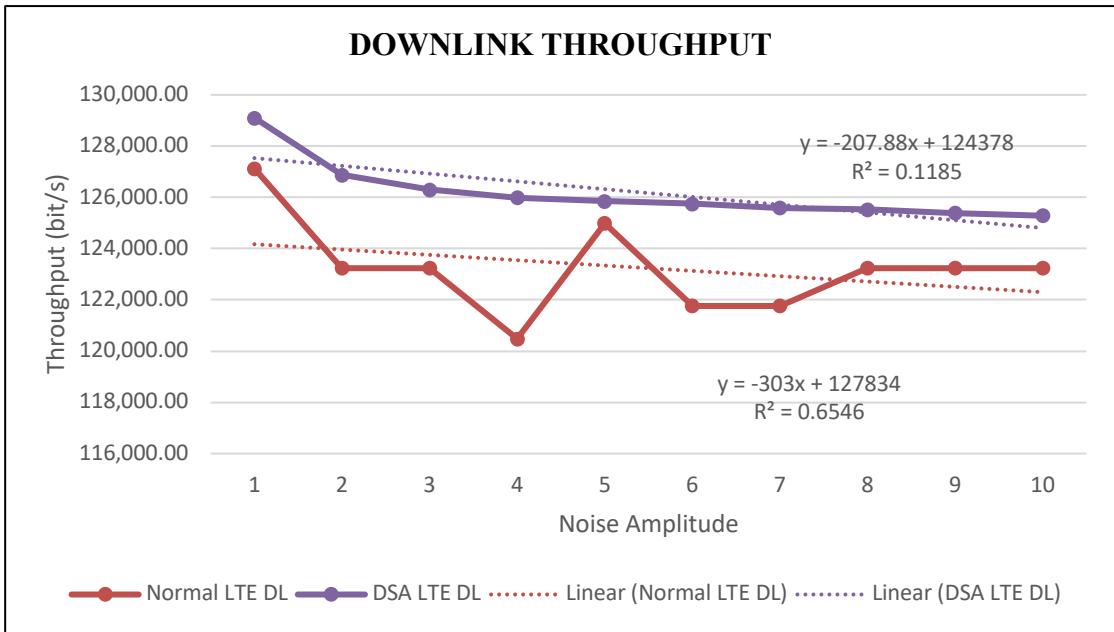
Figure 4.6 Comparison of Throughputs between Typical 4G Configuration and 4G Configuration with DSA Implementation for Downlink Communication
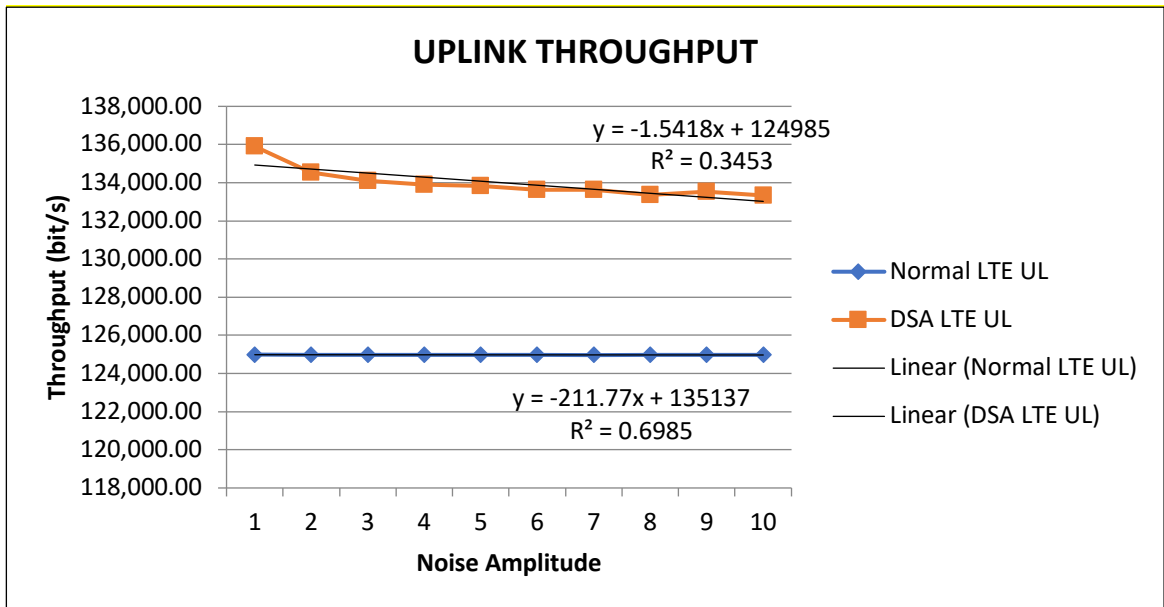
Figure 4.7 Comparison of Throughputs between Typical 4G Configuration and LTE Configuration with DSA Implementation for Uplink Communication

Figure 4.7 shows the graph of comparison of throughputs between typical 4G configuration and 4G configuration with DSA implementation for uplink communication. It can be observed that for the typical 4G configuration, the graph almost remains as a straight horizontal line when the noise amplitude ranges from 1 to 10. As for the 4G configuration with DSA implementation, the graph shows a smooth curve when the noise amplitude ranges from 1 to 10. The throughputs for 4G configuration with DSA implementation are always higher than that of the typical 4G configuration. Besides that, it can be seen that as the noise amplitude increases, the throughput decreases.

Table 4.3 summarizes the average percentage of throughput enhancement for the downlink and uplink configuration. It can be said that the throughput performance of 4G configuration is improved with the implementation of DSA technique, both for downlink and uplink communications. This in turn results in mitigating the cross- tier interference that exists in 4G heterogeneous network.

Table 4.3 Average Percentage of Throughput Enhancement for the 4G DSA Configurations

Item	Downlink Configuration	Uplink Configuration
Average throughput increment with DSA	30%	78%
Throughput Analysis	• **Without DSA implementation** - Low throughput performance that is prone to higher possibility of interference occurrences • **With DSA implementation** - High throughput performance resulting in mitigation of cross-tier interference in 4G heterogeneous network	

4.3.2 The Effectiveness of E-DSA for 5G FBMC Network Using LV Comm

4.3.2.1 Validity of E-DSA Algorithm
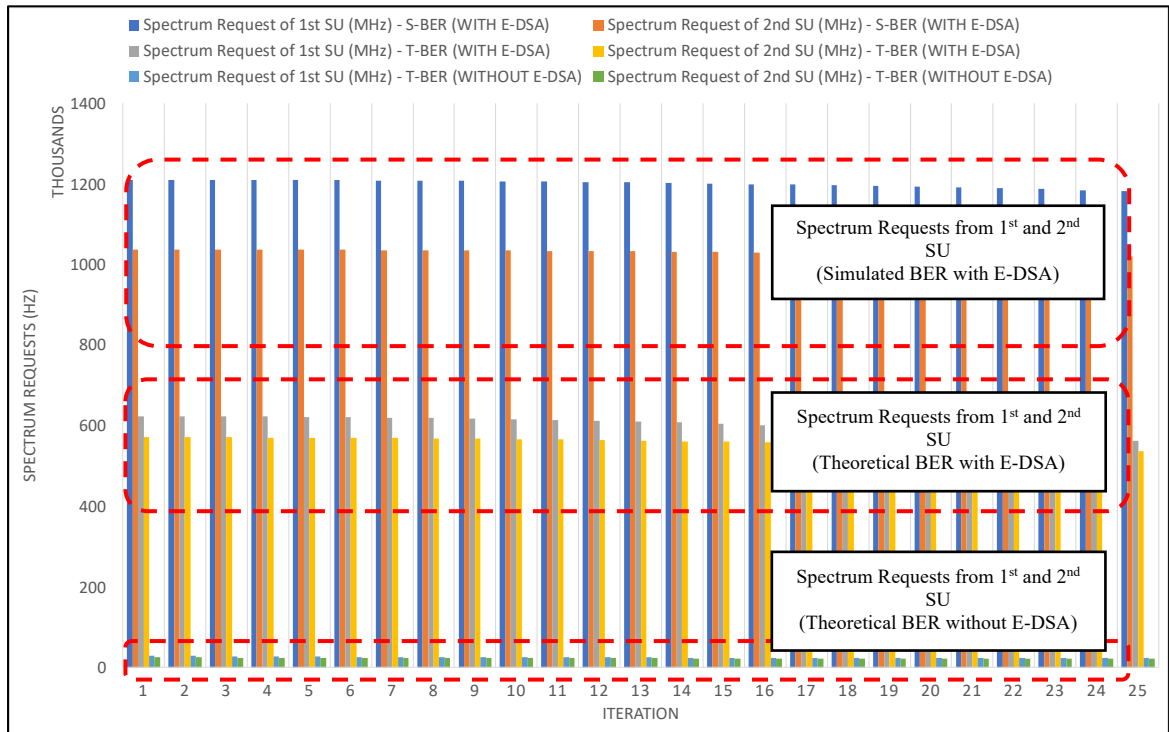
Figure 4.8 Spectrum Requests from 1st SU and 2nd SU

Figure 4.8 depicts the effect of SUs' price weight factors on spectrum allocation for the first and second SUs for both simulated BER (S-BER) and theoretical BER (T-BER). As seen in the figure, there are three different sections that represent different types of spectrum requests. The uppermost section represents the spectrum requests from the first and second SUs using the simulated BER values with E-DSA implementation. The middle section represents the spectrum requests from the first and second SUs using the theoretical BER values with E-DSA implementation. Lastly, the lowest section represents the spectrum requests from the first and second SUs using the theoretical values of BER without E-DSA implementation. It can be observed that the S-BER with E-DSA implementation has the highest spectrum requests, followed by the T-BER with E-DSA implementation, and lastly, the T-BER without E-DSA implementation.

Besides that, it can also be observed that the bandwidths obtained by the first SU for all conditions are always higher than that of the second SU, that is, when the price factor is set to 1 for the first SU and 2 for the second SU. This is because the higher the price weight factor, the higher the unit spectrum price, which may lead to overpayment of costs for the same bandwidth. For these conditions, their bandwidths will be reduced accordingly. Thus, when there is a sudden increment in SU's bandwidth request, the SU's price weight factor is increased by the PU to prevent the SU from gaining an excessive spectrum. This shows that the E-DSA algorithm is valid to be implemented.

4.3.2.2 Effectiveness of E-DSA for 5G FBMC

As explained earlier, the variation in the SINR affects the quality of the signal. SINR indicates the throughput capacity of the channel and is known as the strength of the signal divided by the strength of any interference. Thus, the higher the throughput, the lower the interference.
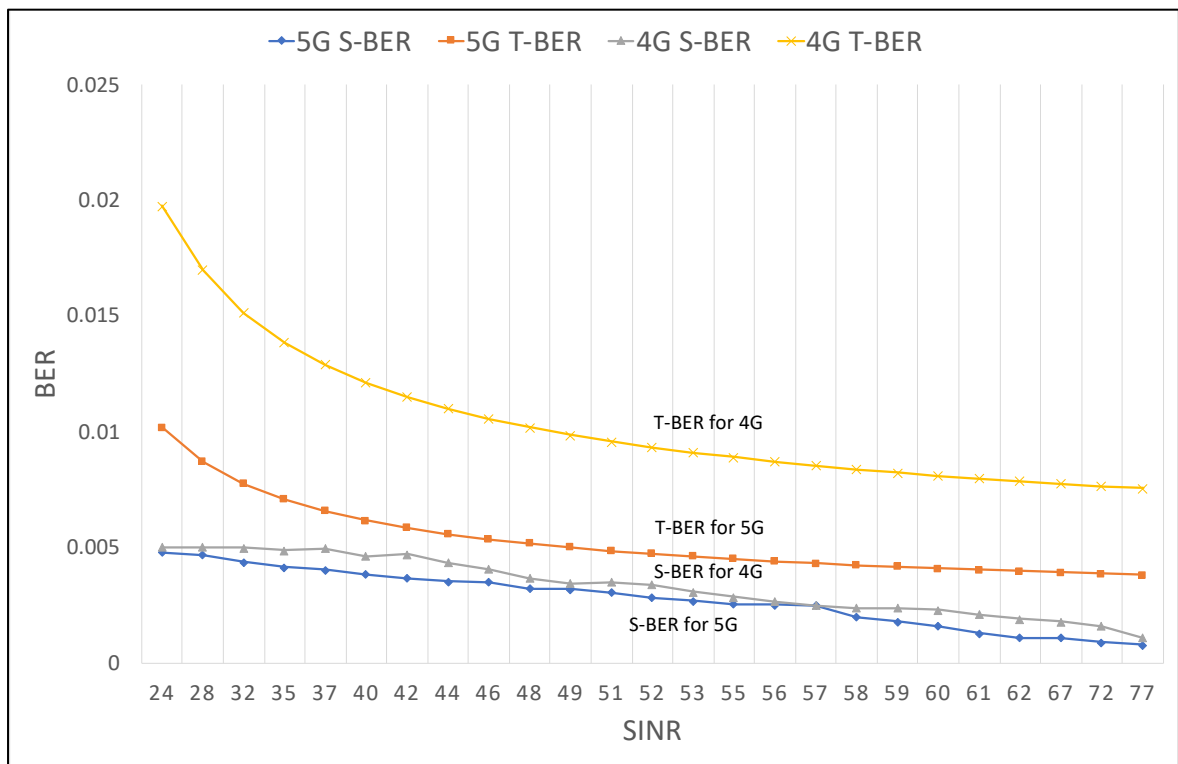
Figure 4.9 BER vs SINR Graph for Simulated and Theoretical BER Values of 4G OFDM and 5G FBMC

90

For this section, the simulated and theoretical BER values of 4G OFDM and 5G FBMC were determined and recorded. Figure 4.9 shows the BER vs SINR graphs for the configurations.

The graph of BER vs SINR was generated for SINR ranging from 0 to 80 dB. From the graph, it can be seen that 5G's simulated BER has the lowest readings as SINR increases. This shows that the simulation design produces a lower BER than the theoretical one. The same goes for the 4G OFDM configuration.

Figure 4.10 shows the throughputs calculated from the S-BERs and T-BERs for 5G FBMC configurations with and without E-DSA implementation. With E-DSA implementations, the throughputs for 5G FBMC configurations are always higher than that without E-DSA implementations for increasing SNR. This is true for both T-BER and S-BER. The average throughput increment for T-BER (Theoretical BER) was calculated from the difference between the throughput of FBMC configuration without E-DSA and the one with E-DSA. These throughputs were determined by implementing the calculated theoretical BER values.
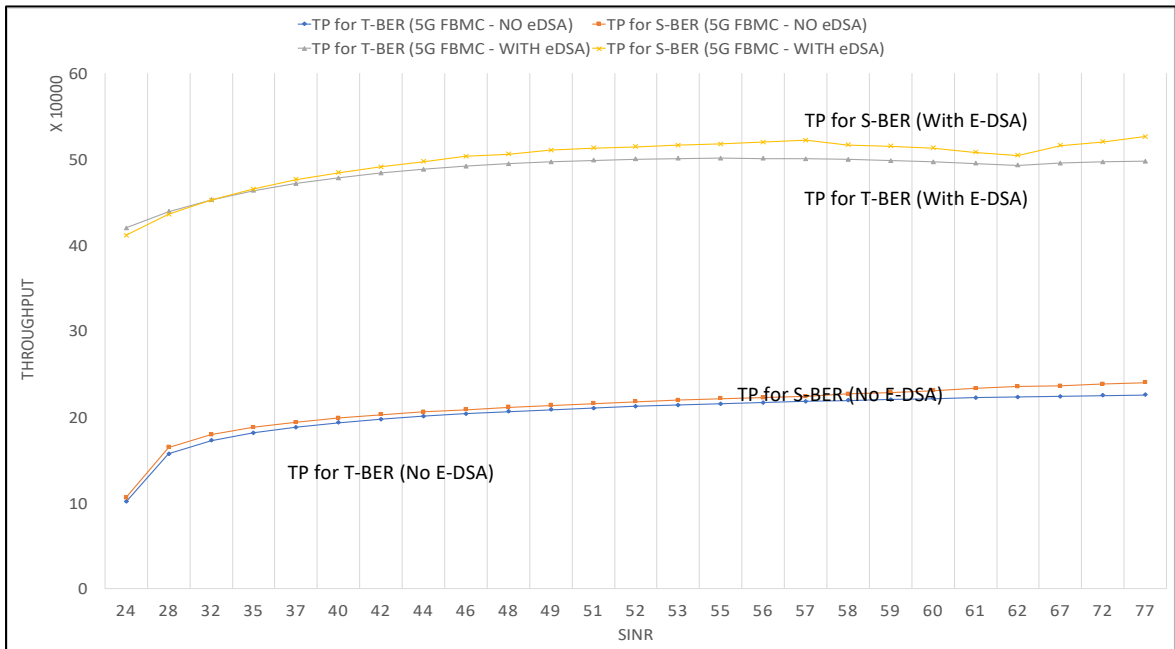
Figure 4.10 Throughput Analysis for T-BER and S-BER 5G FBMC Configuration with and without E-DSA Implementation

Besides that, the average throughput increment for S-BER (Simulated BER) was calculated from the difference between the throughput of FBMC configuration without E-DSA and the one with E-DSA. These throughputs were determined by implementing the BER values generated from the simulations.

By running the simulation design for 5G FBMC using the LV Comm communication software to determine the simulated BER readings for throughput calculation, the throughputs of 4% higher than that when using the theoretical BERs were identified. This shows that the throughput of the 5G configurations can be improved by combining the proposed 5G FBMC design using the software with the proposed E-DSA algorithm. Table 4.4 summarizes the average percentage of throughput enhancement for the configurations.

Table 4.4 Average Percentage of Throughput Enhancement for the Configurations

Item	Throughput Increment		
	Network Configuration		
	DSA 4G OFDM using simulated BER values **(S-BER)** **Othman, N. I. et. al, (2018)**	**Proposed E-DSA FBMC** using theoretical BER values **(T-BER)**	**Proposed E-DSA FBMC** using simulated BER values **(S-BER)**
Increment of percentage	30%	140%	144%
Improvement from DSA to E-DSA (using S-BER values)	114%		

4.4 PSD ANALYSIS USING NI USRP RIO FOR OFDM AND LWF-FBMC

This section presents the outputs from the integration between OFDM and LWF-FBMC simulation configurations using LV Comm software with the implementation of NI USRP 2943R hardware. The outputs were then analyzed using PSD analysis.

4.4.1 Validity of OFDM and FBMC Configurations Using NI USRP 2943R

As explained in Subsection 3.4.1 in Chapter 3, to validate that the transmitter and receiver's antennas are detected by the simulation designs, the transmitter's LED must light up in red (TX1), and the receiver's LED must light up in green (RX2). This means that the NI USRP 2943R is able to transmit and receive the signal successfully by integrating with the simulation design.

Figure 4.11 LED Lights for the Transmitter and Receiver for both OFDM and FBMC Configurations

93

Figure 4.11 shows the result of the LED lights on the NI USRP 2943R after running the simulation. It can be seen that transmitter's LED lights up in red and the receiver's LED lights up in green, which satisfied the signal's transmit and receive rule of the hardware. This means that the simulation designs for both OFDM and FBMC could transmit and receive data simultaneously in real time. Table 4.5 outlines the description of the LED indicators.

Table 4.5 Description of LED Indicators

LED		Description	Colour	State	Indication
RF0	TX1 RX1	Indicates the transmit status of the device.	OFF	-	The device is not active.
			Red	Solid	The device is transmitting data.
			Green	Solid	The device is receiving data.
	RX2	Indicates the receive status of the device.	OFF	-	
			Green	Solid	
RF1	TX1 RX1	Indicates the transmit status of the device.	OFF	-	The device is not active.
			Red	Solid	The device is transmitting data.
			Green	Solid	The device is receiving data.

	RX2	Indicates the receive status of the device.	OFF	-	The device is not receiving data.
			Green	Solid	The device is receiving data.

4.4.1.1 OFDM and LWF-FBMC's Transmitter and Receiver Outputs

Table 4.6 Constellation Outputs for OFDM
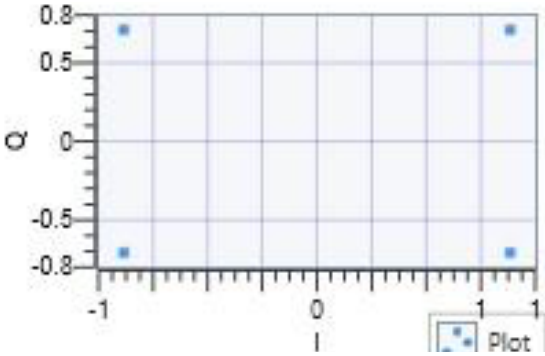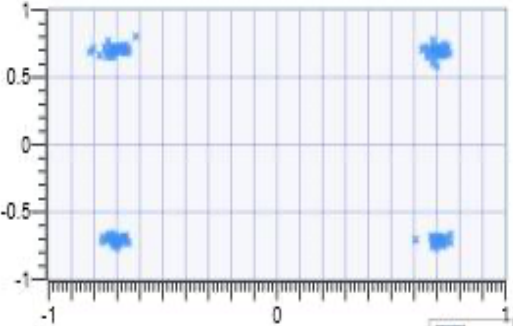
Transmitter
Receiver

Table 4.7 Constellation Outputs for LWF-FBMC

Transmitter
Receiver
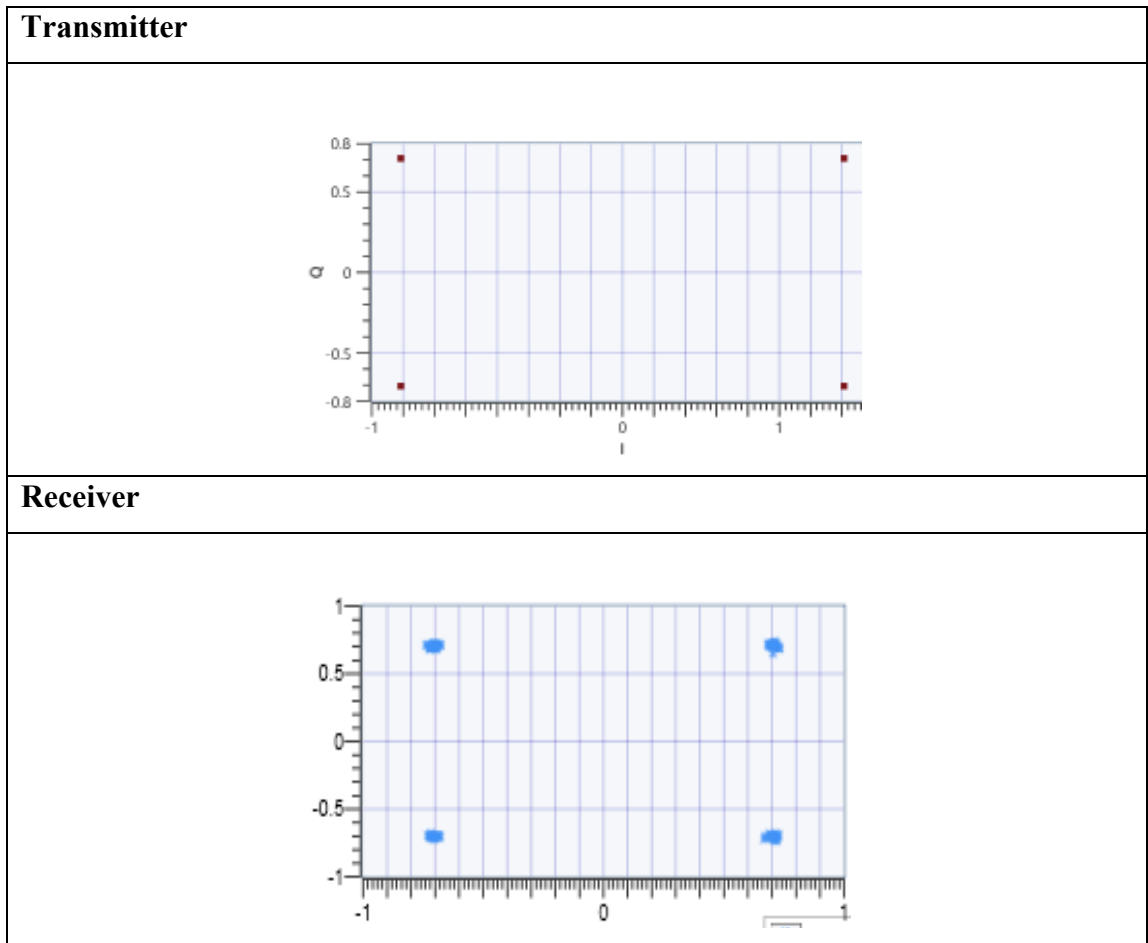
Tables 4.6 and 4.7 show the constellation outputs for OFDM and LWF-FBMC's results. It can be seen that the unequalized and equalized data plots demonstrate that the signal can be generated at any point. Even when interference is present, the receiver can receive almost the precise value of the QAM constellation points from the transmitter. In addition, it is also clear that the accuracy of the constellation diagram at the receiver determines how well the equalization works to reduce Inter-symbol Interference (ISI).

The simulation results found with the help of working setup of OFDM and LWF-FBMC system implementation using LV Comm software and NI USRP RIO hardware which conclude the successful transmission and reception of information bit using the QAM and OQAM techniques with equalized data and amplitude after both the OFDM and LWF-FBMC receivers. Therefore, it can be concluded that the proposed LWF-FBMC and

OFDM setups can successfully transmit and receive data by integrating both the simulation design and hardware implementation.

4.4.2 PSD Analysis

By referring to Table 4.8, it can be seen that LWF-FBMC's modulation strength is closer to the normalized frequency as compared to OFDM. The frequency width for the OFDM configuration is 5 GHz, whereas the frequency width for LWF-FBMC is 2.5 GHz.

Table 4.8 Generated PSD Signals

Generated PSD	
OFDM	

LWF-FBMC	
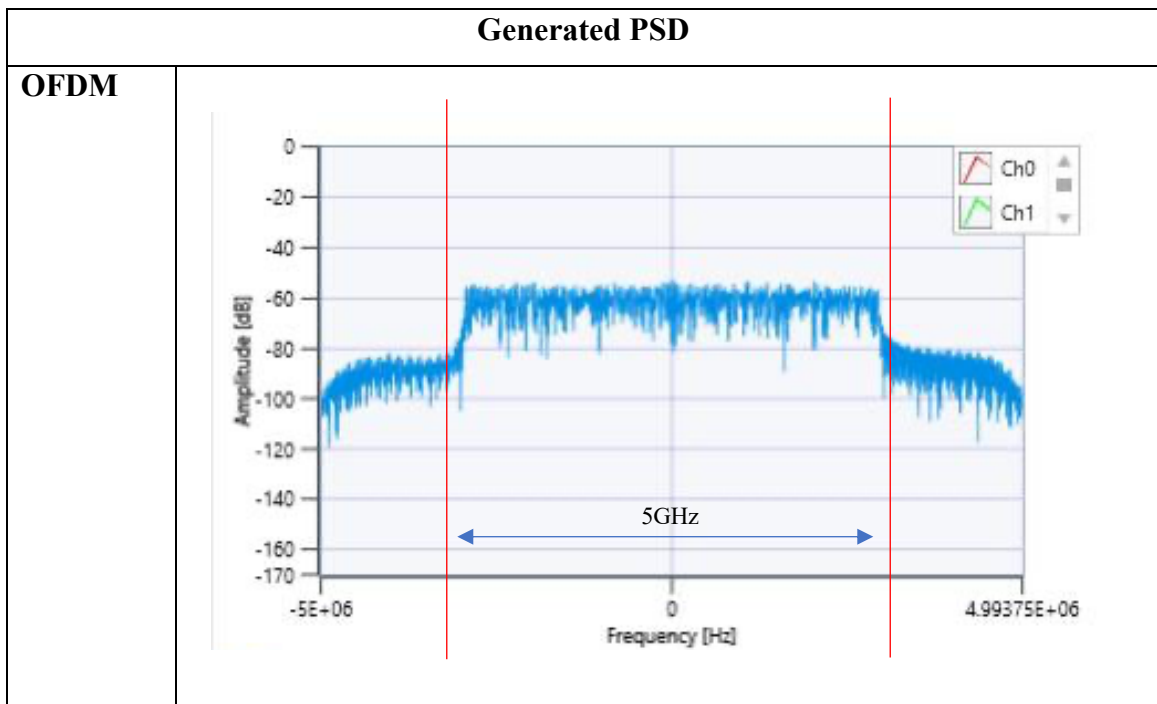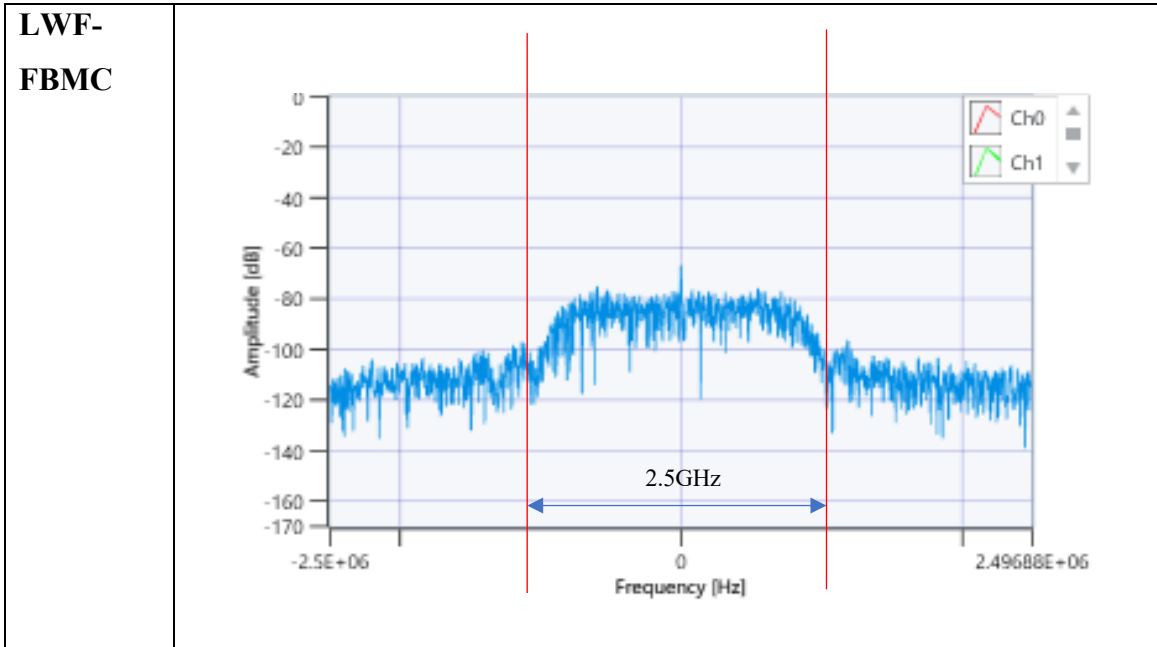
For the PSD analysis, as explained earlier in Chapter 3, if a modulation's strength is closer to the normalized frequency, the spectral density of the modulation is more effective. The signal's strength with time and the potential bandwidth over which bits can be successfully conveyed are represented by the spectral density. Table 4.9 shows the difference in modulation strengths between OFDM and LWF-FBMC.

Table 4.9 Modulation Strengths Generated between OFDM and LWF-FBMC

Configuration Type	Modulation Strength	Percentage Difference
OFDM	5 GHz	50%
LWF-FBMC	2.5GHz	

Besides that, by comparing the two figures in Table 4.8, it can be observed that the rectangular windowing has changed the relative gains of the two waveforms. In contrast to LWF-FBMC, which does not interfere with the nearby sub-channel lobes, OFDM exhibits severe sidelobes. As a result of the polyphase network, where the energy is concentrated within the frequency range of a single subcarrier, we discovered that the OFDM subcarriers are reduced in comparison to FBMC subcarriers.

This shows that LWF-FBMC has higher spectral efficiency than OFDM in real-time analysis. Due to the non-linearity of the high power amplifier (HPA), the advantage of FBMC-OQAM systems over OFDM ones in terms of spectrum localization is lost, and it is crucial to forecast the PSD regrowth of the amplified FBMC-OQAM signal.

On the other hand, the adoption of cyclic prefix in OFDM-based system reduces the total network's spectral efficiency. As a consequence, the FBMC access technique providing better network performance is practical and therefore recommended in the future wireless communication 5G networks.

4.5 DISCUSSION OF RESULTS

4.5.1 Enhanced FBMC as 5G's Multiplexing Method

The spectrum energy distribution that would be found per unit of time is referred to as the power spectral density (PSD). Considering that such a signal's overall energy would typically be infinite. A random or periodic signal's frequency response is referred to as the power spectral density. In terms of power per radian per sample, the power spectral density is determined. The size of the power spectral density and the range of the corresponding normalised frequencies are determined by the length N of the FFT and the values of the input.

The PSD analyses done for both OFDM and FBMC found that FBMC produced the lowest OOB emissions. This is because the FBMC transmit signal is configured for the out-of-band leakage to be minute. This causes an enhanced utilization of the spectrum, leading to improved efficiency of the spectrum usage. With less stringent synchronisation requirements and less spectrum efficiency, FBMC offers solutions to get around OFDM's well-known drawbacks. The properties of FBMC enable a developed PSD and a leading utilisation of the allotted spectrum. Because of this, the FBMC scheme is better than traditional OFDM.

For OFDM, the orthogonality is not ensured for all subcarriers but in FBMC each carrier is individually filtered and orthogonality is achieved by applying Offset-Quadrature Amplitude Modulation (OQAM). Moreover, FBMC instead of using circular convolution, use linear convolution in order to reduce out-of-band (OOB) emission for the sake of robustness against synchronization errors and to protect its spectral density properties

Subsequently, the type of prototype filter used also distinguishes the performance between FBMC and OFDM. The study also performed a PSD analysis for the prototype filters, and the PSD of FBMC outperformed FBMC by 15.4% after applying the newly proposed LWF-Hamming filter to the FBMC's design. Due to the various selections of the various pulse shaping or spectrum shaping filters, it can clearly detect performance disparities such as OOB emission in a shared spectrum framework. It is possible to use the sideband envelope's empirical quantification as an upper bound limit for measurements of OOB emission.

Since the signal's strength with time, or the potential bandwidth over which bits can be successfully conveyed, is represented by the spectral density. If a modulation's strength is nearer to the normalised frequency, the spectral density of the modulation is more effective.

For FBMC, the spectral leakage issue can be mitigated because the filter was designed with the Nyquist pulse shaping theory, whereas OFDM implements a rectangular window filter. This resulted in a very small inter-channel interference (ICI) and inter-symbol interference (ISI) for the FBMC configuration. Hence, it confirms the setup to encompass better spectral efficiency as compared to OFDM.

This was also proven through the hardware implementation test and analysis using NI USRP 2943R, which observed that PSD for the FBMC is 50% higher than that of OFDM. The time frequency localization (TFL) feature, staggered OQAM symbols, actual symbols at twice the symbol rate of QAM, and pulse shaping using an IFFT/FFT-based filter bank are all effectively used by FBMC.

However, this objective did not consider the E-DSA implementation for hardware implementation because of several limitations such as the limited laboratory space and limited research period. This can be done in the near future for better testing of the algorithm in real time.

Even though FBMC is more sophisticated than OFDM, it can offer significantly lower out-of-band emissions, robustness against carrier frequency offset, and superior spectral efficiency because cyclic prefix is not necessary. Table 4.10 shows the summary of the PSD analyses' results between OFDM and FBMC.

Table 4.10 Summary of The PSD Analyses' Results between OFDM and FBMC

| Testing Mechanism | Software / Hardware Used | PSD Analysis | | Percentage of Improvement |
		OFDM	Proposed FBMC	
Prototype Filters	Matlab	Normalized Frequency: -30 GHz	Normalized Frequency: -15 GHz	50%
Simulation Design	LV Comm	Power: -75 dBm	Power: -86 dBm	15.4%
Simulation-Hardware Integration	Software: LV Comm Hardware: NI USRP 2943R	Normalized Frequency: -5 GHz	Normalized Frequency: -2.5 GHz	50%

With OFDM, a frequency selective channel is transformed into N frequency flat channels by dividing the overall bandwidth into N sub-bands with equal spacing. Since the modulating carriers are orthogonal, they do not interfere with one another. Inverse fast Fourier transform (IFFT) is used at the transmitter side to fulfil this criterion. On the receiver side, fast Fourier transform (FFT) is utilised to retrieve the information. The next channel is chosen by leaving a guard band, however the OFDM waveform exhibits a wide sideband. The addition of guard bands renders OFDM spectrally wasteful. As a result, a novel method called FBMC is presented to enhance the spectral efficiency of multi-carrier transmission. The power spectral density (PSD) of the waveform is sharpened by FBMC using extend IFFT, which boosts spectral efficiency.

To further understand regarding the comparison of between OFDM and FBMC based on the percentage of improvements shown in Table 4.10, a summary of the differences and analysis between the two techniques are outlined in Table 4.11. The parameters that were analyzed are the cyclic prefix adoption, modulation type, prototype filter, orthogonality and frequency exploitation.

Table 4.11 Summary of PSD Analyses between OFDM and FBMC

Parameters	Multiplexing Methods		Analysis
	OFDM	Proposed FBMC	
Cyclic Prefix (CP)	CP is needed	No CP needed	Maximized spectral efficiency for FBMC
Modulation type	Higher order of QAM for full duplex	Higher order of OQAM modulation for full duplex. QAM Modulation for half-duplex.	OQAM in FBMC in needed to fully exploit the spectrum and to maintain orthogonality between sub channels
Prototype filter	Rectangular	Proposed LWF-Hamming	Localized frequency coefficients are added in the form of LWF-Hamming filter, which fruits to low OOB emissions
Orthogonality	Requires orthogonality in subcarriers	Requires orthogonality in adjacent sub-channels only	Neighbouring channels orthogonality is achieved using OQAM modulation
Frequency Exploitation	Divides the given frequency into number of sub carriers	Divides the given frequency into number of sub channels	Polyphase Network (PN) along with OQAM accomplish the task for full

			throughput in FBMC

4.5.2 E-DSA as 5G FBMC's Improved Interference Mitigation Technique

Firstly, a DSA scheme can manage different levels of coordination. It can protect the incumbent user from being interfered by secondary users, or it can additionally coordinate secondary users among themselves. The first can be achieved, depending on the incumbent characteristics, by a multi-tier data base approach such as E-DSA for 5G. Concerning the automation of the spectrum allocation, it offers great potential, standardized procedures are already included for machine type communication.

It has been demonstrated that the configuration provides greater throughput for 4G than a heterogeneous network design without the DSA implementation. The simulation results supported the idea that interference in a heterogeneous network can be successfully reduced by providing evidence in its favour. The throughput values were established and computed based on the recorded and compared BER values. The DSA architecture has a better throughput and a lower BER value, according to the data. Interferences must be reduced and system throughput must be increased in order to boost spectral efficiency.

Due to the addition of an intermediary service layer that serves as a private network operator, E-DSA for 5G exhibits a higher level of complexity than DSA for 4G from a complexity perspective. Such a service is helpful in the context of professional applications since it can improve the spectrum quality or the degree of QoS during operation.

However, the proposed E-DSA for 5G FBMC configuration's system model promotes an enhanced spectrum utilization where through spectrum sensing, the SUs obtain information about the PU's available spectrum, including as its size and quality, and relay those details to the base station. Then, with the help of the base station, the SUs negotiate for the spectrum using the Nash bargaining approach to satisfy the communication needs and increase systemwide revenue.

Table 4.12 summarizes the desirable parameter values for both cases, the coordination of primary and secondary users with and without E-DSA implementation. automatic

Table 4.12 Summary of Coordination between PUs and SUs

Parameter	Coordination of PU and SU (Without E-DSA)	Coordination of PU and SU (With E-DSA)
Sharing dimension	- Frequency - Geography - Time	- Frequency - Geography - Time
Sensing	No	Yes
Coordination	Sharing rules	- Sensing - Sharing rules
Deployment	Local	Local
Classification	- Data base access - Set of sharing rules	- Data base access - Set of sharing rules - Sensing - Dynamic interference prediction

A further combination of the improved concepts into a single framework, which combines both mentioned variations of coordination, would significantly increase the application possibilities and significantly increase the efficiency of spectrum utilization.

Secondly, the BER vs SINR analysis showed that 5G's simulated BER has the lowest readings as SINR increases. Hence, the simulation design produces a lower BER than the theoretical one. The same goes for the 4G OFDM configuration. This result indicates that FBMC performs better than OFDM as their BER values are always lower than that of OFDM since the variation in the SINR affects the quality of the signal. the

SINR measures signal quality, which is the strength of the wanted signal compared to the unwanted interference and noise.

Mobile network operators seek to maximize SINR at all sites to deliver the best possible customer experience, either by transmitting at a higher power, or by minimizing the interference and noise. In communications theory, the Shannon's Limit is the theoretical maximum bandwidth of a channel and is a function of the SINR. Thus, optimizing SINR leads to more base station capacity, allows higher order QAM modulation (which are more spectrally efficient), resulting in higher peak data rates, fewer dropped calls, and ultimately improved customer satisfaction.

A healthy SINR is critical to maximizing data capacity and throughput. Even though two subscribers may use the same amount of spectrum, their respective signal quality (SINR) determines their throughput. This is because the higher the SINR, the higher the QAM modulation that can be achieved, and hence the higher the data rate that the subscriber will experience. In the lower frequency bands and for busy cell sites, a low SINR has an outsized negative impact so SINR optimization is particularly important in these cases. This indicates that the E-DSA scheme implemented can reduce the errors contained in the system configuration. The users can receive the signal transmitted more efficiently and with fewer errors.

Thirdly, by comparing the average throughput increments between DSA 4G OFDM and E- DSA 5G FBMC configurations, it is proven that the E-DSA for 5G FBMC produces higher improvements than that of DSA 4G OFDM, that is, by 114%, as shown in Figure 4.13. It can clearly be said that FBMC performs better than OFDM as their BER values are always lower than that of OFDM.

The E-DSA algorithm ensures that the allocation logic would continue to iterate until all subcarriers are occupied. This explains why the algorithm is very efficient and can minimize errors. Therefore, with minimized errors, the interference is also mitigated. As a result, this shows that the BER reduction of the 5G FBMC configuration with E-DSA implementation is better than that of the 4G OFDM configuration even with the DSA implementation.
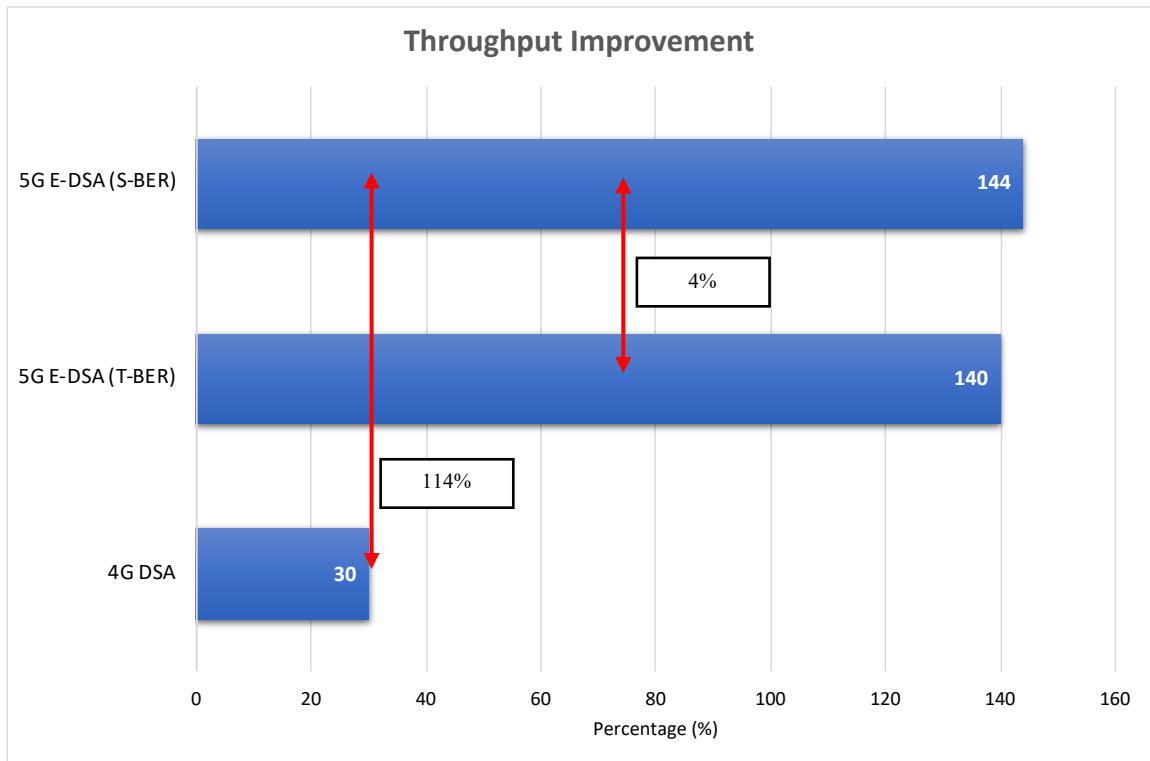
Figure 4.13 Comparison of Throughput Improvements between 4G DSA, 5G E-DSA (T-BER) and 5G E-DSA (S-BER)

The throughput analyses demonstrated that the throughputs could be maximized in both 4G and 5G heterogeneous network setups when implementing DSA for 4G and E-DSA for 5G. This was proven by observing the previous throughput graphs for 4G with DSA implementation that is always higher than that of the typical 4G configuration. It was observed that in a heterogeneous network consisting of macrocell and femtocell and their users, the throughputs can be maximized when implementing the DSA technique.

This in turn results in mitigating the cross-tier interference that exists in 4G heterogeneous network. Crosstalk and noisy call backgrounds are two impacts of interference on voice lines. Calls that are frequently dropped could be the result of interference on control channels. With maximized throughput in a heterogeneous network, unwanted scenarios such as drop calls and loss of signal caused by cross-tier interference can be mitigated.

On the other hand, the same goes when E-DSA was implemented in the 5G configuration. The E-DSA technique's throughput performance outperformed the DSA's by an improvement of 104%. This shows that the E-DSA model implemented in the 5G network can reduce the interference that exist in the network tremendously as compared to the DSA model used for 4G. Figure 4.14 shows the overall summary of the discussions of results for all the three objectives of this research.
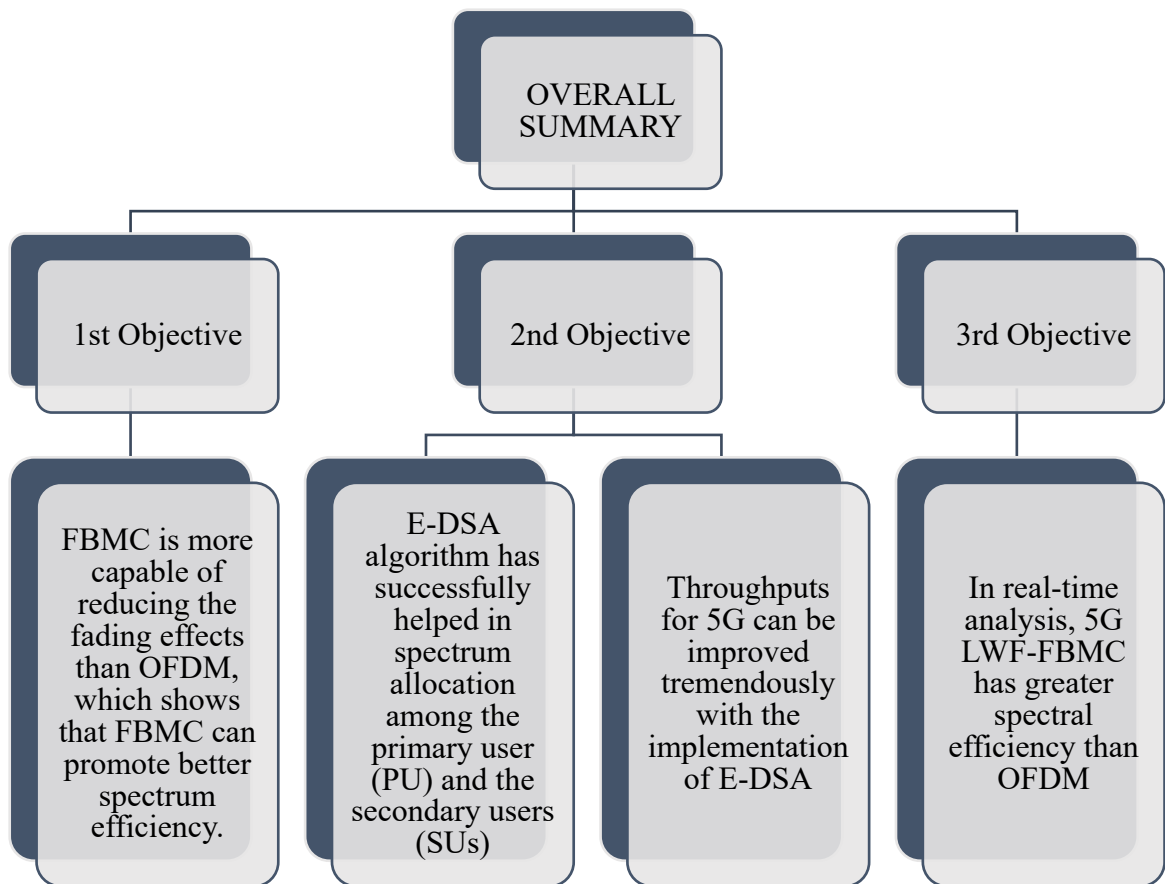
Figure 4.14 Overall Summary of the Discussions of Results for All the Three Objectives

4.6 CHAPTER SUMMARY

Throughout this chapter, the data was collected from the simulations generated using LV Comm software for both 4G OFDM and 5G FBMC configurations and analyzed based on PSD analysis. In addition, an enhanced E-DSA algorithm was developed, and its effectiveness was compared with the DSA for 4G.

The results have also been calculated based on the formulas outlined in Chapter 3 and discussed in terms of their throughput performances. The formulas used were based on the macrocell and microcell network configurations. Lastly, the effectiveness of the OFDM and FBMC simulation designs were tested using NI USRP 2943R hardware.

Based on the collected results, it can be said that the 5G E-DSA configuration coupled with the enhanced FBMC multiplexing method is without a doubt a promising model for interference mitigation in 5G heterogeneous network as it can definitely enhance the throughput performance tremendously within the network.

CHAPTER FIVE

CONCLUSION

5.1 SUMMARY

The emerging demand for the high-speed network has caused many researchers to embark on studies focusing on means of enhancing the performance of the 5G wireless network. The techniques on how to reduce the interference that causes drop calls and loss of signal are being widely researched. Of all the interference mitigation techniques being studied, it has been found that the Dynamic Spectrum Allocation (DSA) technique is one of the best techniques to be implemented in the 5G network. In this research, the proposed Nash Bargaining Solution (NBS) coupled with the FBMC multiplexing method has been shown to successfully produce an enhanced DSA (E-DSA) algorithm. It has been presented that the proposed setup manages to alleviate the interference in the 5G network, in other words maximizing the throughput. A software-defined radio was utilized during the rapid prototyping process To test the performance. The setup offered flexibility in facilitating the development process of an agile communication system, such as OFDM and FBMC.

For the first objective, the spectral analysis of OFDM and LWF-FBMC was carried out by computing the PSD for both configurations. The configurations of OFDM and FBMC were designed and implemented using LabVIEW Communications software (LV Comm). Both the configurations' designs were submitted to the flat fading Rayleigh channel to test the performance in an urban environment. Based on the simulation results, the sidelobe of FBMC's waveform was seen to be 15.4% lower than that of OFDM's, which proved that FBMC has lower out-of-band (OOB) radiation than OFDM. Thus, it can be concluded that FBMC is more capable of reducing the fading effects than OFDM, which shows that FBMC can promote better spectrum efficiency.

For the second objective, an enhanced dynamic spectrum allocation (E-DSA) was developed by combining the FBMC 5G configuration with the cooperative game theory called the Nash Bargaining Solution (NBS) for spectrum allocation to improve the 5G network's throughput performance. The FBMC transceiver was designed and simulated

using LV Comm software to obtain the BER values. The BER values were then incorporated into the E-DSA algorithm to maximize the system's throughput. The first result has shown that the E-DSA algorithm has successfully helped in spectrum allocation among the primary user (PU) and the secondary users (SUs), where the bandwidth requests by the secondary users were supported by the bandwidth availability of the primary user (PU). The price weight factors were used to control and prevent the overpayment of costs of SUs' bandwidth requests. Secondly, for throughput maximization, it was proven that the throughputs for 5G can be improved tremendously with the implementation of E-DSA. An increment of 140% of throughput was theoretically calculated, and 144% of the increment was recorded from the simulation design.

Lastly, for the third objective, with the hardware implementation using NI USRP 2943R as the transceiver, the simulation designs for OFDM and LWF-FBMC had been successfully assembled. The results have shown that between OFDM and LWF-FBMC, the modulation strengths differ by 50%, with LWF-FBMC being closer to the normalized frequency as compared to OFDM. This demonstrates that in real-time analysis, LWF-FBMC has greater spectral efficiency than OFDM.

5.2 IMPLICATIONS

This study has shown that the 5G configuration in a heterogeneous network environment with E-DSA implementation has a greater throughput than one without the DSA implementation. The outcomes of the simulations supported the idea that interference in a heterogeneous network can be admirably reduced. In this light, spectral efficiency can be improved by avoiding interferences and maximizing system throughput. In this regard, this study has demonstrated that the research goals outlined in Chapter 1 of this thesis have been met. Additionally, it could be possible to pursue empirical analysis incorporating a more extensive implementation using NI USRP RIO hardware in the very near future. Extended designs like MIMO and multiple-channel setups may be used. The parameters proposed in this thesis, which are compatible with the constraints of the laboratory, will serve as the foundation for the experimental results. The results can support hardware system compatibility, which validates that it can be used in practical settings.

5.3   RECOMMENDATIONS

Based on the newly proposed LWF-FBMC modulation and E-DSA technique in mitigating interference in the 5G heterogeneous network, the study makes the following recommendations for directions in future research:

1.   Experimental Scenarios

The E-DSA results in this study were solely derived from simulations run on the LV Comm software platform. Future comparisons between the simulation findings and the real-time configuration should take into account a hardware implementation. It is also recommended to use a frequency of 2.6 GHz for 4G and a frequency of 3.5 GHz for 5G configurations.

2.   Performance Metrics

Besides PSD, BER, and throughput, other metrics such as peak average-to-power ratio (PAPR) and the Error Vector Magnitude measurement against the output power of the hardware could also be included for analysis.

3.   Adaptive Features

Future research could examine adaptive characteristics, including varying the distance between the transmitter and receiver, the SINR, the allotted subcarrier per channel quality need, and the transform scheme (such as wavelet).

REFERENCES

Abdulhakeem, B. S., Gwassi, O. A. & Hasan, R. S. (2022). *Spectrum Sharing Techniques for Improving the Quality of Service*. International Symposium on Multidisciplinary Studies and Innovative Technologies (ISMSIT), 2770-7954.

Ahmadi, H., Katzis, K., Shakir, M. Z., Arvaneh, M. & Gatherer, A. (2020). *Wireless Communication and the Pandemic: The Story So Far*. ComSoc Technology News (CTN), CTN Issue: April 2020

Al-Amodi, A. M. A. & Datta, A. (2020). *The Impact of Heterogenous Ultra-dense Network Technologies on the Performance of 4G and 5GNetworks*. International Journal of Innovative Technology and Exploring Engineering (IJITEE). Volume-10 Issue-1.

Al-Jawhar, Y. A., Ramli, K. N., Taher, M. A., Shah, N. S. M., Mostafa, S. A. & Khalaf, B. A. (2020). *Improving PAPR performance of filtered OFDM for 5G communications using PTS*. ETRI Journal. 2021;43(2):209–220.

Alam, M. J., Hossain, M. R., Azad, S. & Chugh, Ritesh. (2023). *An overview of LTE/LTE-A heterogeneous networks for 5Gand beyond*. Transactions on Emerging Telecommunications Technologies published by John Wiley & Sons Ltd, e4806.

Altay, C. & Koca, M. (2019). *Capacity Analysis and Optimization for Energy Efficient Heterogeneous Networks*. IEEE Wireless Communications and Networking Conference (WCNC), 1525-3511.

Anand, A., de Veciana, G. & Shakkottai, S. (2020). *Joint scheduling of URLLC and eMBB traffic in 5G wireless networks*. IEEE/ACM Network, volume 28, no. 2, pp. 477–490.

Bellanger, M. (2010). *Physical layer for future broadband radio systems*. 2010 IEEE Radio and Wireless Symposium (RWS).

Bithas, P. S. & López-Martínez, F. J. (2021). *Throughput Analysis in a Wireless Powered Mobile Communication System*. IEEE Access Vol. 9.

Bogale, T. E. & Le, L. B. (2016). *Massive MIMO and mmWave for 5G Wireless HetNet*. IEEE vehicular technology magazine, 1556-6072/16.

Chalaliya, H. A., Dave, N. T. & Dastoor, S. K. (2018). *Interference Mitigation Technique for Downlink Cellular Network by Advanced Receiver and Scheduling Mechanism*. International Journal of Engineering Research & Technology (IJERT), Vol. 7 Issue 02.

Choudhary, G., Kim, J. & Sharma, V. (2019). *Security of 5G-Mobile Backhaul Networks: A Survey*. Journal of Wireless Mobile Networks, Ubiquitous Computing, and Dependable Applications (JoWUA), 9:4, pp. 41-70.

Devi, M., Sarma, N., & Deka, S. K. (2021). *A Double Auction Framework for Multi-Channel Multi-Winner Heterogeneous Spectrum Allocation in Cognitive Radio Networks*. IEEE Access, Volume 9.

Ericsson. (2013). *5G Radio Access, Research and Vision*. White paper.

FP7-ICT Future Networks PHYDYAS—PHYsical Layer for DYnamic AccesS and Cognitive Radio Project (ICT-211887).

Franzin, R.P. & Lopes, P.B. (2017). *A Performance Comparison between OFDM and FBMC in PLC Applications*. 2017 IEEE Second Ecuador Technical Chapters Meeting (ETCM).

Fooladivanda D. & Rosenberg C. (2013). *Joint resource allocation and user association for heterogeneous wireless cellular networks*, IEEE Transactions on Wireless Communications, 12(1):248–257.

Gentile, K. (2007). *Digital Pulse-Shaping Filter Basics*. Analog Devices AN-922 APPLICATION NOTE.

Jakes, W. (1974). *Microwave Mobile Communications*. New York: Wiley.

JENDELA Report. (2021). *Network Complaints by Service Provider*. 7 April 2021.

Irram, F., Ali, M., Maqbool, Z., Qamar, F. & Rodrigues, J. J. (2020). *Coordinated Multi-Point Transmission in 5G and Beyond Heterogeneous Networks*. IEEE 23rd International Multitopic Conference (INMIC), doi:10.1109/inmic50486.2020.9318091.

Kansal, P. & Shankhwar, A. K. (2017). *FBMC vs OFDM Waveform Contenders for 5G Wireless Communication System*. Wireless Engineering and Technology, 2017, 8, 59-70.

Kebede, T., Wondie, Y., Steinbrunn, J., Kassa, H. B., and Kornegay, K. T. (2022). *Multi-Carrier Waveforms and Multiple Access Strategies in Wireless Networks: Performance, Applications, and Challenges*. IEEE Access, Volume 10.

Koley, S., Bepari, D. & Mitra, D. (2019). *Predictive Multi-user Dynamic Spectrum Allocation Using Hidden Semi-Markov Model*. Journal of Communications Technology and Electronics, Volume 63, Issue 12.

Kumar, T. D. & Venkatesan, P. (2019). *Performance estimation of multicarrier CDMA using adaptive brain storm optimization for 5G communication system in frequency*

selective fading channel. Kumar, T. D., & Venkatesan, P. (2019). Transactions on Emerging Telecommunications Technologies, e3829.

Liu, Z. (2011). *The Modelling and Simulation of Rayleigh Flat Fading Channels Based on SCILAB*. IEEE International Workshop on Open-Source Software for Scientific Computation, 12-14 Oct 2011.

Metis. (2013). *Scenarios, requirements and KPIs for 5G mobile and wireless system*. ICT-317669 METIS project.

MT Rayleigh Selective Fading profile (Jakes). Available online: ni.com/documentation/en/labview-comms/1.0/mt-node-ref/mt-rayleigh-selective-fade-profile-jakes/ (accessed on 1st April 2022).

Nakamura, T., Nagata, S., Benjebbour, A., Kishiyama, Y., Tang, H., Shen, X., Yang, N. & Li, N. (2013). *Trends in Small Cell Enhancements in LTE Advanced.* IEEE Communications Magazine, volume 51, no. 2, pp. 98 – 105.

Nash, J. F. (1950). *The bargaining problem*. Econometrica, 18 (195), 155 - 162.

Othman, N. I., Ismail, A. F., Hasan, M. K., Badron. K. & Hashim, W., *Throughput Analysis on Dynamic Spectrum Al-location Technique to Mitigate Interference on LTE Heterogeneous Network*. Vol. 11, No. 4 (2018), pp.95-104.

Proakis, J. G. & Manolaokis, D. G. (2013). *Digital Signal Processing: Principles, Algorithms, And Application*. 4th Edition, Pearson Education, pp.654.

Raghavan, V. (2005). *A Comparative Study of Rayleigh Fading Wireless Channel Simulators*. A thesis submitted to Texas A&M University.

Rani, S. S. (2016). *Power Spectral Density in Communication Systems*. Conference: Faculty Development Program, Sri Ramakrishna Institute of Technology.

Roessler, A. (2019). *5G waveform candidates*. Rohde & Schwarz GmbH & Co. KG, Application Note, 1MA271, Munich, Germany, pp.1-60.

Siddiqui, M. U. A, Qamar, F, Ahmed, F., Nguyen, Q. N. & Hassan, R. (2021). *Interference Management in 5G and Beyond Network: Requirements, Challenges and Future Directions*. IEEE Access, 9, 68932–68965.

Shami, T. M., Grace, D., Burr, A. & Vardakas, J. S. (2019). *Load balancing and control with interference mitigation in 5G heterogeneous networks*. EURASIP Journal on Wireless Communications and Networking, Article number: 177.

Shi, J., Yang, L-L & Ni, Q. (2017). Novel Intercell Interference Mitigation Algorithms for Multicell OFDMA Systems With Limited Base Station Cooperation. IEEE Transactions on Vehicular Technology, Volume: 66, Issue: 1.

Suhaib Ahmed, Mudasir Bashir & Ashish Suri. (2014). *Low Pass FIR Filter Design and Analysis Using Hamming, Blackman and Kaiser Windows*. International Journal of Advanced Research in Electrical, Electronics and Instrumentation Engineering. Vol. 3, Issue 4, April 2014.

Sundus Naseer, Qurratul-Ain Minhas, Khalid Saleem, Ghazanfar Farooq Siddiqui, Naeem Bhatti & Hasan Mahmood. (2021). *A game theoretic power control and spectrum sharing approach using cost dominance in cognitive radio networks*. PeerJ Comput. Sci. 7:e617 DOI 10.7717/peerj-cs.617.

Han, T., Mao, G., Li, Q., Wang, L. & Zhang, J. (2017). *Interference Minimization in 5G Heterogeneous Networks*. Mobile Networks and Applications, vol. 20, no. 6, pp. 756-762

Xie, J. & Liu, C-C. (2018). *Multi-agent systems and their applications*. Journal of International Council on Electrical Engineering, 7:1, 188-197.

Yang, F., Wang, Y., Ding, L. & Qian, L. (2021). *An improved equalization with real interference prediction scheme of the FBMC/OQAM system*. China Communications, Volume: 18, Issue: 1.

Yu, W., Rhee, W., Boyd, S. & Cioffi, J. M. (2004). *Iterative waterfilling for Gaussian vector multiple-access channels*. IEEE Transactions on Information Theory, vol. 50, no. 1, pp. 145–152.

Zhang, Y., He, D., He, W., Xu, Y., Guan, Y. & Zhang, W. (2020). *Dynamic Spectrum Allocation by 5G Base Station*. International Wireless Communications and Mobile Computing (IWCMC), 2376-6492.

APPENDIX I – MATLAB Code - Prototype Filters Comparison (51 lines)

```matlab
clear; close all;

fs                      = 15.36e6;          % Sampling Rate: 1024*15kHz
F                       = 15e3;             % Subcarrier Spacing: 15kHz

dt = 1/fs;

%% Define Prototype Filters! Orthogonal for T=T0 and F=2/T0!


%FIR Hamming


p_FIR_Hamming_04 = @(t,T0) ((t<=(4*T0/2))&(t>-4*T0/2)).*(0.25+...
    0.02546*cos(2*pi*1/4*t/T0)+...
    0.243*cos(pi*2/4*t/T0))/sqrt(T0);

% Root raised cosine filter in time (low latency)
p_timeRRC = @(t,T0) ((t<=(T0/2))&(t>-T0/2)).*sqrt(1+(...
      cos(pi*1*2*t/T0)  ...
    ))/sqrt(T0);

% Reference rectangular prototype filter, orthogonal for T=T0, F=1/T0!
p_Rectangular = @(t,T0) (1/sqrt(T0).*((t<=(T0/2))&(t>-T0/2)));


%% Plot Filters
T0  = 1/F;
t   = (-200*T0/2:dt:(200*T0/2)).'; t(end)=[]; % so that fft becomes
real

% Time domain
p_FIR_Hamming_04_Samples= p_FIR_Hamming_04(t,T0);
p_timeRRC_Samples       = p_timeRRC(t,T0);
p_Rectangular_Samples   = p_Rectangular(t,T0);

% Plot the prototype filters in time
figure();
plot(t/T0,p_FIR_Hamming_04_Samples*sqrt(T0),'red');
hold on;
plot(t/T0,p_timeRRC_Samples*sqrt(T0),'magenta');
plot(t/T0,p_Rectangular_Samples*sqrt(T0),'black');
xlim([-2 2]);
ylabel('p(t)');
xlabel('Normalized Time, t/T0');
legend({'FIRHamm','RRC','Rectangular'});

% Frequency domain
df  = 1/(length(t)*dt);
f   = (-length(t)/2:(length(t)/2-1))*df;
P_FIR_Hamming_04_FFT= circshift(abs(fft(p_FIR_Hamming_04_Samples)),[-
length(t)/2,0]);
```

```
P_timeRRC_FFT         = circshift(abs(fft(p_timeRRC_Samples)),[-
length(t)/2,0]);
P_Rectangular_FFT   = circshift(abs(fft(p_Rectangular_Samples)),[-
length(t)/2,0]);

Normalize             = max(max([P_FIR_Hamming_04_FFT P_timeRRC_FFT
P_Rectangular_FFT]));

% Plot the prototype filters in frequency
figure();
plot(f*T0,20*log10(P_FIR_Hamming_04_FFT/Normalize),'red');
hold on;
plot(f*T0,20*log10(P_timeRRC_FFT/Normalize),'magenta');
plot(f*T0,20*log10(P_Rectangular_FFT/Normalize),'black');
ylim([-100 0]);
xlim([-10 10]);
ylabel('P(f)');
xlabel('Normalized Frequency, f T0');
legend({'FIRHamm','RRC','Rectangular'});
```

APPENDIX II – MATLAB Code – PSD Comparison between f-OFDM, OFDM and LWF-FBMC

```matlab
clear; close all;

L                             = 24;
% Number of subcarriers
K_OFDM                        = 10;
% Number of OFDM symbols in time
K_FBMC                        = 105;
% For FBMC we use a higher number of time-symbols so that the frequency
resolution is better. Without that, the figure would look ugly.

NrRepetitions                 = 200;
% Number repetitions for the simulation
QAM_ModulationOrder           = 16;
% Modulation order, 4,16,64,...

Simulate                      = true;
% Perform also a simulation in order to check the theoretical Power
Spectral Density (PSD)

SubcarrierSpacing             = 15e3;
% Subcarrier spacing (15kHz, same as LTE)
SamplingRate                  = SubcarrierSpacing*L*14;
% We need oversampling (14) in order to see out of band emissions.
Furthermore 14 fits the CP length of OFDM.

OverlappingFactor             = 4;
% Overlapping factor for FBMC.
IntermediateSubcarrier        = 50;
% Shift frequency (for presentation purposes)

% Parameterset 1
TF_FilteredAndWindowedOFDM    = 1.09;
FilterLengthTXandRX_FOFDM     = 1.18*1/(14*SubcarrierSpacing);

ColorFBMC   = [1 0 1]*0.5;
ColorOFDM   = [0 0 1];
ColorFOFDM  = [1 0 0]*0.7;


CP_LengthFilter = (TF_FilteredAndWindowedOFDM-1)*1/(SubcarrierSpacing);

%% FBMC Object
FBMC = Modulation.FBMC(...
    L,...                                                       %
Number subcarriers
    K_FBMC,...                                                  %
Number FBMC symbols (determines the frequency resolution!)
    SubcarrierSpacing,...                                       %
Subcarrier spacing (Hz)
```

```matlab
    SamplingRate,...                                    %
Sampling rate (Samples/s)
    SubcarrierSpacing*IntermediateSubcarrier,...        %
Intermediate frequency first subcarrier (Hz)
    false,...                                           %
Transmit real valued signal
    'LPFIR-OQAM',...                                    %
Prototype filter
    OverlappingFactor, ...                              %
Overlapping factor (also determines oversampling in the frequency
domain)
    0, ...                                              %
Initial phase shift
    true ...                                            %
Polyphase implementation
    );
%% OFDM Object
OFDM = Modulation.OFDM(...
    L,...                                               %
Number subcarriers
    K_OFDM,...                                          %
Number OFDM Symbols
    SubcarrierSpacing,...                               %
Subcarrier spacing (Hz)
    SamplingRate,...                                    %
Sampling rate (Samples/s)
    SubcarrierSpacing*IntermediateSubcarrier,...        %
Intermediate frequency first subcarrier (Hz)
    false,...                                           %
Transmit real valued signal
    1/(14*SubcarrierSpacing), ...                       %
Cyclic prefix length (s)
    0 ...                                               %
Zero guard length (s)
    );


%% Filtered OFDM
FOFDM = Modulation.FOFDM(...
    L,...                                               %
Number subcarriers
    K_OFDM,...                                          %
Number OFDM Symbols
    SubcarrierSpacing,...                               %
Subcarrier spacing (Hz)
    SamplingRate,...                                    %
Sampling rate (Samples/s)
    SubcarrierSpacing*IntermediateSubcarrier,...        %
Intermediate frequency first subcarrier (Hz)
    false,...                                           %
Transmit real valued signal
    0, ...                                              %
Cyclic prefix length (s)
    0, ...                                              %
```

```matlab
                                                                 Zero guard length (s)
    FilterLengthTXandRX_FOFDM, ...                               %
Filter length at TX (s)
    FilterLengthTXandRX_FOFDM, ...                               %
Filter length at RX (s)
    CP_LengthFilter ...                                          %
Addional cyclic prefix for the filtering (s)
);


%% Get TX and RX matrices to calculate SIR for FOFDM and UFMC due to
ISI/ICI
G_TX_FOFDM = sparse(FOFDM.GetTXMatrix);
G_RX_FOFDM = sparse(FOFDM.GetRXMatrix);


D_FOFDM = G_RX_FOFDM*G_TX_FOFDM;

% Inband Signal to interference ratio due to filtering (the filter
length is longer than the CP to improve filter characteristics)
SIR_dB_FOFDM =
10*log10(sum(abs(diag(D_FOFDM)).^2)/(sum(sum(abs(D_FOFDM-
diag(diag(D_FOFDM))).^2,2),1)));


%% Information
fprintf('==================================================\n');
fprintf('                  |(complex)TF-Spacing| Bandwidth(LF)| \n');
fprintf('OFDM (with CP) |%17.2f  |%8.2f MHz  | \n',
OFDM.PHY.TimeSpacing*OFDM.PHY.SubcarrierSpacing ,
OFDM.PHY.SubcarrierSpacing*OFDM.Nr.Subcarriers/1e6);
fprintf('FBMC           |%17.2f  |%8.2f MHz  | \n',
FBMC.PHY.TimeSpacing*FBMC.PHY.SubcarrierSpacing*2 ,
FBMC.PHY.SubcarrierSpacing*FBMC.Nr.Subcarriers/1e6);
fprintf('FOFDM          |%17.2f  |%8.2f MHz  | \n',
FOFDM.PHY.TimeSpacing*FOFDM.PHY.SubcarrierSpacing ,
FOFDM.PHY.SubcarrierSpacing*FOFDM.Nr.Subcarriers/1e6);
fprintf('==================================================\n');
fprintf('SIR [dB] for FOFDM: %2.2f   \n', full(SIR_dB_FOFDM));
fprintf('SIR [dB] for FBMC:  %2.2f   \n', FBMC.GetSIRdBDoublyFlat);
% Interference due to imperfect prototype filter


%% Calculate the Power Spectral Density (PSD)
[PSD_FBMC_Theory,f_FBMC]    =
FBMC.PlotPowerSpectralDensityUncorrelatedData;
[PSD_OFDM_Theory,f_OFDM]    =
OFDM.PlotPowerSpectralDensityUncorrelatedData;
[PSD_FOFDM_Theory,f_FOFDM] =
FOFDM.PlotPowerSpectralDensityUncorrelatedData;
```

```matlab
% Normalize over energy
PSD_FBMC_Theory  =
PSD_FBMC_Theory/(sum(PSD_FBMC_Theory)*SamplingRate/FBMC.Nr.SamplesTotal
);
PSD_OFDM_Theory  =
PSD_OFDM_Theory/(sum(PSD_OFDM_Theory)*SamplingRate/OFDM.Nr.SamplesTotal
);
PSD_FOFDM_Theory =
PSD_FOFDM_Theory/(sum(PSD_FOFDM_Theory)*SamplingRate/FOFDM.Nr.SamplesTo
tal);

% Normalize to 0dB
NormalizationFactor_Theory = max([PSD_FBMC_Theory]);
PSD_FBMC_Theory  = PSD_FBMC_Theory/NormalizationFactor_Theory;
PSD_OFDM_Theory  = PSD_OFDM_Theory/NormalizationFactor_Theory;
PSD_FOFDM_Theory = PSD_FOFDM_Theory/NormalizationFactor_Theory;


figure();
plot([-12 -12], [-150,20],'color', [0.8 0.8 0.8]);
hold on;
plot([12 12], [-150,20],'color', [0.8 0.8 0.8]);
plot(f_OFDM/OFDM.PHY.SubcarrierSpacing-IntermediateSubcarrier-
ceil(L/2)+1/2,10*log10([PSD_OFDM_Theory]),'Color', ColorOFDM);
plot(f_FOFDM/FOFDM.PHY.SubcarrierSpacing-IntermediateSubcarrier-
ceil(L/2)+1/2,10*log10([PSD_FOFDM_Theory]),'Color',ColorFOFDM);
plot(f_FBMC/FBMC.PHY.SubcarrierSpacing-IntermediateSubcarrier-
ceil(L/2)+1/2,10*log10([PSD_FBMC_Theory]),'Color', ColorFBMC);
ylim([-100 4]);
xlim([-50 50]);
xlabel('Normalized Frequency, f/F');
ylabel('Power Spectral Density [dB]');
set(gca,'XTick',[-50:10:50]);


if Simulate
tic
QAM = Modulation.SignalConstellation(QAM_ModulationOrder,'QAM');
PAM = Modulation.SignalConstellation(sqrt(QAM_ModulationOrder),'PAM');
PSD_FBMC_Simulation  = zeros(FBMC.Nr.SamplesTotal,1);
PSD_OFDM_Simulation  = zeros(OFDM.Nr.SamplesTotal,1);
PSD_FOFDM_Simulation = zeros(FOFDM.Nr.SamplesTotal,1);
for i_rep = 1:NrRepetitions
    x_OFDM = QAM.SymbolMapping(randi(QAM_ModulationOrder,L,K_OFDM));
    x_PAM  =
PAM.SymbolMapping(randi(sqrt(QAM_ModulationOrder),L,K_FBMC));

    s_FBMC  = FBMC.Modulation(x_PAM);
    s_OFDM  = OFDM.Modulation(x_OFDM);
    s_FOFDM = FOFDM.Modulation(x_OFDM);

    PSD_FBMC_Simulation  = PSD_FBMC_Simulation + abs(fft(s_FBMC)).^2;
    PSD_OFDM_Simulation  = PSD_OFDM_Simulation + abs(fft(s_OFDM)).^2;
    PSD_FOFDM_Simulation = PSD_FOFDM_Simulation + abs(fft(s_FOFDM)).^2;
```

```matlab
        TimePassed = toc;
        if mod(i_rep,100)==0
            disp(['Realization ' int2str(i_rep) ' of '
int2str(NrRepetitions) '. Time left: '
int2str(TimePassed/i_rep*(NrRepetitions-i_rep)/60) 'minutes']);
        end
end

% Normalize over energy
PSD_FBMC_Simulation =
PSD_FBMC_Simulation/(sum(PSD_FBMC_Simulation)*SamplingRate/FBMC.Nr.Samp
lesTotal);
PSD_OFDM_Simulation =
PSD_OFDM_Simulation/(sum(PSD_OFDM_Simulation)*SamplingRate/OFDM.Nr.Samp
lesTotal);
PSD_FOFDM_Simulation =
PSD_FOFDM_Simulation/(sum(PSD_FOFDM_Simulation)*SamplingRate/FOFDM.Nr.S
amplesTotal);

% LS Estimation to normalize to 0dB
NormalizationFactor_Simulation =
1./mean((PSD_FBMC_Simulation'*PSD_FBMC_Theory)./(PSD_FBMC_Simulation'*P
SD_FBMC_Simulation));
PSD_FBMC_Simulation =
PSD_FBMC_Simulation/NormalizationFactor_Simulation;
PSD_OFDM_Simulation =
PSD_OFDM_Simulation/NormalizationFactor_Simulation;
PSD_FOFDM_Simulation =
PSD_FOFDM_Simulation/NormalizationFactor_Simulation;

figure();
plot(f_OFDM/OFDM.PHY.SubcarrierSpacing-IntermediateSubcarrier-
ceil(L/2)+1/2,10*log10([PSD_OFDM_Theory PSD_OFDM_Simulation]),'Color',
ColorOFDM);
hold on;
plot(f_FOFDM/FOFDM.PHY.SubcarrierSpacing-IntermediateSubcarrier-
ceil(L/2)+1/2,10*log10([PSD_FOFDM_Theory
PSD_FOFDM_Simulation]),'Color', ColorFOFDM);
plot(f_FBMC/FBMC.PHY.SubcarrierSpacing-IntermediateSubcarrier-
ceil(L/2)+1/2,10*log10([PSD_FBMC_Theory PSD_FBMC_Simulation]),'Color',
ColorFBMC);
plot([-12 -12], [-150,20],'color', [0.8 0.8 0.8]);
plot([12 12], [-150,20],'color', [0.8 0.8 0.8]);
ylim([-100 4]);
xlim([-50 50]);
xlabel('Normalized Frequency, f/F');
ylabel('Power Spectral Density [dB]');
set(gca,'XTick',[-50:10:50]);
title('Theory vs Simulation');

end
```